THE INTERACTION OF TARGETED AND NON-TARGETED NANOPARTICLES WITH CELLS AND MODEL MEMBRANES

by

Pascale Raymonde Leroueil

A dissertation submitted in partial fulfillment
of the requirements for the degree of
Doctor of Philosophy
(Chemistry)
in The University of Michigan
2008

Doctoral Committee:

Professor Mark M. Banaszak Holl, Co-Chair
Professor Bradford G. Orr, Co-Chair
Professor James R. Baker Jr.
Assistant Professor Ioan Andricioaei

DEDICATION

To Mom

If there ever comes a day when we can't be together
keep me in your heart, I'll stay there forever.

-- Winnie the Pooh

ACKNOWLEDGEMENTS

Committee: Mark M. Banaszak Holl, Bradford G. Orr, James R. Baker, Jr., Ioan Andricioaie

Dr. Mark M. Banaszak-Holl is an overflowing source of ideas. More often than not, I would sit back amazed thinking, "How did he come up with that?" Despite this, he always tried to make it seem like he too had difficulties with science on par with my own, although I'm quite sure the vast majority of these were made up for my benefit. It was clear Mark's intention was to make his graduate students the best scientists and members of society they could be. He encouraged personal development outside the lab, as well as the occasional friendly bet within the lab (none of which I ever won – NOTE: If Hillary Clinton wins the Presidency in 2008, my losing streak will have ended!).

As an advisor, **Dr. Bradford (Brad) G. Orr** always kept his door open, ready to discuss experiments (or Supreme Court Justices, as the case may be). Even when I was way off on the evaluation of my data, I never walked out of his office thinking, "You idiot, Pascale!" More often than not, I actually walked out thinking, "You genius, Pascale! That's what you meant all along!" I am truly grateful for Brad's patience and encouragement, as well as his genuine concern for my well-being throughout my graduate career. Also, I would like to thank Brad's wife, **Diane Conde** and sons **Matthew** and **Stephen**: I will always look back on the parties with them fondly. Well, not all of the parties: I lost too much money at some of them.

Dr. Christine Orme served as my advisor at Lawrence Livermore National Lab and was extremely helpful in my adventures in force pulling spectroscopy, as well as making me feel welcome in her lab. Plus, she buys the best chocolate for chocolate tasting competitions.

As a member of the Michigan Nanotechnology Institute for Medicine and Biological Sciences, **(MNiMBS)**, I have had the privilege of working with a number of talented scientists.

Dr. James R. Baker, Jr.'s vast knowledge and Superman-like qualities still astound me, even after more than 4 years. I am thankful for the work Dr. Baker has done, and continues to do. I wish him success and an occasional round of golf at a course with no cell phone reception.

Dr. Ania Bielinska once called me a 'cat,' independent and stubborn. Despite this oftentimes-truthful description of me, she was willing to lend a much-needed helping hand. Or knock me down a few steps as the case may be.

Dr. Thommey Thomas has been a great source of information and encouragement. He has always been willing to explain the obvious details of an experiment to those of us that felt the obvious details weren't so obvious.

The entire **Banaszak-Holl and Orr Group** has at one time or another helped me along the way. However, there are a few members that have pushed me a little harder, both in regards to science and life.

Dr. Zuzanna Cygan was perfectly suited to explain how you screwed up. I still covet that skill today.

Dr. Stassi C. DiMaggio was here for less than a year following Hurricane Katrina but she left an indelible mark on many us. Her candor, charm and obsession with doing what was right and good have made her one of my favorite people to shoot the breeze with over a Tangaray and Tonic.

Blake Erickson has been a very thoughtful and scientifically rigorous addition to the Banaszak Holl/Orr Lab this past year. He always had an open an ear and was willing to push the envelope on levels of appropriateness.

Dr. Jessica (Blunt) Hessler was my mentor, my big sister and one of my first very good friends here at Michigan. She called you out when you were and bought you a punching bag when things weren't going so well in science and in life. Despite her tough exterior, it was clearly her heart and sense of justice that drove her.

In my first year in graduate school, **Dr. Seungpyo Hong** told me he was going to serve as my 'big brother.' Although he later told me he was a bit worried about me when I first

started out, he was a constant source of advice and encouragement. Our talks at Charlie's and subsequent trips to the arcade, as well as other adventures that I still laugh about, are truly priceless memories.

Within thirty minutes of meeting **Channing (Chan) Huntington**, I informed him of my fool-proof plan for solving all the problems in the Middle East – it was the start of a beautiful friendship full of coffee runs and rib shots. His Jon Stewartesque humor and appreciation of good food and discussions have made these last two years all the more entertaining.

One minute **Prashant Padmanabhan** would be explaining why most pits are just so fun and the next he would be reciting a treatise on the rights of Man that Paine himself would envy. He filled the shoes of both a boy and a wise man well.

Christopher V. Kelly has served as the sounding board for my most insane ideas, science related and otherwise. For this, West Hall 271 will forever house some of my most treasured conversations in graduate school. He has become one of my absolute best friends here at Michigan and I will miss him dearly. **Chris'** better half **Katie Kelly**, has been one of my favorite sources of smiles and enjoyable outings. She is truly a sweetheart that I am glad to have had the pleasure of meeting. In addition to being wonderful friends, the **Kellys** have served as wonderful landlords these past 6 months.

Damian Khan loves knowledge. More than that, he loves to teach what he knows. If ever I was confused about a model going through my head, you could be sure that Damian would drop everything to help me out.

The future medical Drs. **Mary-Margaret (Maggie) Kober** and **Stephanie A. Berry** do nothing but amaze me. Both were top-notch scientists and truly wonderful people with infectious smiles. They helped me with many an experiment and kept things interesting around the lab.

Kevin Landmark, physicist-turned-chemist, is someone I remember meeting and thinking, "he can't be *that* nice." But he is.

Dr. Bonnie (Laack) Ludwig on the exterior is a shining example of what I thought a Midwesterner was before I came to Michigan. I soon learned, however, that the girl has a bite equal to that of any New Yorker. She remains a mentor, a giver of chocolate, a joke-teller and a good friend.

Although rumor has it he never smiles, I rarely saw **Daniel (Dan) McNerny** without a smile on his face. Of course, most of them are code for "I know something…" Dan has been a dedicated scientist and friend. I wish he and **Erin Gatenby** many adventures together.

During graduate school, I jokingly referred to myself as living in the shadow of **Dr. Almut Mecke.** She has a German precision about her with which my emotionally driven French nature simply cannot compete. Nonetheless, our mutual love of chocolate and European tendencies allowed us to get along wonderfully.

Douglas (Doug) Mullen, sailor and singer extraordinaire, is as good-natured and sweet as his dimples suggest. Always up for a drink (unless it conflicts with "practice"), a chat, or just a hug, Doug makes this world a happier place.

Kami L. Hull, my roommate and confidante for nearly all of graduate school is one of the most generous and caring individuals I have ever met. *Ever*. A giver to nearly a fault, her level-headed talks, infinite drives to and from the airport and delicious brownies made graduate school that much more bearable.

Shanna Shaked and Jasper Kok, my two physicist friends who I stole from **Chris Kelly.** I met both of them much later than I would have liked because the last year spent with them has been *wonderful*. I smile in happiness knowing that these two brilliant, warm-hearted and caring individuals have found each other. I'm convinced that they will one day be one of those 80 year old couples you see sitting on a bench holding hands…talking about physics.

Shokelleroueil, the household of **Shanna, Jasper, Chris, Katie and Pascale**. How could I not acknowledge the union that left many confused but us buckled over in fits of laughter? Happy memories were truly had.

I met **Gabrielle Soucy** on a soccer field and suffice it to say, I never stopped running. She was here for too short a time but the girl from Montreal took me on more than a few enjoyable rollercoaster rides. I have always been a sucker for those.

Mary Christine (Chris) Mackowiak,, mother of my future husband, has been a source of laughter and travel re-imbursements throughout my graduate career. From lunches to random chats, she served as a constant reminder that life ought to be entertaining.

Although **Drs. Katie and Jeremy Mitchell-Koch** left Ann Arbor for Kansas during my second year here, our continued friendship has meant more to me than they'll ever know. Sunday dinner still brings back fond memories. And for my other Kansas friend, **Dr. Leilani Welbes** who often went to her 'happy place' when wine and chocolate were present – she still makes me smile. I am pleased to announce that both **Katie** and **Leilani** will be making **Kami** and I honorary aunts this Spring!

While not an official member of the **Melanie Sanford Group**, they always made me feel welcome whenever I came searching for my housemate, or just happened to be in the Chemistry Building.

Charles Sutton, the man who ran the Applied Physics Office, could be counted on to provide directions to where **Brad** (or a pizza) was stashed**.** He watched out for me and handed me advice when I needed it.

Although the entire **Chemistry Staff** has helped me throughout my stay her, **Linda Van Blaircum** and **Aiko Nakatino** in particular have made things go much smoother than they would have otherwise.

Duane, Kate, Doug and the rest of **Physics OCS** have saved me on more than once occasion and for that I am incredibly grateful.

And finally, for my family who throughout my life has been behind me, cheering at the top of their lungs. My grandpa and grandma, **Leslie H. Clark** and **Patricia H. Clark**, have always been the proud grandparents every child deserves. They sacrificed. They smiled. They taught me spelling. They were wonderful. My aunt **Stephanie A. Clark** proofread my essays when I was younger and my research papers when I was older, all while preserving her goofy sense of humor. My aunt **Karen Clark**, maintained an interest in my work and well-being, particularly when I needed it most. My uncle **Dr. Doug L. Clark** and aunt **Dr. Shu-Ming Wang Clark** always encouraged me to go for the gold, even if it was located on top of a mountain and under a rock.

My big brother **Pierre A. Leroueil**, left this world earlier than any of us would have hoped. His 'fuck it' attitude was the inspiration for many of my most daring adventures, in and out of graduate school.

My little brother **Marc M. Leroueil**, a giant in stature and in character, has always been wise beyond his years. Our shared sense of humor and his easy-going nature made it such that we rarely fought as children. Or adults. I look forward to living off the interest of his riches.

And finally, my parents, Mom (**Christine C. Leroueil**) and Papa (**Pierre E. Leroueil**). They gave me every opportunity to excel and change the world for the better. Their commitment to their children and to each other shaped my life like nothing else. Merci Mama et Papa.

TABLE OF CONTENTS

LIST OF TABLES

LIST OF FIGURES

CHAPTER 1

INTRODUCTION

1.1 BACKGROUND

Nanoparticles are loosely defined as structures with diameters of ~1-100 x 10^{-9} m.[1] Invisible to the eye, and indeed most measurement techniques, nanoparticles have revolutionized how our cars are made, how our computer chips are made, and even how we play tennis. By simply taking a piece of common material such as gold and shrinking it until it is very small, we can make new materials that bear very little resemblance to their bulk counterparts.[2, 3] The potential held within these very small structures is clearly great, both from a consumer, as well as financial standpoint.[4] In addition to infiltrating our everyday products, nanoparticles have changed the way we think about medicine. Our ability to make particles comparable in size to that of the proteins has opened up a wide range of possible medical applications, including gene therapy[5-8] and targeted drug delivery.[6, 7, 9-11]

Despite these current and potential benefits, there is growing concern regarding the interaction of nanoparticles with their environment.[12-19] For the most part, nanoparticles have been developed under the assumption that we could expect 1 kilo of nanoparticle ***X*** to have the same toxicity concerns as 1 kilo of bulk ***X***. This assumption would be correct if elemental composition dictated all the properties of the material. However, given the multitude of physical, electrical and optical properties possible using

the same molecule as a building block, this assumption is clearly faulty.[2, 20-24] Indeed, nanostructure plays a key role in dictating the interactions of nanoparticles with their environments. It is from this perspective that this thesis addresses the selectivity of targeted and non-targeted nanoparticles with cells and model cell membranes.

1.2 TARGETED NANOPARTICLES FOR GENE AND DRUG DELIVERY

In 1907, the Nobel Prize winning Paul Ehrlich coined the term "magic bullet" in reference to a compound that could selectively target and deliver toxin to an organism.[25] The magic bullet has since been the holy grail of cancer treatment.[26] Traditional treatment relies heavily on the systemic administration of highly toxic drugs that kill not only cancerous cells, but healthy cells as well. Most cancer drugs possess a very narrow therapeutic range resulting in the need to administer sub-optimal dosages to patients. A targeted drug delivery platform would allow for a patient to be given the appropriate drug dosage necessary to retard or stop tumor growth while minimizing non-selective side effects.[27] In addition, targeted drug delivery would enable the patient to be given therapeutics in quicker succession. This is important given that it may not be immediately apparent which drug or drug combination is appropriate for a particular cancer. By using a targeted delivery system, the patient could be treated continuously with a variety of drugs without fear of doing irreparable damage to the healthy cells.

The field of targeted drug delivery has been largely divided into two classes of targeting systems: those that utilize (1) passive targeting and those that utilize (2) active targeting. Passive targeting systems rely on the enhanced permeability and retention (EPR) effect.[28] Large macromolecules are sequestered in tumors due to the leaky

vascular system associated with tumor growth. The result is that nanoparticles modified to include traditional cancer fighting drugs are retained in the tumor, thereby selectively delivering the toxin to the offending cells. However, a limitation of passive targeting is that it requires the tumor to be of substantial size such that the surrounding vascular system is sufficiently compromised.[29] Active targeting circumvents this problem by targeting not the tumor mass, but instead particular receptors or moieties present on the surface of individual cancer cells[27] **(Figure 1.1).** In principle, an active targeted platform will bind and internalize into only those cells which express the target. Small molecules such as folic acid,[10] RGD peptides,[5] and aptamers[30] have been employed as targeting agents because their respective receptors are shown to be over-expressed on a range of cancer cell lines.[5, 31]

1.2.1 Type of nanoparticles used for the development of targeted drug delivery.

An important component when developing a targeted drug delivery platform is the choice of the scaffold that serves as the backbone of the platform. The requirements for an effective scaffold are that they must be: (1) highly water soluble (2) easily functionalizable and (3) biocompatible. An assortment of scaffolds including liposomes,[32, 33] gold,[2, 6, 34] and polymers[7, 9, 10, 35] have been used in the fabrication of targeted platforms. Unfortunately, however, many of these platforms fail because they lack one or more of the three requirements noted above. The result is lack of directed toxicity at best, and unintended toxicity at worst.

1.2.2 MNiMBS development of a multivalent targeted drug delivery nanoparticle using a PAMAM dendrimer as a scaffold.

The development of an active targeted drug delivery platform has been the focus of much of the Michigan Nanotechnology Institute for Medicine and Biological Sciences (MNiMBS). Our group has utilized a particular type of nanoparticle called a Generation 5 (G5) PAMAM dendrimer as our scaffold. This nanoparticle is a highly modifiable, relatively mono-disperse and water-soluble branched polymer. In addition, unlike many other polymers developed for targeted delivery, acetylated dendrimers have been shown to be non-immunogenic.[10, 35]

The versatility of the dendrimer in both size and chemical termination has allowed for the attachment of various targeting agents (folic acid (FA), herceptin), therapeutics (methotrexate, taxol) and imaging agents (FITC, AlexFluor*488*).[36] FA, the primary targeting agent used by our group, was chosen because its receptor, FAR, is known to be over-expressed on several epithelial cancer cell lines.[31, 37]

1.2.3 Use and Quantification of Multivalency

Targeted drug delivery using a single targeting agent represents a vast improvement over the administration of free drug.[10] However, a further increase in targeting has been shown through the attachment of multiple FAs to the PAMAM dendrimer scaffold. It was found that those devices with a larger number of FAs conjugated to their surface showed an increase in binding to real and model FARs (folate binding proteins, FBPs).[38] This improvement has been quantified using confocal microscopy, flow cytometry and surface plasmon resonance (SPR). Although our understanding of the bulk binding effects has been greatly increased using these techniques, they have failed to detail the interaction between a single G5-FA_n and receptor.

Chapter 2 addresses this issue using force pulling spectroscopy, a single molecule technique, to obtain the forces associated with the G5-FA_n binding to the FBP substrate. A series of G5 dendrimers with varying numbers of FA molecules (2-8) were used in conjunction with this technique. It was found that the rupture force associated with the unbinding of these modified dendrimers from the FBP substrate scales with the bulk measurements previously obtained by Hong et al.[38]

1.3. NON-TARGETED NANOPARTICLES

In the process of developing our targeted platform, we found that amine terminated dendrimers exhibited a great deal of non-specific binding. These interactions were of concern because they resulted in unintended cytotoxicity to surrounding cells. It was only upon full acetylation of the terminal amines that these non-specific interactions were suppressed. This was particularly interesting from our perspective because many 'targeted' nanoparticles developed by other research groups suffer from the same selectivity issues we had when we employed non-acetylated targeted dendrimers.[10] A hypothesis was formed that stated that the protonated amines present on PAMAM dendrimers at physiological pH were responsible, at least in part, for the non-specific interactions.

In order to explore the effect that dendrimer charge had on mediating non-specific interactions with cells, a variety of assays including enzyme leakage, dye diffusion, flow cytometry and confocal microscopy were employed. These cell-level assays provided a relatively cheap avenue through which nanoparticle selectivity and cytotoxicity could be assessed. Indeed, cell-level assays have served as the backbone for toxicity assays

because they address the fundamental question of "at what level does a material's selectivity (or non-selectivity) result in toxicity?" A deficiency in cell-level studies, however, is that they do not allow us to obtain a nanoscale understanding of the interaction between nanoparticle and cell. Atomic force microscopy (AFM), in conjunction with supported lipid bilayers (SLBs), a simple model of the very complex cellular membrane, allows us to achieve nanoscale resolution of this interaction. Consisting of one or more types of lipid, SLBs do not contain the proteins, sugars or cholesterol found in a true cell membrane**. (Figure 1.2)** Nonetheless, this model has been shown to correlate with whole-cell level assays which found that cell-membrane disruption increased as the number of amine groups present on the dendrimer increased.[39, 40] Given the wide range of nanoparticles currently in development, and indeed already on the market, we were interested in examining how other physical characteristics of charged nanoparticles affected their interaction with cell membranes.

Chapters 3-4 examine the interaction of our model cell membrane with non-targeted nanoparticles while varying a variety of physical characteristics, including charge density, size, flexibility and chemistry. By understanding the details of this nanoscale interaction, we can predict nanoparticle selectivity, and therefore tune their physical characteristics to alleviate unintended toxicity effects. It was found that polycationic polymers induce defect formation and/or expansion within SLBs whereas neutral polymers do not. Other types of polycationic materials (Au-NH_2, Si-NH_2, TAT protein, MSI-78) were also investigated using the AFM-SLB assay. Each of these materials induce the formation and/or expansion of defects within SLBs. Taken as a

whole, these studies suggest that interactions between charged non-targeted nanoparticles and membranes are governed grossly by surface area and charge density.[35, 39, 40]

The nanoparticles investigated above are formed through covalent linkages of their respective sub-parts, resulting in a stable complex. To address the importance of nanoparticle stability, we chose to examine charged 'nanoparticles' with non-stable structures. Above critical micelle concentration (CMC), detergents form a non-stable complex (micelle) that is similar in size to those nanoparticles investigated in Chapters 3-4. Chapter 5 examines the interaction of two charged, non-covalently linked complexes with model membranes using the AFM-SLB assay. Like the covalently linked nanoparticles investigated above, we find that the above CMC charged detergents SDS and CTAB remove lipid from SLBs. Interestingly, pre-existing defects within the SLBs are occluded when these same detergents are introduced at concentrations below their respective CMCs. These studies show that even transient aggregations of charged material are sufficient to induce hole formation in cell membranes.

1.4. OUTLINE AND THESIS ORGANIZATION

This thesis details the interaction of targeted and non-nanoparticles with real and model membranes. Chapter 2 addresses the binding of a targeted nanoparticle, G5-FA_n to a model cell receptor surface. Chapters 3-5 focus on the interaction of a variety of non-targeted charged nanoparticles with real and model membranes. Chapter 6 serves as a summary of this thesis and provides direction for relevant future studies.

1.5 FIGURES

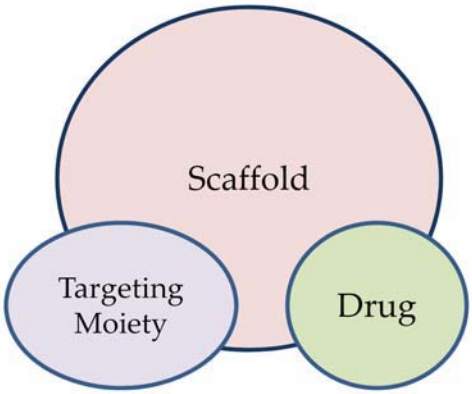

Figure 1.1. Schematic illustrating the general design of a targeted drug delivery platform. The drug and targeting moiety are attached to a scaffold. The choice and drug and targeting moiety are dependent on the type of cancer being treated.

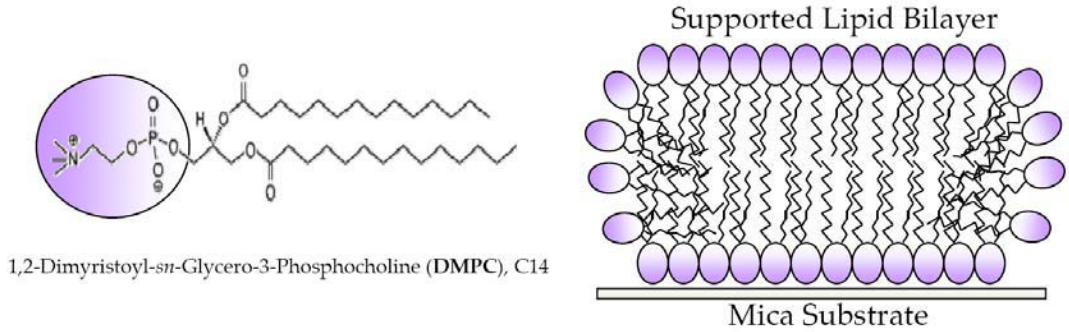

Figure 1.2. Cartoon showing a mica-supported 1,2-Dimyristoyl-*sn*-Glycero-3-Phosphocholine (DMPC) lipid bilayer. DMPC supported lipid bilayers serve model membrane used in all AFM studies completed within this thesis.

1.6 REFERENCES

1. Oberdorster, G.; Oberdorster, E.; Oberdorster, J., Nanotoxicology: An emerging discipline evolving from studies of ultrafine particles. *Environmental Health Perspectives* **2005,** 113, (7), 823-839.

2. West, J. L.; Halas, N. J., Engineered nanomaterials for biophotonics applications: Improving sensing, imaging, and therapeutics. *Annual Review of Biomedical Engineering* **2003,** 5, 285-292.

3. Li, M.; Schnablegger, H.; Mann, S., Coupled synthesis and self-assembly of nanoparticles to give structures with controlled organization. *Nature* **1999,** 402, (6760), 393-395.

4. Woodrow Wilson International Center for Scholars: Project on Emerging Technologies. http://www.nanotechproject.org/ (October 2, 2007)

5. Schiffelers, R. M.; Ansari, A.; Xu, J.; Zhou, Q.; Tang, Q. Q.; Storm, G.; Molema, G.; Lu, P. Y.; Scaria, P. V.; Woodle, M. C., Cancer siRNA therapy by tumor selective delivery with ligand-targeted sterically stabilized nanoparticle. *Nucleic Acids Research* **2004,** 32, (19).

6. Zhi, P. X.; Qing, H. Z.; Gao, Q. L.; Ai, B. Y., Inorganic nanoparticles as carriers for efficient cellular delivery. *Chemical Engineering Science* **2006,** 61, (3), 1027-1040.

7. Satchi-Fainaro, R.; Duncan, R.; Barnes, C. M., Polymer therapeutics for cancer: Current status and future challenges. In *Polymer Therapeutics Ii: Polymers as Drugs, Conjugates and Gene Delivery Systems*, 2006; Vol. 193, pp 1-65.

8. Hood, J. D.; Bednarski, M.; Frausto, R.; Guccione, S.; Reisfeld, R. A.; Xiang, R.; Cheresh, D. A., Tumor regression by targeted gene delivery to the neovasculature. *Science* **2002,** 296, (5577), 2404-2407.

9. Brannon-Peppas, L.; Blanchette, J. O., Nanoparticle and targeted systems for cancer therapy. *Advanced Drug Delivery Reviews* **2004,** 56, (11), 1649-1659.

10. Quintana, A.; Raczka, E.; Piehler, L.; Lee, I.; Myc, A.; Majoros, I.; Patri, A. K.; Thomas, T.; Mule, J.; Baker, J. R., Design and function of a dendrimer-based therapeutic nanodevice targeted to tumor cells through the folate receptor. *Pharmaceutical Research* **2002,** 19, (9), 1310-1316.

11. Kreuter, J., Nanoparticulate systems for brain delivery of drugs. *Advanced Drug Delivery Reviews* **2001,** 47, (1), 65-81.

12. Borm, P. Y. A.; Costa, D.; Castranova, V.; Donaldson, K.; Driscoll, K.; Dungworth, D.; Green, F.; Greim, H.; Harkema, J.; Jarabek, A.; Kane, A. B.; Kuempel,

E. D.; Mauderly, J. L.; McCunney, R. J.; Miller, F.; Morgan, D.; Mossman, B.; Muhle, H.; Nauss, K.; Nikula, K.; Oberdorster, G.; Olin, S. S.; Pepelko, W.; Pinkerton, K. E.; Schultz, M.; Utell, M. J.; Vallyathan, V.; Vu, V.; Warheit, D. B.; Witschi, H., The relevance of the rat lung response to particle overload for human risk assessment: A workshop consensus report. *Inhalation Toxicology* **2000,** 12, (1-2), 1-17.

13. Warheit, D. B.; Webb, T. R.; Colvin, V. L.; Reed, K. L.; Sayes, C. R., Pulmonary bioassay studies with nanoscale and fine-quartz particles in rats: Toxicity is not dependent upon particle size but on surface characteristics. *Toxicological Sciences* **2007,** 95, (1), 270-280.

14. Maynard, A. D.; Kuempel, E. D., Airborne nanostructured particles and occupational health. *Journal of Nanoparticle Research* **2005,** 7, (6), 587-614.

15. Oberdorster, E., Manufactured nanomaterials (Fullerenes, C-60) induce oxidative stress in the brain of juvenile largemouth bass. *Environmental Health Perspectives* **2004,** 112, (10), 1058-1062.

16. Gwinn, M. R.; Vallyathan, V., Nanoparticles: Health effects - Pros and cons. *Environmental Health Perspectives* **2006,** 114, (12), 1818-1825.

17. Wittmaack, K., Search of the most relevant parameter for quantifying lung inflammatory response to nanoparticle exposure: Particle number, surface area, or what? *Environmental Health Perspectives* **2007,** 115, (2), 187-194.

18. Hussain, S. M.; Hess, K. L.; Gearhart, J. M.; Geiss, K. T.; Schlager, J. J., In vitro toxicity of nanoparticles in BRL 3A rat liver cells. *Toxicology in Vitro* **2005,** 19, (7), 975-983.

19. Nel, A.; Xia, T.; Madler, L.; Li, N., Toxic potential of materials at the nanolevel. *Science* **2006,** 311, (5761), 622-627.

20. Kamat, P. V., Photophysical, photochemical and photocatalytic aspects of metal nanoparticles. *Journal of Physical Chemistry B* **2002,** 106, (32), 7729-7744.

21. Shipway, A. N.; Katz, E.; Willner, I., Nanoparticle arrays on surfaces for electronic, optical, and sensor applications. *Chemphyschem* **2000,** 1, (1), 18-52.

22. Murray, C. B.; Kagan, C. R.; Bawendi, M. G., Synthesis and characterization of monodisperse nanocrystals and close-packed nanocrystal assemblies. *Annual Review of Materials Science* **2000,** 30, 545-610.

23. Link, S.; El-Sayed, M. A., Shape and size dependence of radiative, non-radiative and photothermal properties of gold nanocrystals. *International Reviews in Physical Chemistry* **2000,** 19, (3), 409-453.

24. Jackson, J. B.; Halas, N. J., Silver nanoshells: Variations in morphologies and optical properties. *Journal of Physical Chemistry B* **2001,** 105, (14), 2743-2746.

25. Shukla, S. K.; Petrucci, F.; Caimi, S.; Alimonti, A.; Cusumano, R., Cancer 'Chemotherapia specifica' ninety years after Paul Ehrlich. *Chemotherapy* **2007,** 53, (5), 309-312.

26. Allen, T. M.; Cullis, P. R., Drug delivery systems: Entering the mainstream. *Science* **2004,** 303, (5665), 1818-1822.

27. Braun, K.; Pipkorn, R.; Waldeck, W., Development and characterization of drug delivery systems for targeting mammalian cells and tissues: A review. *Current Medicinal Chemistry* **2005,** 12, (16), 1841-1858.

28. Maeda, H., The enhanced permeability and retention (EPR) effect in tumor vasculature: The key role of tumor-selective macromolecular drug targeting. In *Advances in Enzyme Regulation, Vol 41*, 2001; Vol. 41, pp 189-207.

29. Jain, R. K., Barriers to Drug-Delivery in Solid Tumors. *Scientific American* **1994,** 271, (1), 58-65.

30. Farokhzad, O. C.; Jon, S. Y.; Khadelmhosseini, A.; Tran, T. N. T.; LaVan, D. A.; Langer, R., Nanopartide-aptamer bioconjugates: A new approach for targeting prostate cancer cells. *Cancer Research* **2004,** 64, (21), 7668-7672.

31. Ross, J. F.; Chaudhuri, P. K.; Ratnam, M., Differential Regulation of Folate Receptor Isoforms in Normal and Malignant-Tissues in-Vivo and in Established Cell-Lines - Physiological and Clinical Implications. *Cancer* **1994,** 73, (9), 2432-2443.

32. Dubey, P. K.; Mishra, V.; Jain, S.; Mahor, S.; Vyas, S. P., Liposomes modified with cyclic RGD peptide for tumor targeting. *Journal of Drug Targeting* **2004,** 12, (5), 257-264.

33. Andresen, T. L.; Jensen, S. S.; Jorgensen, K., Advanced strategies in liposomal cancer therapy: Problems and prospects of active and tumor specific drug release. *Progress in Lipid Research* **2005,** 44, (1), 68-97.

34. Paciotti, G. F.; Myer, L.; Weinreich, D.; Goia, D.; Pavel, N.; McLaughlin, R. E.; Tamarkin, L., Colloidal gold: A novel nanoparticle vector for tumor directed drug delivery. *Drug Delivery* **2004,** 11, (3), 169-183.

35. Duncan, R.; Izzo, L., Dendrimer biocompatibility and toxicity. *Advanced Drug Delivery Reviews* **2005,** 57, (15), 2215-2237.

36. Majoros, I. J.; Myc, A.; Thomas, T.; Mehta, C. B.; Baker, J. R., PAMAM dendrimer-based multifunctional conjugate for cancer therapy: Synthesis, characterization, and functionality. *Biomacromolecules* **2006,** 7, (2), 572-579.

37. Sudimack, J.; Lee, R. J., Targeted drug delivery via the folate receptor. *Advanced Drug Delivery Reviews* **2000,** 41, (2), 147-162.

38. Hong, S.; Leroueil, P. R.; Majoros, I. J.; Orr, B. G.; Baker, J. R.; Holl, M. M. B., The binding avidity of a nanoparticle-based multivalent targeted drug delivery platform. *Chemistry & Biology* **2007,** 14, (1), 105-113.

39. Mecke, A.; Majoros, I. J.; Patri, A. K.; Baker, J. R.; Holl, M. M. B.; Orr, B. G., Lipid bilayer disruption by polycationic polymers: The roles of size and chemical functional group. *Langmuir* **2005,** 21, (23), 10348-10354.

40. Hong, S. P.; Leroueil, P. R.; Janus, E. K.; Peters, J. L.; Kober, M. M.; Islam, M. T.; Orr, B. G.; Baker, J. R.; Holl, M. M. B., Interaction of polycationic polymers with supported lipid bilayers and cells: Nanoscale hole formation and enhanced membrane permeability. *Bioconjugate Chemistry* **2006,** 17, (3), 728-734.

CHAPTER 2

MEASURING THE BINDING OF A MULTIVALENT TARGETED NANOPARTICLE USING FORCE PULLING SPECTROSCOPY

2.1. BACKGROUND

A limitation of many medical treatments, particularly chemotherapeutics, is that they are administered systemically resulting in the destruction of both sick and healthy cells.[1, 2] The collateral damage associated with this systemic administration of drugs often results in premature cessation of treatment for the patient. A device capable of delivering a drug to only those cells in need of treatment would be preferred. By conjugating a targeting agent and a traditional therapeutic to a scaffold, one could selectively deliver the therapeutic to those cells expressing a particular receptor, or other target moiety.

Many targeted delivery platforms have been developed since the 1970s using a variety of scaffolds[3-7] and targeting agents.[3, 7-13] Attempts have been made to further increase specific binding affinity by employing multivalency, the simultaneous binding of multiple ligands to multiple receptors. Previous *in vitro* studies using multivalent inhibitors have shown a 1 to 9 order increase in binding avidity over their monovalent form whereas multivalent effectors have shown a 1 to 2 order increase.[14-19] However, unintended targeting of healthy cells expressing the target-moiety, and non-selective toxicity resulting from the targeted-therapeutic remaining sequestered within the patient, have made many of these same targeted-therapeutics less promising *in vivo*. [3, 20, 21]

Our own group has developed a targeted platform using folic acid (FA) as a targeting agent, methotrexate (MTX) as a therapeutic, and an acetylated generation 5 PAMAM dendrimer (G5) as a scaffold. FA was chosen as the targeting agent because the folate receptor (FAR) is known to be over-expressed on the surface of several epithelial cancer cell lines.[22-25] Like other targeted therapeutics, G5-FA_n-MTX has been shown to be effective *in vitro*.[15] However, it is the proven effectiveness of this multivalent (~5 FAs) platform at shrinking tumor size *in vivo* without causing detectable side effects that is truly remarkable.[26]

Hong *et al.* recently completed a study in which the number of FAs, *n*, conjugated to the surface of a G5 was systematically varied. Using surface plasmon resonance (SPR), a ~2,500- to 170,000-fold reduction in the dissociation constant (K_D) over free FA was measured between G5-FA_n (where n = ~ 3 to 14) and a model FAR (folate binding protein, FBP) surface **(Figure 2.1)**. In addition, it was found that there is an exponential decrease in k_d with *n* while k_a only increases linearly with *n* **(Figure 2.2).** [27] The drastic decrease in K_D of the G5-FA_n conjugates as compared to free FA is therefore due to the increase in residence time of the targeted-platform on the FAR expressing cell. Note that the enhancement in K_D measured for the G5-FA_n series is significantly higher than the 10-100 fold enhancement reported by another group utilizing a different multivalent FA platform.[28] Fluorescence activated cell-sorting (FACS) studies showed a similar trend **(Figure 2.3).**[27] Given the success of this multivalent targeted therapeutic both *in vitro* and *in vivo*, we used force pulling spectroscopy to examine in greater detail how the binding of a *single* G5-Ac_{70}-FA_n to a FBP surface varies with *n*.

2.2. EXPERIMENTAL

Preparation of Dendrimers

G5 PAMAM dendrimers were synthesized and purified to remove low molecular weight impurities as well as high molecular weight dimers, according to previous reports.[26, 29, 30] After purification, the dendrimers were partially acetylated (70 of the 110 total primary amines) resulting in G5-Ac_{70}.[31] The G5-Ac_{70} in H_2O was allowed to react with FA pre-activated by 1-[3-(dimethylamino)propyl]-3-ethylcarbodiimide/HCl (EDC) in DMF/DMSO at different molar ratios (0:1, 3:1, 6:1, 9:1) of FA to G5-Ac_{70}. Following further purification, the dendrimers were characterized. Based on GPC and UV-Vis results, the following conjugates were formed: G5-Ac_{70}-FA_0, G5-Ac_{70}-$FA_{2.7}$, G5-Ac_{70}-$FA_{4.7}$, and G5-Ac_{70}-$FA_{7.2}$. Note that the remaining amines present on the dendrimers were not acetylated as they are required for the attachment to the AFM tip.

For the purpose of this text, all discussion relating to a single G5-Ac_{70}-FA_n will be referred to by its bulk description. For example, a G5-Ac_{70}-FA_n taken from a solution labeled 'G5-Ac_{70}-$FA_{2.7}$' will be denoted as a 'G5-Ac_{70}-$FA_{2.7}$,' regardless of how many FAs that *particular* G5-Ac_{70}-FA_n may have conjugated to its surface.

Preparation of Biacore Substrates:

Folate binding protein (FBP) substrates were prepared in the same manner as those used in SPR binding studies.[27] Substrates were prepared using a BIAcore X (Pharmacia Biosensor AB, Uppsala, Sweden). FBP extracted from bovine milk was immobilized on the sensor chip surface of a carboxylated dextran-coated gold film (CM 5 sensor chip) by amine coupling as described elsewhere.[8, 21, 28, 32] Briefly, 70 μL of a mixed solution of NHS/ECD (1:1, v/v) was first injected into the BIAcore to activate the

carboxylated dextran, followed by injection of 70 μL of 2.5 mg/mL FBP dissolved in 100 mM potassium phosphate buffer, pH 5.0, supplemented with 4 mM mercaptoethanol and 10% (v/v) glycerol. 1 M ethanolamine in water, pH 8.5 was then injected to deactivate residual NHS-esters on the sensor chip. The immobilization process was performed at a flow rate of 10 μL/min, resulting in the binding of ~6 ng/mm2 (~ 5,900 RU) of FBP per channel.

Preparation of AFM Tips for Forcepulling:

Prior to tip modification, silicon nitride (Si_3N_3) tips (Veeco Probes) were placed in a piranha solution (sulfuric acid/H2O2, 7:3) for 20 minutes. The tips were rinsed 3 times with Millipore water and then 3 times with 200-proof ethanol (EtOH), dried using a nitrogen stream and then placed in a 110°C oven for 10 minutes to remove any remaining water. The tips were then silanized by suspending them in a nitrogen-purged glass vial for 1 hour containing a 1:15 (low density G5-Ac_{70}-FA_n coverage) or 1:5 (high density G5-Ac_{70}-FA_n coverage) ratio of aminopropyltriethoxylsilane (APTES) to methyltriethoxysilane (MTES) dissolved in chloroform. The silanized tips were subsequently placed in a 110°C oven for 10 minutes. Expected surface coverage based on respective vapor pressures (APTES (0.02 hPa @20˚C) and MTES (14.66 hPa @20˚C)) is 1:100 APTES:MTES for "low density coverage" and 1:20 APTES:MTES for "high density coverage" Tips were then pegylated by placing tips in a 10 mg/mL solution of SMB-PEG-SMB in chloroform (Nektar) for two minutes and then rinsed 3 times with fresh chloroform and steam dried with nitrogen. G5-Ac_{70}-FA_n were attached by covering tips in a solution containing equal volumes of 1 mg/mL G5-Ac_{70}-FA_n and phosphate buffer (pH 8, no salts). Tips were left undisturbed for 30 minutes and

subsequently washed 3 times in phosphate buffer (pH 7, no salts). Modified tips were utilized the same day they were prepared and kept in a nitrogen box when not in use. Based on tip dimensions and APTES:MTES surface coverage, ~2 G5-Ac_{70}-FA_n (low density coverage) or ~6 G5-Ac_{70}-FA_n (high density coverage) were expected to be in contact with the FBP substrate during measurements.

Measurements.

Using an atomic force microscope (AFM), tips modified with solutions of one of the four targeted platforms (G5-Ac_{70}-FA_n, where n = 0, 2.7, 4.7 or 7.2) were brought into contact with a FBP substrate and then retracted **(Figure 2.4)**. This process was recorded (**Figure 2.5**) and the force required to rupture the specific FA-FBP bonds were extracted as described below. Note that forces obtained are *relative* and not absolute.[33] Dislocation forces, which are currently thought to represent the partial unbinding of G5-Ac_{70}-FA_n from the FBP substrate, were also extracted from those force-distance curves exhibiting the characteristic PEG-stretch. Experiments were completed using an Asylum MFP-3D. At low density coverage, ~2000 force-distance curves (up down motions) were obtained for G5-Ac_{70}-FA_0, G5-Ac_{70}-$FA_{2.7}$, G5-Ac_{70}-$FA_{4.7}$ and G5-Ac_{70}-$FA_{7.2}$. At high density coverage, ~1000 force-distance curve were obtained for G5-Ac_{70}-$FA_{2.7}$, G5-Ac_{70}-$FA_{4.7}$ and G5-Ac_{70}-$FA_{7.2.}$ The position of the tip in relation to the FBP substrate was changed 10 times, or after every 200 force-distance curves. The distance retracted from the surface was 300-500 nm. The rate used for these measurements was 1 Hz.

Blocking experiments using free FA were completed to show that the rupture forces measured were due to FA-FBP binding, and not simply due to non-specific interactions. Blocking experiments were conducted by first incubating the FBP substrate

with 10 u*M* free FA for 40 minutes before obtaining ~2000 force vs. distance curves using a tip modified with G5-Ac_{70}-$FA_{7.2.}$ This experiment was completed using the exact same tip used for G5-Ac_{70}-$FA_{7.2}$ under low density coverage conditions. Sensitivity and spring constants were calculated for each modified tip. All measurements were completed in phosphate buffered solution (pH 7) using the Asylum fluid cell.

Extracting rupture forces from force-distance curves. The modified AFM tips approached the FBP substrate (**Figure 2.5-a, red**) and finally contacted the surface. The tip was then retracted (**Figure 2.5-a, blue**). Non-specific interactions between the G5-Ac_{70}-FA_n were first broken **(a)**, leaving the specific G5-Ac_{70}-FA_n–bound FA-FBP interactions. As the tip was pulled further from the surface, the PEG polymer linking to the G5-Ac_{70}-FA_n stretched resulting in the characteristic PEG-stretch **(b-c)** until finally the G5-Ac_{70}-FA_n–bound FA and FBP interactions were broken **(c-d)**. The force required to break the specific G5-Ac_{70}-FA_n – FBP interactions was extracted from the force-distance curves by determining the difference in force-magnitude between **(c)** and **(d)**. The entire force distributions for G5-Ac_{70}-FA_n are displayed in **Figure 2.6** (low density G5-Ac_{70}-FA_n coverage) and **Figure 2.7** (high density G5-Ac_{70}-FA_n coverage)**.** The force distribution for G5-Ac_{70}-$FA_{7.2}$ following blocking conditions is displayed in **Figure 2.8.**

Extracting dislocations from force-distance curves. Dislocation forces were extracted from those rupture force curves which exhibited both (1) a characteristic PEG stretch and (2) dislocation in the rupture portion of the force-distance curve. Dislocation forces were obtained by determining the difference in force-magnitude between **(c)** and **(d)**, and **(e)** and **(f)** for force distance curves similar to **Figure 2.5-b.** These are thought to correspond to the partial and complete unbinding, respectively, of the G5-Ac_{70}-FA_n

from the FBP substrate. Dislocations are displayed in **Figure 2.9** (low density G5-Ac_{70}-FA_n coverage) and **Figure 2.10** (high density G5-Ac_{70}-FA_n coverage).

2.3. RESULTS

I. Results for low-density G5-Ac_{70}-FA_n coverage

Rupture forces measured for G5-Ac_{70}-FA_0, G5-Ac_{70}-$FA_{2.7}$, G5-Ac_{70}-$FA_{4.7}$, and G5-Ac_{70}-$FA_{7.2}$. A total of 2000 curves were obtained for a tip modified with each dendrimer sample. The first force event, **Figure 2.5a,** region a-b, was present for 70% of the curves whereas the remaining 30% smoothly retracted with a discernable force interaction. The second force event, region b-c-d, was present for 14 (G5-Ac_{70}-FA_0), 598 (G5-Ac_{70}-$FA_{2.7}$), 440 (G5-Ac_{70}-$FA_{4.7}$), and 596 (G5-Ac_{70}-$FA_{7.2}$) of the curves measured. Histograms of the measured rupture forces for region b-c-d are displayed in **Figure 2.6**. The maximum number of counted events occur at 0.68 (G5-Ac_{70}-FA_0), 0.08 (G5-Ac_{70}-$FA_{2.7}$), 0.22 (G5-Ac_{70}-$FA_{4.7}$) and 0.21 nN (G5-Ac_{70}-$FA_{7.2}$). Mean measured rupture forces are 0.66 (G5-Ac_{70}-FA_0), 0.14 nN (G5-Ac_{70}-$FA_{2.7}$), 0.24 (G5-Ac_{70}-$FA_{4.7}$) and 0.23 nN (G5-Ac_{70}-$FA_{7.2}$). Median measured rupture forces are 0.67 (G5-Ac_{70}-FA_0), 0.08 nN (G5-Ac_{70}-$FA_{2.7}$), 0.26 (G5-Ac_{70}-$FA_{4.7}$) and 0.23 nN (G5-Ac_{70}-$FA_{7.2}$). The values provided in this paragraph are derived from *all* measured interactions presented in **Figure 2.6**.

Rupture forces measured following incubation of FBP-substrate with free FA. The incubation of 10μ*M* free FA with the FBP substrate prior to performing force measurements using a G5-Ac_{70}-$FA_{7.2}$ tip resulted in 163 force events (b-d-c) from 2000 measured curves **(Figure 2.8).** This is a 56% reduction in counted force events as

compared to the measurement performed with no free folic acid present for the 0-08 nN region and a 63% reduction for the 0-0.4 nN region. For the 0-0.8 nN region, the average measured rupture force in the presence of 10μ*M* free FA was 0.35 nN while the median rupture force was 0.31 nN for rupture forces. For the 0-0.4 nN region, the average measured rupture force in the presence of 10μ*M* free FA was 0.26 nN while the median rupture force was 0.26 nN.

Dislocations present in some force-distance curves. Dislocations (*see* **Figure 2.5b**) were found in 0 (G5-Ac_{70}-FA_0), 3 (G5-Ac_{70}-$FA_{2.7}$), 24 (G5-Ac_{70}-$FA_{4.7}$) and 83 (G5-Ac_{70}-$FA_{7.2}$) of the 2000 force curves taken for each G5-Ac_{70}-FA_n. The mean dislocation rupture force was 0.26 nN (G5-Ac_{70}-$FA_{2.7}$), 0.10 nN (G5-Ac_{70}-$FA_{4.7}$), and 0.14 nN (G5-Ac_{70}-$FA_{7.2}$). The median dislocation rupture force was 0.26 nN (G5-Ac_{70}-$FA_{2.7}$), 0.08 nN (G5-Ac_{70}-$FA_{4.7}$), and 0.13 nN (G5-Ac_{70}-$FA_{7.2}$). The distribution of low density coverage dislocations is displayed in **Figure 2.9**.

II. Results for high-density G5-Ac_{70}-FA_n coverage

Rupture forces measured for G5-Ac_{70}-$FA_{2.7}$, G5-Ac_{70}-$FA_{4.7}$, and G5-Ac_{70}-$FA_{7.2}$. A total of 1000 curves were obtained for a tip modified with each dendrimer sample. The b-c-d- region of **Figure 2.5a** was present for 221 (G5-Ac_{70}-$FA_{2.7}$), 258 (G5-Ac_{70}-$FA_{4.7}$), and 233 (G5-Ac_{70}-$FA_{7.2}$) of the curves measured. The maximum number of counted events occur at 0.16 (G5-Ac_{70}-$FA_{2.7}$), 0.14 (G5-Ac_{70}-$FA_{4.7}$) and 0.18 (G5-Ac_{70}-$FA_{7.2}$). Mean measured rupture forces are 0.36 (G5-Ac_{70}-$FA_{2.7}$), 0.30 (G5-Ac_{70}-$FA_{4.7}$) and 0.36 nN (G5-Ac_{70}-$FA_{7.2}$). Median measured rupture forces are 0.29 (G5-Ac_{70}-$FA_{2.7}$),

0.24 (G5-Ac_{70}-$FA_{4.7}$) and 0.30 nN (G5-Ac_{70}-$FA_{7.2}$). The distribution of rupture forces at high density coverage is displayed in **Figure 2.7**.

Number of PEG stretches force-distance curves at high density G5-Ac_{70}-FA_n coverage. The number of PEG stretches found within the 1000 force curves taken for G5-Ac_{70}-$FA_{2.7}$ was: **0**(778), **1**(87), **2**(67), **3**(38), **4**(13), **5**(14), **6**(1), **7**(2) and **8**(0). The number of PEG stretches found within the 1000 force curves taken for G5-Ac_{70}-$FA_{4.7}$ was: **0**(741), **1**(127), **2**(78), **3**(37), **4**(9), **5**(5), **6**(0), **7**(2) and **8**(1). The number of PEG stretches found within the 1000 force curves taken for G5-Ac_{70}-$FA_{7.2}$ was: **0**(768), **1**(154), **2**(54), **3**(30), **4**(17), **5**(9), **6**(6), **7**(1) and **8**(1). Representative force distance curves obtained at high and low density G5-Ac_{70}-FA_n coverage is presented in **Figure 2.11.** Note the presence of multiple PEG stretches in the high density coverage example

Dislocations present in some force-distance curves at high density G5-Ac_{70}-FA_n coverage. Dislocations **(***see* **Figure 2.5b)** were found in 53 (G5-Ac_{70}-$FA_{2.7}$), 60 (G5-Ac_{70}-$FA_{4.7}$) and 102 (G5-Ac_{70}-$FA_{7.2}$) of the 1000 force curves taken for each G5-Ac_{70}-FA_n. The mean dislocation rupture force was 0.35 nN (G5-Ac_{70}-$FA_{2.7}$), 0.22 nN (G5-Ac_{70}-$FA_{4.7}$), and 0.29 nN (G5-Ac_{70}-$FA_{7.2}$). The median dislocation rupture force was 0.28 nN (G5-Ac_{70}-$FA_{2.7}$), 0.18 nN (G5-Ac_{70}-$FA_{4.7}$), and 0.24 nN (G5-Ac_{70}-$FA_{7.2}$). Dislocation distribution obtained at high density G5-Ac_{70}-FA_n coverage are displayed in Figure **2.10.**

2.4. DISCUSSION

Summary of measured rupture forces after removing events not related to folic acid/FBP binding from low density G5-Ac_{70}-FA_n coverage. The raw data

summary provided above include some events that we believe are not related to FA/FBP binding. The rupture force histogram (**Figure 2.6**) includes 14 b-c-d events for the dendrimer containing no FA (G5-Ac_{70}-FA_0). These 14 events are localized in the 0.40 to 0.80 nN force range which does not overlap with the major portion of any of the three histograms ascribed to FA/FBP binding for the other samples. Furthermore, examination of the inhibition data (**Figure 2.8**) shows that forces measured in the 0.40 – 0.80 nN range are not reduced in count frequency by the presence of free FA. The fact that these forces are present for conjugates containing no FA, and that they are not inhibited by the presence of free FA, indicates that these are not FA/FBP related events. Therefore, the measured rupture forces are summarized below with the data in the 0.40-0.80 nN range excluded from the noted means and medians. The mean rupture forces for G5-Ac_{70}-$FA_{2.7}$, G5-Ac_{70}-$FA_{4.7,}$ G5-Ac_{70}-$FA_{7.2}$, and G5-Ac_{70}-$FA_{7.2}$ are 0.12, 0.22, 0.21 nN respectively. The median rupture forces for G5-Ac_{70}-$FA_{2.7}$, G5-Ac_{70}-$FA_{4.7}$, G5-Ac_{70}-$FA_{7.2}$, and G5-Ac_{70}-$FA_{7.}$ are 0.10, 0.21, 0.21 nN respectively. Excluding the events in the 0.40 to 0.80 nN range does not change the force at which the maximum number of events is counted for any of these samples. Additionally, the median and average rupture force for G5-Ac_{70}-$FA_{7.2}$ under blocking conditions excluding the events in the 0.4 nN to 0.80 nN range is 0.26 nN. The distribution of rupture forces obtained between 0-0.4 nN is displayed in **Figure 2.12**

Distribution of FAs on the surface of the G5-Ac_{70}-FA_n makes assignment of rupture forces very difficult. A criticism of this work is that we have only used a single G5-Ac_{70}-FA_n per experiment to determine the binding of a nanodevice with *n* FAs. This is problematic in that the actual number of FAs on a single G5-Ac_{70}-FA_n used for the

force experiment can differ significantly from the average, *n*. **Figure 2.13** shows the expected distribution of FAs on the G5 scaffold within a solution of G5-Ac_{70}-FA_n. This analysis was based on the random addition of FA to the surface of the G5 dendrimer with 110 available conjugation points until an average of *n* folic acids per conjugate was obtained. This resulted in a Poisson distribution. Note that there is a significant overlap in the expected distributions for the three G5-Ac_{70}-FA_n conjugates making the likelihood of having the stated number of FAs *n* present on each of the conjugates much lower than desired. For example, the likelihood of obtaining a G5-Ac_{70}-FA_3, G5-Ac_{70}-FA_5 *and* G5-Ac_{70}-FA_7 is less than 1 percent **(**(G5-Ac_{70}-FA_3 (23%), G5-Ac_{70}-FA_5 (19%) G5-Ac_{70}-FA_7 (17%)**).** Recall that for the purpose of this text, all discussion relating to a single G5-Ac_{70}-FA_n will be referred to by its bulk description. For example, a G5-Ac_{70}-FA_n taken from a solution labeled 'G5-Ac_{70}-$FA_{2.7}$' will be denoted as a 'G5-Ac_{70}-$FA_{2.7}$,' regardless of how many FAs that *particular* G5-Ac_{70}-FA_n may have conjugated to its surface.

Comparison of the low density G5-Ac_{70}-FA_n coverage rupture forces to previously performed SPR studies. Despite not knowing the exact number of FAs present on the each of the G5-Ac_{70}-FA_ns used for the studies, the trend seen in the low density G5-Ac_{70}-FA_n coverage data is remarkably consistent with trend seen in the SPR as well as FACs studies. These SPR studies showed that the change in K_D per FA greatly decreased after more than 5 FAs were added per G5-Ac_{70}-FA_n. The correlation between the bulk measurements (SPR and FACS) to the single molecule measurements presented here is interesting although not altogether understood. Two hypotheses have been put forward to explain the near-saturation of the K_D and rupture force at ~5 FAs: (1) the G5-Ac_{70}-FA_n can only reach ~5 FBPs and (2) the binding is sterically limited by the

flexibility of dendrimer platform itself **(Figure 2.14).** The first hypothesis was discussed in detail within the paper.[27] The second, however, was not explicitly discussed but is in some ways correlated to the first in that the sterics are related to our choice of a G5 PAMAM dendrimer as the scaffold. Once some number of FAs bind to the FBP substrate, the remaining FAs are severely hampered in their ability to bind to the FBP substrate. Due to steric constraints, a saturation in binding is obtained, regardless of how many FAs are present on the G5-Ac_{70}-FA_n. One could imagine increasing the size of the scaffold (i.e., generation of the dendrimer) to increase the effective reach of the targeted platform. This could prove helpful in cases in which targeted receptors are not closely situated near each other on the cell membrane surface. The caveat to this is that larger dendrimer generations lose their flexibility because the density of end groups on the outer shell of the dendrimer necessarily increases with increasing generation. Therefore, one must be cognizant of the inherent size-flexibility tradeoff when altering the nature of the dendrimer scaffold.

At high G5-Ac_{70}-FA_n coverage, measurements yield very similar rupture force distributions for G5-Ac_{70}-$FA_{2.7}$, G5-Ac_{70}-$FA_{4.7}$, and G5-Ac_{70}-$FA_{7.2}$. In examining forces obtained at high G5-Ac_{70}-FA_n coverage, we see that over half the force curves exhibit multiple PEG stretches, indicating multiple G5-Ac_{70}-FA_n binding events per pull. Interestingly, the measured rupture forces for G5-Ac_{70}-$FA_{2.7}$, G5-Ac_{70}-$FA_{4.7}$, and G5-Ac_{70}-$FA_{7.2}$ largely overlap, suggesting that an equal number of FAs per G5-Ac_{70}-FA_n bind to the FBP surface per pull. In other words, at this density coverage, increasing the number of FAs per G5 does not increase the average measured rupture force per single G5-Ac_{70}-FA_n.

We have developed an incomplete hypothesis based on steric hindrance describing the difference in G5-Ac_{70}-FA_n-FBP interaction low and high density coverage. At high density coverage, the G5-Ac_{70}-FA_n may be unable to bind optimally to the substrate surface. This argument is based on the phenomena of prozone in which very high concentrations of antibody or antigen significantly inhibit immunological reactions.[34] The result is that the binding that does occur is weaker than one would expect had the G5-Ac_{70}-FA_n been more isolated from other G5-Ac_{70}-FA_n as they would at low density coverage. Still unresolved, however, is the discrepancy in the magnitude of the measured rupture forces obtained for the low and high density coverage G5-Ac_{70}-FA_n data. If the above analysis is correct, one would expect the measured rupture forces obtained at high density coverage to be lower in magnitude than those measured at the low density coverage. However, this is not the case. As noted in the results section, the average rupture force for the low density coverage data is significantly lower than that of the high density coverage data.

Although the low and high density coverage were obtained on the same instrument, the measurements for these two sets of data were taken months apart. It should be noted that the high density G5-Ac_{70}-FA_n coverage data was obtained first and although we have no obvious reason to question the validity of this data, more familiarity with the technique during the acquisition of the low density G5-Ac_{70}-FA_n coverage data makes me as the experimentalist more trusting of this data. In summary, no self-consistent explanation for the low and high density data is apparent at this juncture.

Implications of the distribution forces seen under blocking conditions versus non-blocking conditions. The FBP substrate was incubated with free FA such that free

FA would block or reduce binding of the G5-Ac_{70}-$FA_{7.2}$ when it was brought into contact with the FBP substrate. Although there was a decrease in frequency of binding, it is interesting to note that the average rupture force under blocking conditions is actually higher than under non-blocking conditions. A hypothesis that has been put forth to explain this phenomena is that the lower rupture forces represent the binding of "few" FAs whereas the higher rupture forces represent the binding of "more" folic acids. Under blocking conditions, the G5-Ac_{70}-$FA_{7.2}$ in question must compete with the free FA in order to bind to the receptor surface. If "few" FAs per G5-Ac_{70}-$FA_{7.2}$ are optimally aligned with the receptor surface, one may bind but the free FA may then compete the G5-Ac_{70}-$FA_{7.2}$ off the FBP substrate during the 1 sec time scale of the pull. However, if "more" G5-Ac_{70}-$FA_{7.2}$-bound FAs are aligned optimally and therefore bind to the receptor surface, these FAs would be less likely to be out competed by the free FA in solution **(Figure 2.15).**

These experiments must be repeated using more tips per G5-Ac_{70}-FA_n in order to obtain reliable data. These experiments must be repeated in order to be sure that the distribution of forces obtained are representative of the G5-Ac_{70}-FA_n noted. Having only performed these studies using a single tip for each experimental condition, it does not appear possible to discuss the assignment of the forces in relation to the number of FAs present on the targeted nanodevice. One would need to adequately sample each solution of G5-Ac_{70}-FA_n to determine which rupture forces measured are, for example, associated with a true G5-Ac_{70}-FA_3 and which are associated with a G5-Ac_{70}-FA_1, G5-Ac_{70}-FA_2, G5-Ac_{70}-FA_3, etc, all of which would be present in the G5-Ac_{70}-FA_3 solution. Requiring a Poisson distribution of FAs per G5-Ac_{70}-FA_n, we would need to perform

these studies on 11, 19 and 27 G5-Ac_{70}-FA_ns per solution of G5-Ac_{70}-FA_3, G5-Ac_{70}-FA_5 and G5-Ac_{70}-$FA_{7,}$ respectively to be 95% confident the average number of FAs on those particular G5-Ac_{70}-FA_ns had an average of $n \pm 1$ FAs.

Dynamic force microscopy would allow us to obtain absolute forces and evaluate aid us in our evaluation of the binding configurations of the G5-Ac_{70}-FA_n. Looking at the force distribution obtained under low density conditions for the G5-Ac_{70}-$FA_{n,}$ we see two large distributions: one for G5-Ac_{70}-$FA_{2.7}$, and one for G5-Ac_{70}-$FA_{4.7}$ and G5-Ac_{70}-$FA_{7.2}$. One could imagine assigning the entire force distribution of the G5-Ac_{70}-$FA_{2.7}$ to the binding of 1 FA, 2 FAs, 3 FAs or a distribution of these three. One could do a similar assignment to the rupture forces of G5-Ac_{70}-$FA_{4.7}$ and G5-Ac_{70}-$FA_{7.2,}$ and potentially determine the probability of binding for some number of FAs as a function of the number of FAs present on the G5-Ac_{70}-FA_n. The studies presented here are performed at a single loading rate. Therefore the rupture forces obtained in these studies are proportionally but not absolutely correct. If one performed these same studies at a variety of loading rates for each conjugate, one could then plot the average rupture force (pN) vs. *ln*((loading rate)(pN/s)) and extrapolate out to a zero applied force to obtain the absolute force required to rupture the G5-Ac_{70}-FA and FBP bonds.[35-37] Ideally, one could also then obtain the force required to rupture a single FA-FBP bond either by synthesizing a G5-Ac_{70}-$FA_{1,}$ or using the focal point of a dendron as a FA-conjugation site thereby ensuring only a single FA is present. If both the dynamic force and the single-FA measurements were obtained, one could determine the distribution of binding configurations of a G5-Ac_{70}-FA_n to the FBP receptor surface.

2.5. CONCLUSIONS AND SUMMARY

We have shown that the rupture forces obtained from force pulling studies at low density coverage of G5-Ac_{70}-FA_n follow a similar trend to that seen in previously completed SPR and FACS studies. The rupture forces obtained for a G5-Ac_{70}-$FA_{7.2}$ at low density coverage under free FA blocking conditions have a higher average rupture force than under non-blocking conditions. At this time, it is not clear what the distributions of forces obtained from the high density coverage of G5-Ac_{70}-FA_n represent.

These studies must be repeated such that the distribution of G5-Ac_{70}-FA_n within a solution of G5-Ac_{70}-FA_n is adequately sampled. In addition, dynamic force microscopy should be performed to obtained absolute rupture forces for each sample. In doing this, one could potentially determine the distribution of binding configurations for each G5-Ac_{70}-FA_n.

2.6. FIGURES

Targeted Nanodevice	Dissociation Constant K_D (M)[a]	Fold Increase over Free FA[b]	Fold Increase over Free FA[c]
Free FA	$5 \pm 3 \times 10^{-6}$	—	—
G5-Ac-AF488-$FA_{2.6}$	$2 \pm 1 \times 10^{-9}$	2,500	1,000
G5-Ac-AF488-$FA_{4.7}$	$7 \pm 6 \times 10^{-11}$	71,400	15,200
G5-Ac-AF488-$FA_{7.2}$	$7 \pm 2 \times 10^{-11}$	71,400	9,900
G5-Ac-AF488-$FA_{11.5}$	$5 \pm 1 \times 10^{-11}$	100,000	8,700
G5-Ac-AF488-$FA_{13.7}$	$3 \pm 2 \times 10^{-11}$	166,700	12,200

[a] Obtained by averaging at least three different runs of SPR measurements. The values are averages ± standard deviations taken from different runs.
[b] Fold increase based on dendrimer concentrations. Also known as multivalency parameter β.
[c] Fold increase based on FA concentrations.

Figure 2.1. Dissociation constants (K_D) obtained using SPR for a series of G5-FA_n. This data was obtained by S. Hong.

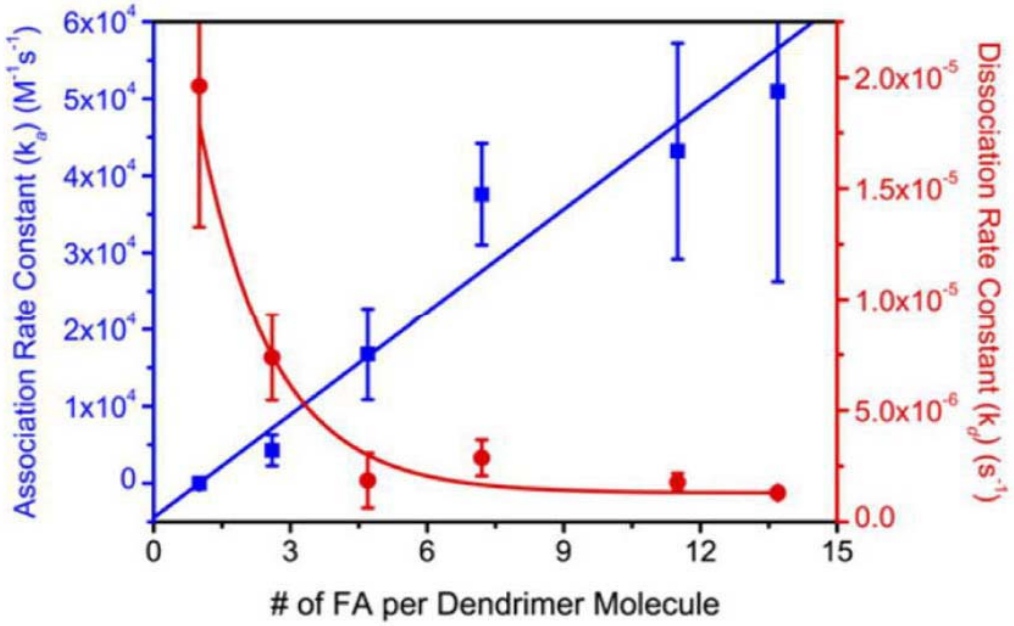

Figure 2.2. Graph showing a linear increase in k_a and exponential decrease in k_d with increasing number of FAs, *n*. This data was obtained by S. Hong and analyzed by P. Leroueil.

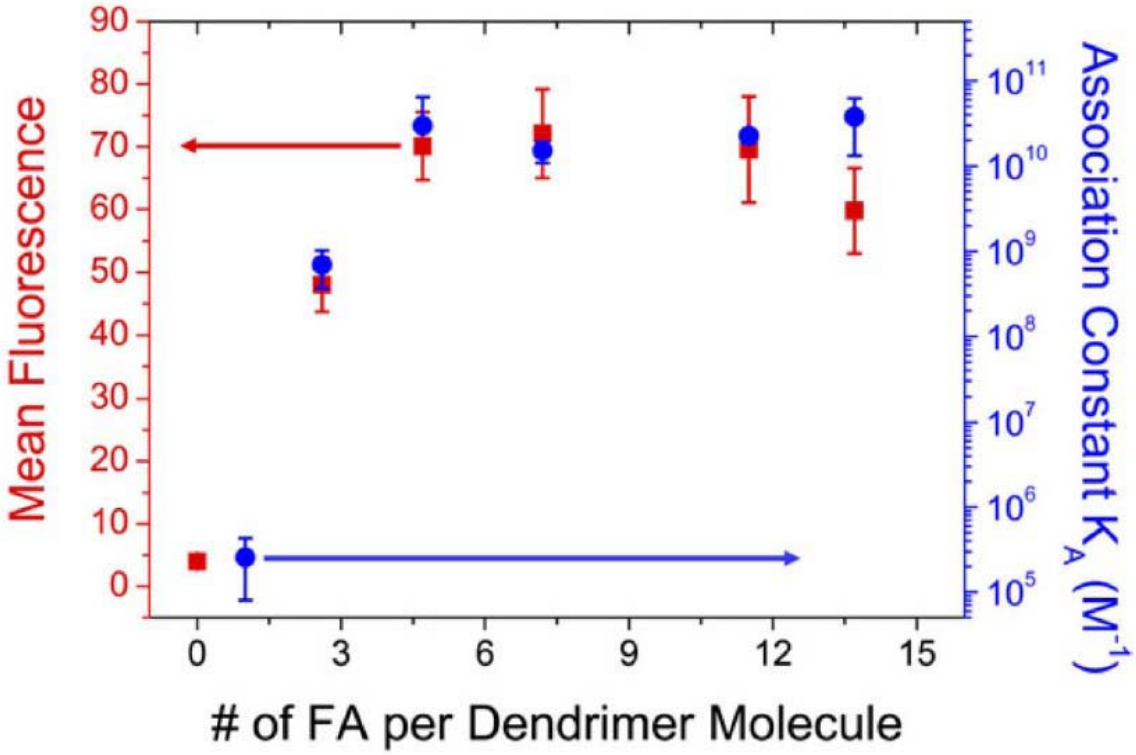

Figure 2.3. The effect of the number of FAs, *n,* on G5-FA_n binding as previously measured by surface plasmon resonance (SPR) and fluorescent activated cell sorting (FACS) (S. Hong). Note that blue circles and red squares represent SPR and FACS results, respectively. The error bars represent standard deviations. The nanodevice with 2.6 FA shows a lower degree of cellular binding and association constant K_A than the rest of the nanodevices. FACS data were obtained after incubation with dendritic nanodevices with FAR over-expressing KB cells at 37ºC and represent averaging from 12 different samples at each condition. Association constants were averaged values from at least three SPR measurements for each point. The association constant ($K_A = 1/K_D$) is plotted in this case as it provides the best visual comparison to the FACS data. [27] (S. Hong)

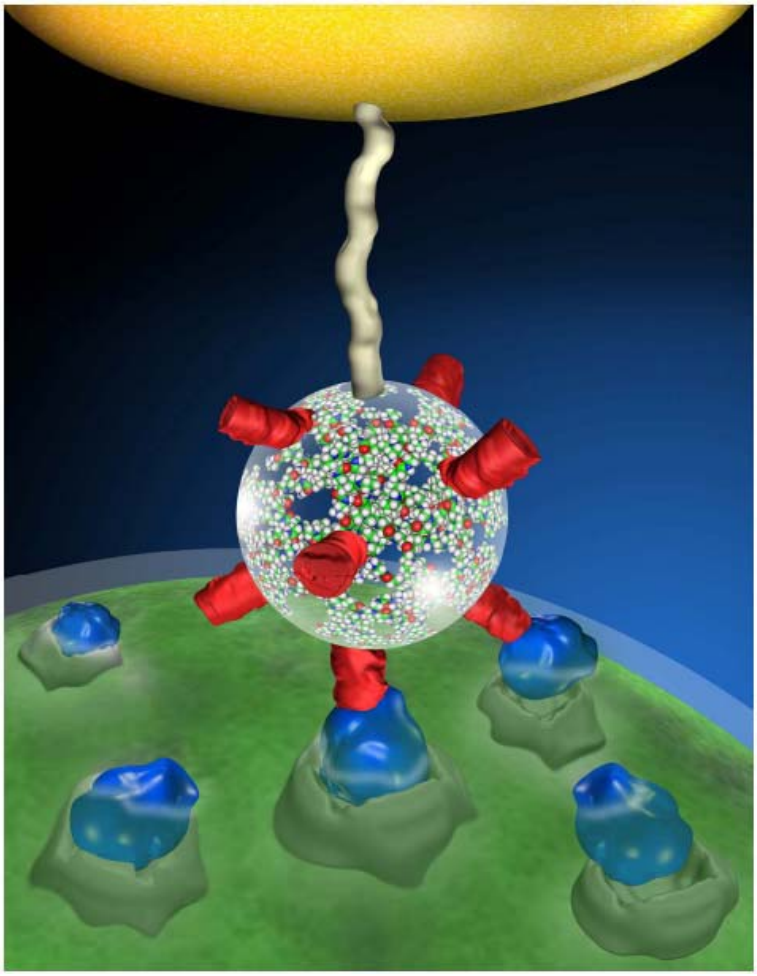

Figure 2.4. Depiction of experimental set-up. A G5-FAn dendrimer is attached to an AFM tip (gold) via a PEG linker (tan). Here, 7 FAs (red) are conjugated to the surface of the G5 dendrimer. During force-pulling measurements, the AFM tip is lowered, allowing the G5-FA_n to interact with the FBP substrate surface. The number of FAs per G5-FA_n that bind to the FBP substrate is dependent on *n*. As the AFM tip is retracted, the FA-FBP bonds are ruptured. This process is repeated until 2000 force-distance curves are obtained. (Art provided by Paul Trombley)

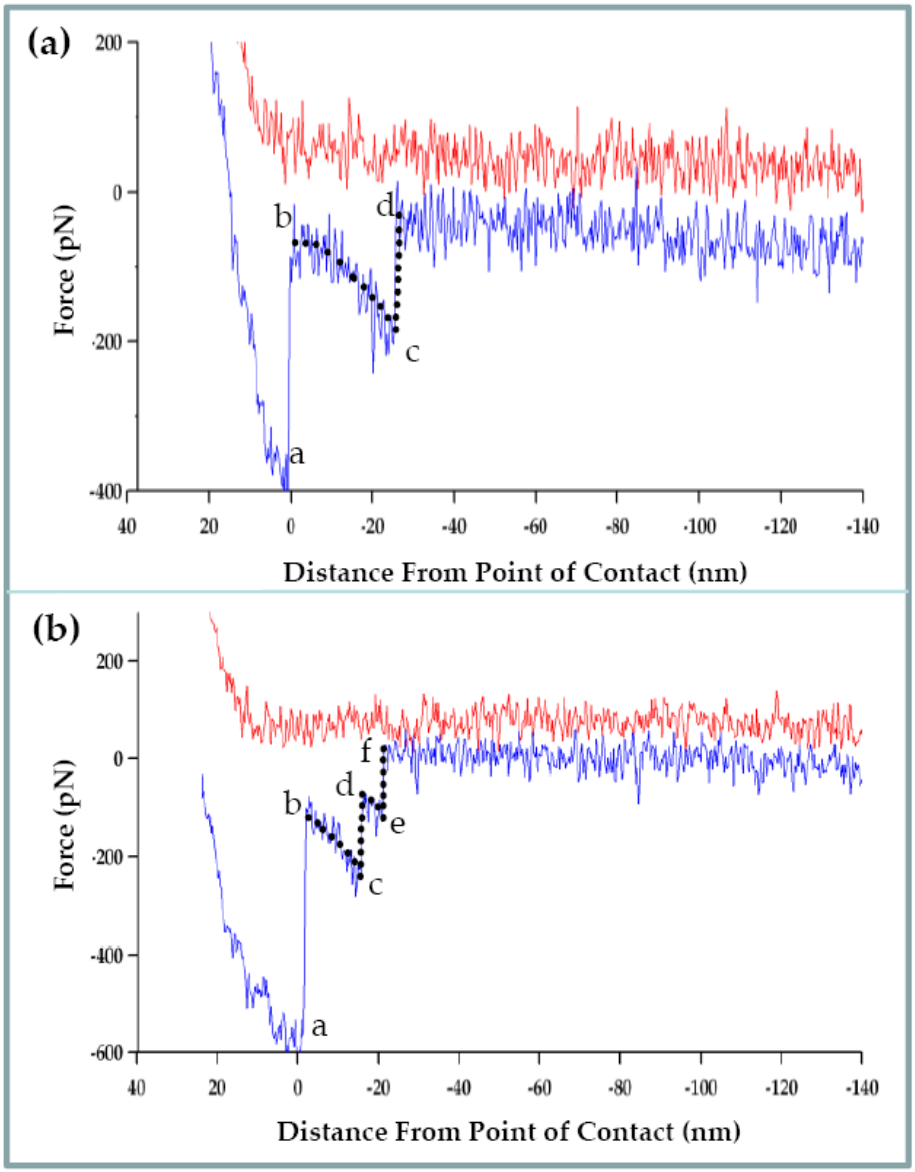

Figure 2.5. Force (pN) vs. distance (nm) curves showing **(a)** specific G5-FA_n binding to the FBP substrate and **(b)** specific G5-FA_n and partial unbinding in the form of a 'dislocation.' Rupture forces were extracted from force-distance curves by determining the magnitude of **(a)** (d-c) and **(b)** (*d-c)* and (*f-e).* Both **(a)** and **(b)** were taken from curves obtained from G5-FA_7 measurements.

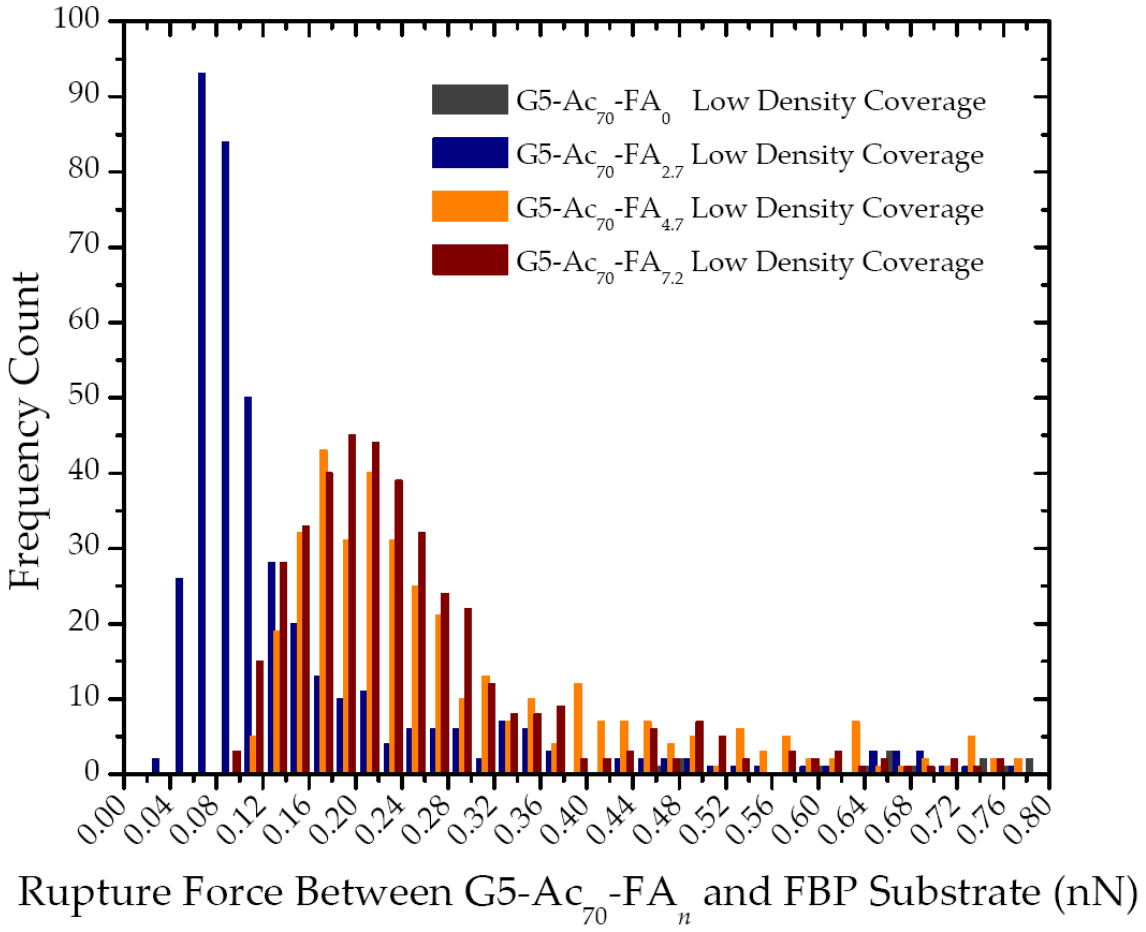

Figure 2.6. Histogram of rupture forces spanning 0-0.8 nN for G5-Ac_{70}-FA_n at low density G5-Ac_{70}-FA_n coverage. The maximum number of counted events occur at 0.68 (G5-Ac_{70}-FA_0), 0.08 (G5-Ac_{70}-$FA_{2.7}$), 0.22 (G5-Ac_{70}-$FA_{4.7}$) and 0.21 nN (G5-Ac_{70}-$FA_{7.2}$). Mean measured rupture forces are 0.66 (G5-Ac_{70}-FA_0), 0.14 nN (G5-Ac_{70}-$FA_{2.7}$), 0.24 (G5-Ac_{70}-$FA_{4.7}$) and 0.23 nN (G5-Ac_{70}-$FA_{7.2}$). Median measured rupture forces are 0.67 (G5-Ac_{70}-FA_0), 0.08 nN (G5-Ac_{70}-$FA_{2.7}$), 0.26 (G5-Ac_{70}-$FA_{4.7}$) and 0.23 nN (G5-Ac_{70}-$FA_{7.2}$). The median and means presented here are based on the 0-0.80 nN force region.

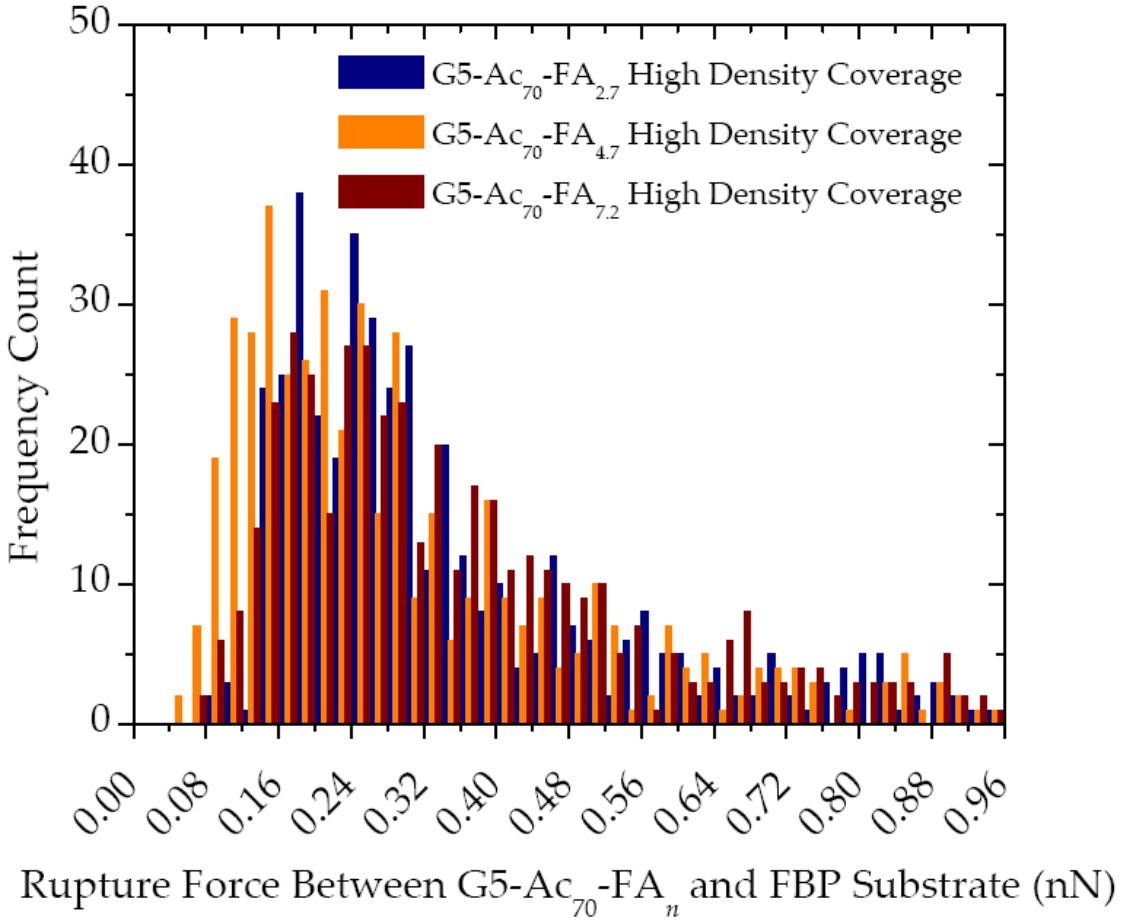

Figure 2.7. Histogram of rupture forces spanning 0-0.96 nN for G5-Ac_{70}-FA_n at high density G5-Ac_{70}-FA_n coverage. The maximum number of counted events occur at 0.16 (G5-Ac_{70}-$FA_{2.7}$), 0.14 (G5-Ac_{70}-$FA_{4.7}$) and 0.18 (G5-Ac_{70}-$FA_{7.2}$). Mean measured rupture forces are 0.36 (G5-Ac_{70}-$FA_{2.7}$), 0.30 (G5-Ac_{70}-$FA_{4.7}$) and 0.36 nN (G5-Ac_{70}-$FA_{7.2}$). Median measured rupture forces are 0.29 (G5-Ac_{70}-$FA_{2.7}$), 0.24 (G5-Ac_{70}-$FA_{4.7}$) and 0.30 nN (G5-Ac_{70}-$FA_{7.2}$).

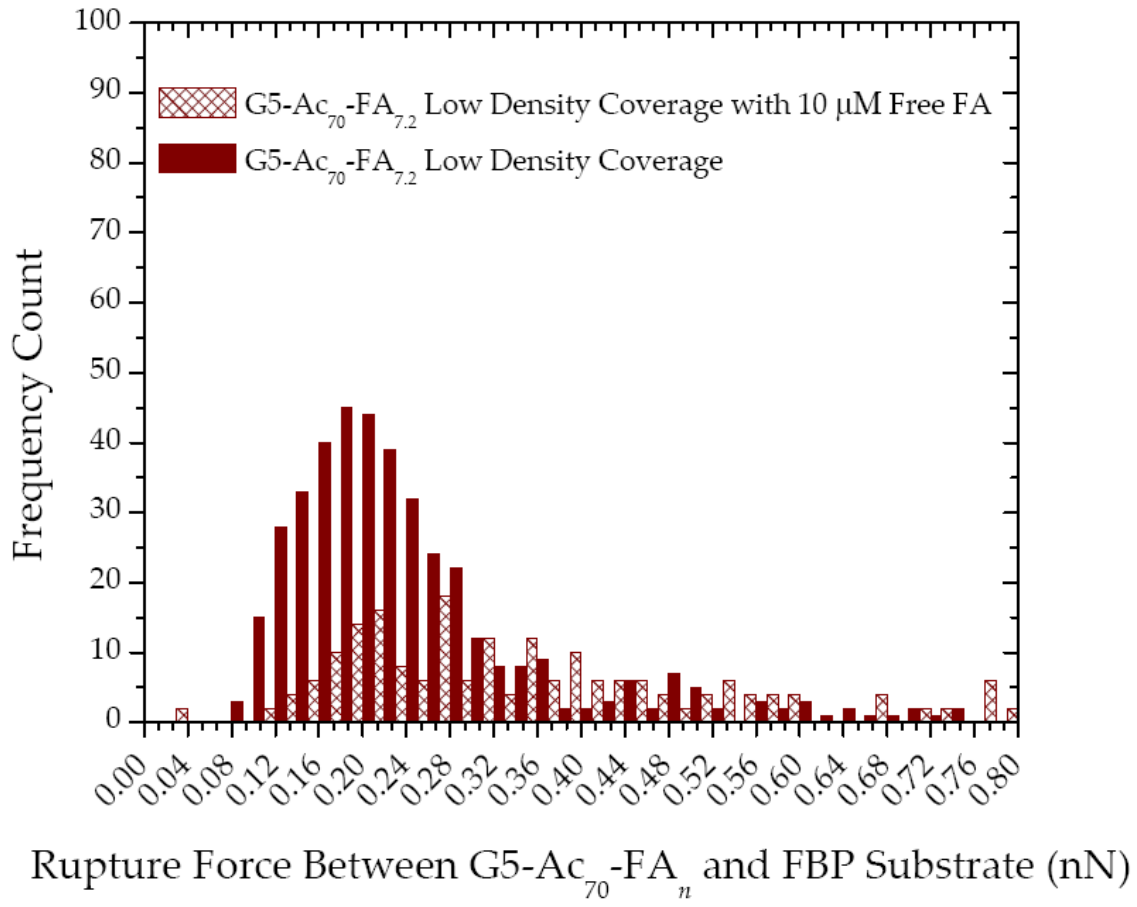

Figure 2.8. Histogram of rupture forces spanning 0-0.8 nN following incubation with free FA for G5-Ac_{70}-$FA_{7.2}$ at low density coverage. This is a 56% reduction in counted force events as compared to the measurement performed with no free folic acid present for the 0-08 nN region and a 63% reduction for the 0-0.4 nN region. For the 0-0.8 nN region, the average measured rupture force in the presence of 10μ*M* free FA was 0.35 nN while the median rupture force was 0.31 nN for rupture forces. For the 0-0.4 nN region, the average measured rupture force in the presence of 10μ*M* free FA was 0.26 nN while the median rupture force was 0.26 nN.

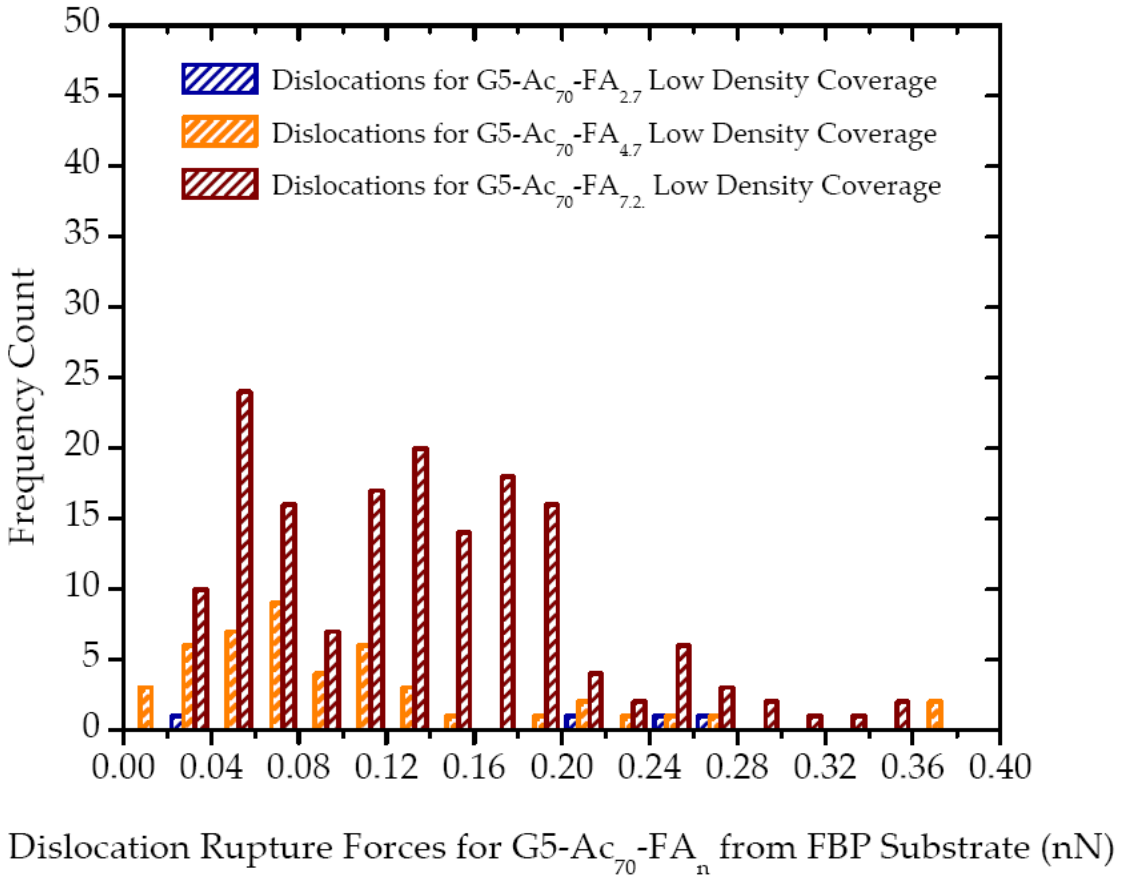

Figure 2.9. Histogram of dislocations obtained for G5-Ac_{70}-FA_n at low density G5-Ac_{70}-FA_n coverage. The mean dislocation rupture force was 0.26 nN (G5-Ac_{70}-$FA_{2.7}$), 0.10 nN (G5-Ac_{70}-$FA_{4.7}$), and 0.14 nN (G5-Ac_{70}-$FA_{7.2}$). The median dislocation rupture force was 0.26 nN (G5-Ac_{70}-$FA_{2.7}$), 0.08 nN (G5-Ac_{70}-$FA_{4.7}$), and 0.13 nN (G5-Ac_{70}-$FA_{7.2}$). The median and means presented here are based on the 0-0.40 nN force region.

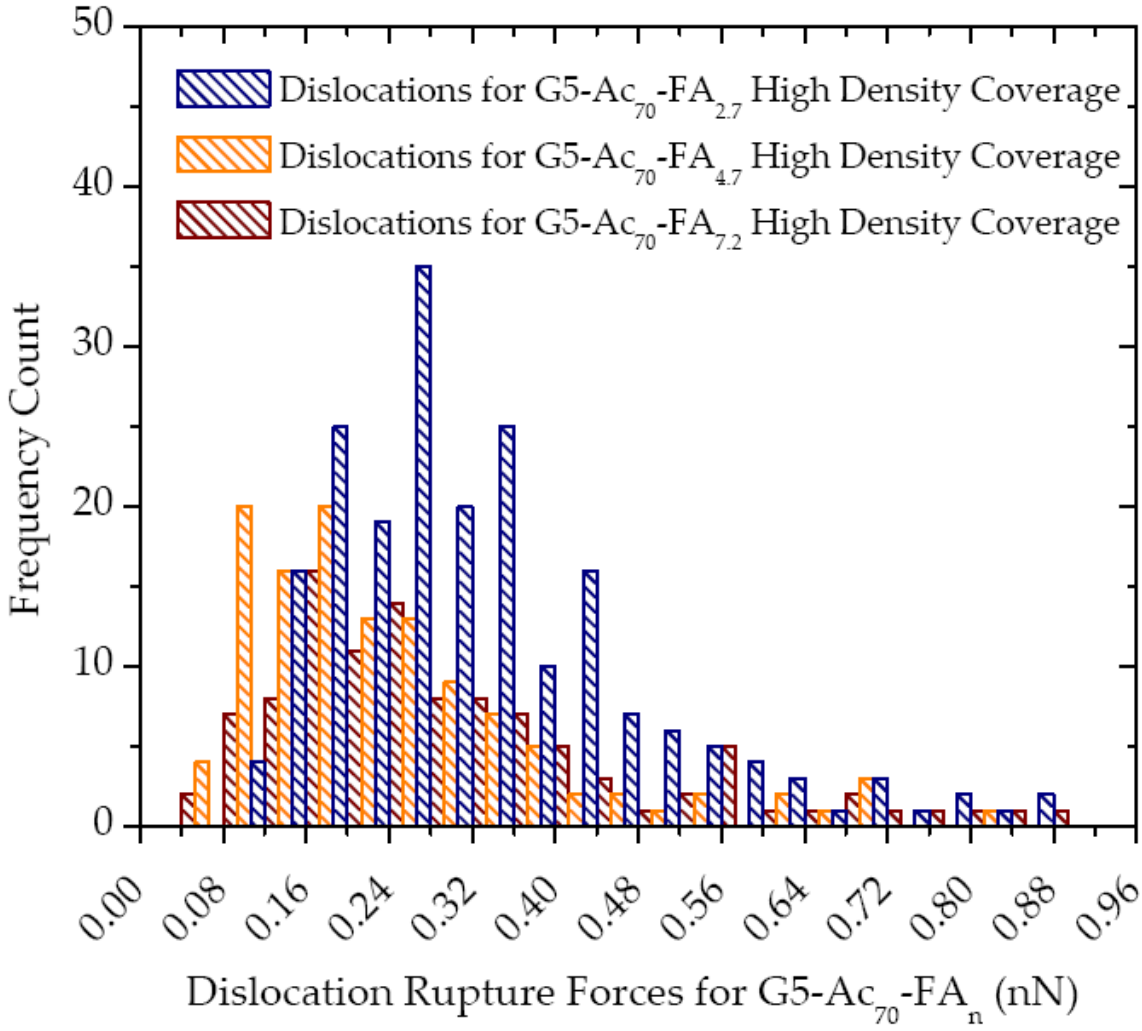

Figure 2.10. Histogram of dislocations obtained for G5-Ac_{70}-FA_n at high density G5-Ac_{70}-FA_n coverage. The mean dislocation rupture force was 0.35 nN (G5-Ac_{70}-$FA_{2.7}$), 0.22 nN (G5-Ac_{70}-$FA_{4.7}$), and 0.29 nN (G5-Ac_{70}-$FA_{7.2}$). The median dislocation rupture force was 0.28 nN (G5-Ac_{70}-$FA_{2.7}$), 0.18 nN (G5-Ac_{70}-$FA_{4.7}$), and 0.24 nN (G5-Ac_{70}-$FA_{7.2}$). The median and means presented here are based on the 0-0.96 nN force region.

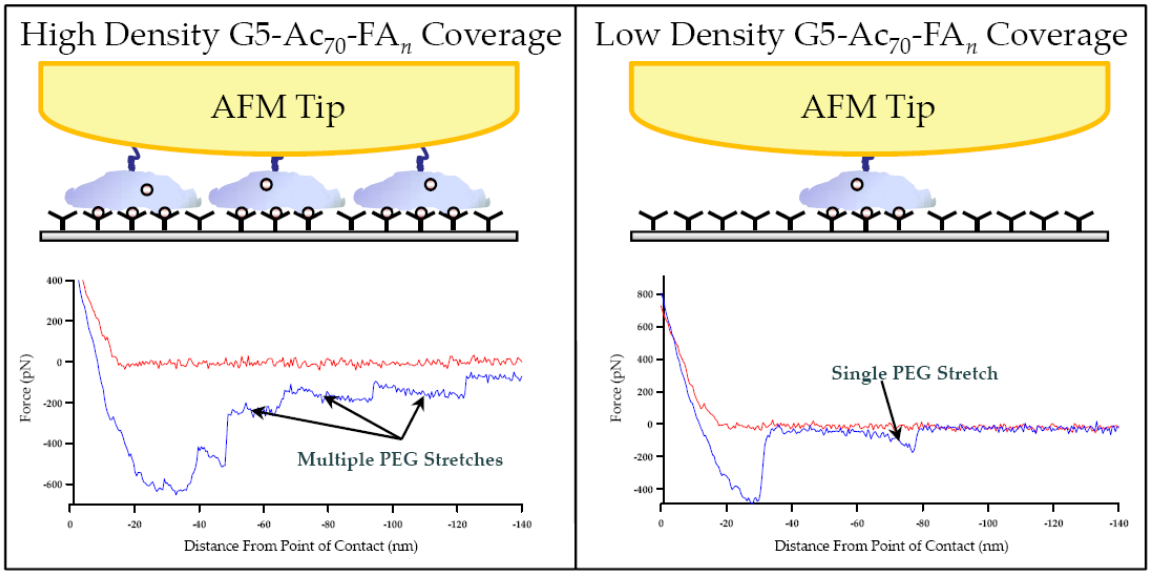

Figure 2.11. Schematic distinguishing between high density G5-Ac_{70}-FA_n coverage and low density G5-Ac_{70}-FA_n coverage. Force-distance curves below each schematic serve as an experimental distinction between the two degrees of coverage. Note that 'high density' coverage results in multiple PEG stretches whereas 'low density' coverage results in a single PEG stretch. The length of each PEG stretch is 20-30 nm which is consistent with what one would expect for a PEG (20 nm) + G5 PAMAM dendrimer (5-10 nm).

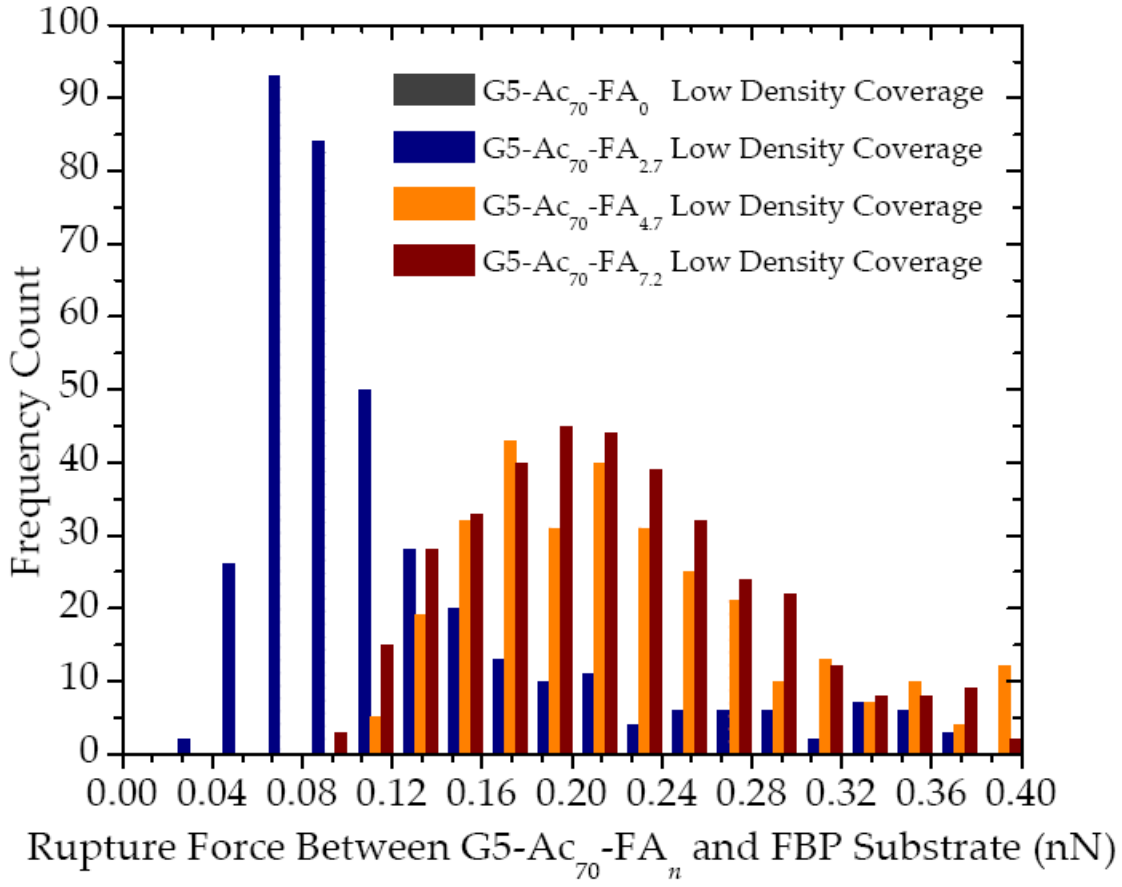

Figure 2.12. Histogram of rupture forces obtained for G5-Ac_{70}-FA_n at low density coverage spanning rupture forces from 0-0.40 nN. Ruptures above 0.40 nN are believed not to be FA-FBP specific. The mean rupture forces for G5-Ac_{70}-$FA_{2.7}$, G5-Ac_{70}-$FA_{4.7,}$ G5-Ac_{70}-$FA_{7.2}$, and G5-Ac_{70}-$FA_{7.2}$ are 0.12, 0.22, 0.21 nN respectively. The median rupture forces for G5-Ac_{70}-$FA_{2.7}$, G5-Ac_{70}-$FA_{4.7}$, G5-Ac_{70}-$FA_{7.2}$, and G5-Ac_{70}-$FA_{7.}$ are 0.10, 0.21, 0.21 nN respectively.

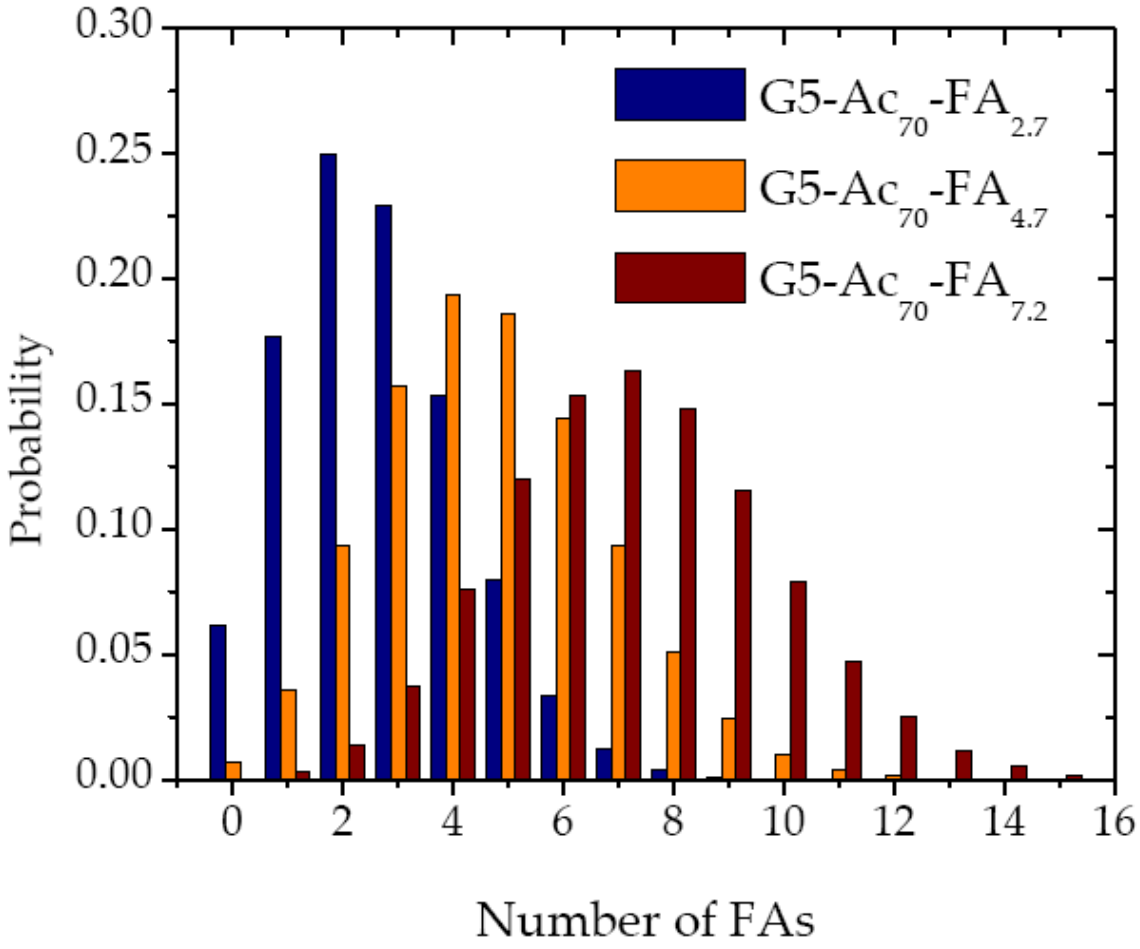

Figure 2.13. Expected Poisson distribution of FAs on a dendrimer within a solution of G5-Ac_{70}-FA_n. This analysis was based on the random addition of FA to the surface of the G5 dendrimer with 110 available conjugation points until there is an average of *n* FAs per G5-Ac_{70}-FA_n.

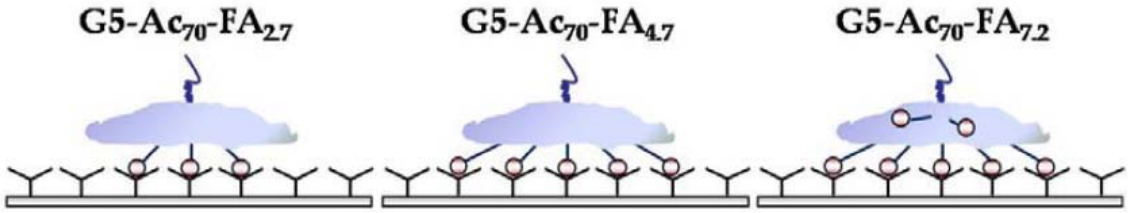

Figure 2.14 Schematic depicting the possibility that the saturation of binding seen in both the SPR and force pulling studies is due to steric inhibition of the entire G5-Ac_{70}-FA_n once some number of FAs has bound. Figure 2.14 shows that this inhibition occurs at 5 FA-FBP interactions but this number can be as low as 2 FA-FBP interactions. Our data does not answer the question of the maximum number of FAs that bind to the FBP substrate under these conditions.

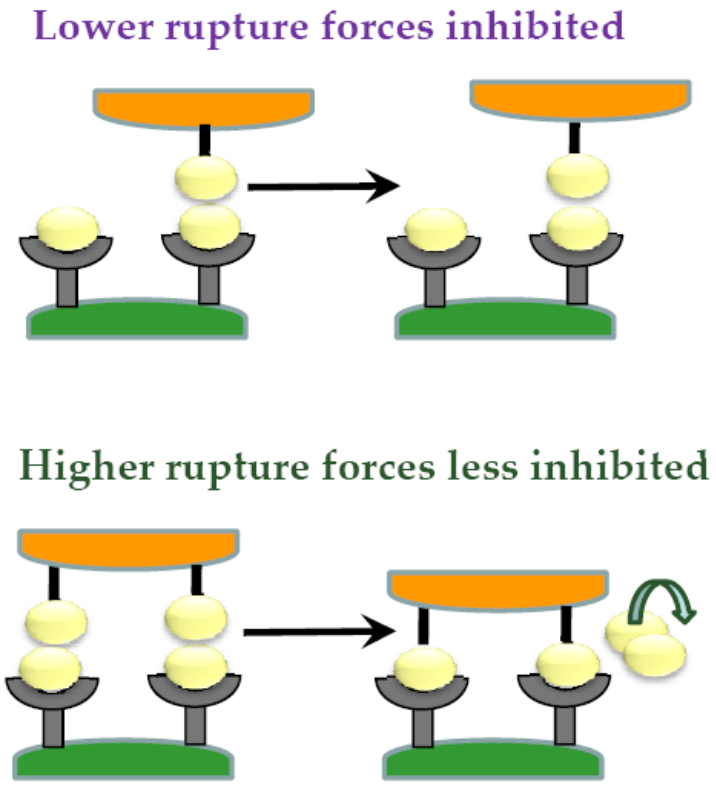

Figure 2.15. Schematic depicting hypothesis as to why the average rupture force between a G5-Ac_{70}-FA_n and FBP substrate increases in the presence of free FA. Note that the use of 1 and 2 FAs binding to the receptor surface is intended only to illustrate the idea of 'more' and 'fewer' FA-FBP bonds. It is believed that the higher rupture forces represent 'more' FAs binding to the FBP substrate than the lower rupture forces. Because of the difference in local concentration between those G5-Ac_{70}-FA_n that are binding via 'more' FAs versus those that are binding with 'fewer' FAs, those bound via 'more' are more likely to displace the free FA bound to the FBP substrate.

2.7. REFERENCES

1. Uckun, F. M.; Narla, R. K.; Zeren, T.; Yanishevski, Y.; Myers, D. E.; Waurzyniak, B.; Ek, O.; Schneider, E.; Messinger, Y.; Chelstrom, L. M.; Gunther, R.; Evans, W., In vivo toxicity, pharmacokinetics, and anticancer activity of genistein linked to recombinant human epidermal growth factor. *Clinical Cancer Research* **1998,** 4, (5), 1125-1134.

2. Meadows, D. C.; Gervay-Hague, J., Targeting HIV. *Chemmedchem* **2006,** 1, (1), 16-29.

3. Artemov, D.; Mori, N.; Ravi, R.; Bhujwalla, Z. M., Magnetic resonance molecular imaging of the HER-2/neu receptor. *Cancer Research* **2003,** 63, (11), 2723-2727.

4. Duncan, R., The dawning era of polymer therapeutics. *Nature Reviews Drug Discovery* **2003,** 2, (5), 347-360.

5. Pillai, O.; Dhanikula, A. B.; Panchagnula, R., Drug delivery: an odyssey of 100 years. *Current Opinion in Chemical Biology* **2001,** 5, (4), 439-446.

6. Langer, R., Drug delivery and targeting. *Nature* **1998,** 392, (6679), 5-10.

7. Winter, P. M.; Caruthers, S. D.; Kassner, A.; Harris, T. D.; Chinen, L. K.; Allen, J. S.; Lacy, E. K.; Zhang, H. Y.; Robertson, J. D.; Wickline, S. A.; Lanza, G. M., Molecular Imaging of angiogenesis in nascent vx-2 rabbit tumors using a novel alpha(v)beta(3)-targeted nanoparticle and 1.5 tesla magnetic resonance imaging. *Cancer Research* **2003,** 63, (18), 5838-5843.

8. Salmaso, S.; Semenzato, A.; Caliceti, P.; Hoebeke, J.; Sonvico, F.; Dubernet, C.; Couvreur, P., Specific antitumor targetable beta-cyclodextrin-poly(ethylene glycol)-folic acid drug delivery bioconjugate. *Bioconjugate Chemistry* **2004,** 15, (5), 997-1004.

9. Gu, F. X.; Karnik, R.; Wang, A. Z.; Alexis, F.; Levy-Nissenbaum, E.; Hong, S.; Langer, R. S.; Farokhzad, O. C., Targeted nanoparticles for cancer therapy. *Nano Today* **2007,** 2, (3), 14-21.

10. Carrithers, M. D.; Lerner, M. R., Synthesis and characterization of bivalent peptide ligands targeted to G-protein-coupled receptors. *Chemistry & Biology* **1996,** 3, (7), 537-542.

11. Luo, Y.; Bernshaw, N. J.; Lu, Z. R.; Kopecek, J.; Prestwich, G. D., Targeted delivery of doxorubicin by HPMA copolymer-hyaluronan bioconjugates. *Pharmaceutical Research* **2002,** 19, (4), 396-402.

12. Napier, M. E.; Desimone, J. M., Nanoparticle drug delivery platform. *Polymer Reviews* **2007,** 47, (3), 321-327.

13. Liu, Y.; Steiniger, S. C. J.; Kim, Y.; Kaufmann, G. F.; Felding-Habermann, B.; Janda, K. D., Mechanistic studies of a peptidic GRP78 ligand for cancer cell-specific drug delivery. *Molecular Pharmaceutics* **2007,** 4, (3), 435-447.

14. Jin, Z. H.; Josserand, V.; Foillard, S.; Boturyn, D.; Dumy, P.; Favrot, M. C.; Coll, J. L., In vivo optical imaging of integrin alpha(v)-beta(3) in mice using multivalent or monovalent cRGD targeting vectors. *Molecular Cancer* **2007,** 6.

15. Thomas, T. P.; Majoros, I. J.; Kotlyar, A.; Kukowska-Latallo, J. F.; Bielinska, A.; Myc, A.; Baker, J. R., Targeting and inhibition of cell growth by an engineered dendritic nanodevice. *Journal of Medicinal Chemistry* **2005,** 48, (11), 3729-3735.

16. Gopalakr.Pv; Karush, F., Antibody Affinity .7. Multivalent Interaction of Anti-Lactoside Antibody. *Journal of Immunology* **1974,** 113, (3), 769-778.

17. Montet, X.; Funovics, M.; Montet-Abou, K.; Weissleder, R.; Josephson, L., Multivalent effects of RGD peptides obtained by nanoparticle display. *Journal of Medicinal Chemistry* **2006,** 49, (20), 6087-6093.

18. Maaheimo, H.; Renkonen, R.; Turunen, J. P.; Penttila, L.; Renkonen, O., Synthesis of a Divalent Sialyl-Lewis-X O-Glycan, a Potent Inhibitor of Lymphocyte-Endothelium Adhesion - Evidence That Multivalency Enhances the Saccharide Binding to L-Selectin. *European Journal of Biochemistry* **1995,** 234, (2), 616-625.

19. Chen, X. Y.; Plasencia, C.; Hou, Y. P.; Neamati, N., Synthesis and biological evaluation of dimeric RGD peptide-paclitaxel conjugate as a model for integrin-targeted drug delivery. *Journal of Medicinal Chemistry* **2005,** 48, (4), 1098-1106.

20. Nigavekar, S. S.; Sung, L. Y.; Llanes, M.; El-Jawahri, A.; Lawrence, T. S.; Becker, C. W.; Balogh, L.; Khan, M. K., H-3 dendrimer nanoparticle organ/tumor distribution. *Pharmaceutical Research* **2004,** 21, (3), 476-483.

21. Quintana, A.; Raczka, E.; Piehler, L.; Lee, I.; Myc, A.; Majoros, I.; Patri, A. K.; Thomas, T.; Mule, J.; Baker, J. R., Design and function of a dendrimer-based therapeutic nanodevice targeted to tumor cells through the folate receptor. *Pharmaceutical Research* **2002,** 19, (9), 1310-1316.

22. Ross, J. F.; Chaudhuri, P. K.; Ratnam, M., Differential Regulation of Folate Receptor Isoforms in Normal and Malignant-Tissues in-Vivo and in Established Cell-Lines - Physiological and Clinical Implications. *Cancer* **1994,** 73, (9), 2432-2443.

23. Weitman, S. D.; Weinberg, A. G.; Coney, L. R.; Zurawski, V. R.; Jennings, D. S.; Kamen, B. A., Cellular-Localization of the Folate Receptor - Potential Role in Drug Toxicity and Folate Homeostasis. *Cancer Research* **1992,** 52, (23), 6708-6711.

24. Weitman, S. D.; Lark, R. H.; Coney, L. R.; Fort, D. W.; Frasca, V.; Zurawski, V. R.; Kamen, B. A., Distribution of the Folate Receptor Gp38 in Normal and Malignant-Cell Lines and Tissues. *Cancer Research* **1992,** 52, (12), 3396-3401.

25. Campbell, I. G.; Jones, T. A.; Foulkes, W. D.; Trowsdale, J., Folate-Binding Protein Is a Marker for Ovarian-Cancer. *Cancer Research* **1991,** 51, (19), 5329-5338.

26. Kukowska-Latallo, J. F.; Candido, K. A.; Cao, Z. Y.; Nigavekar, S. S.; Majoros, I. J.; Thomas, T. P.; Balogh, L. P.; Khan, M. K.; Baker, J. R., Nanoparticle targeting of anticancer drug improves therapeutic response in animal model of human epithelial cancer. *Cancer Research* **2005,** 65, (12), 5317-5324.

27. Hong, S.; Leroueil, P. R.; Majoros, I. J.; Orr, B. G.; Baker, J. R.; Holl, M. M. B., The binding avidity of a nanoparticle-based multivalent targeted drug delivery platform. *Chemistry & Biology* **2007,** 14, (1), 105-113.

28. Stella, B.; Arpicco, S.; Peracchia, M. T.; Desmaele, D.; Hoebeke, J.; Renoir, M.; D'Angelo, J.; Cattel, L.; Couvreur, P., Design of folic acid-conjugated nanoparticles for drug targeting. *Journal of Pharmaceutical Sciences* **2000,** 89, (11), 1452-1464.

29. Majoros, I. J.; Thomas, T. P.; Mehta, C. B.; Baker, J. R., Poly(amidoamine) dendrimer-based multifunctional engineered nanodevice for cancer therapy. *Journal Of Medicinal Chemistry* **2005,** 48, (19), 5892-5899.

30. Hong, S. P.; Bielinska, A. U.; Mecke, A.; Keszler, B.; Beals, J. L.; Shi, X. Y.; Balogh, L.; Orr, B. G.; Baker, J. R.; Holl, M. M. B., Interaction of poly(amidoamine) dendrimers with supported lipid bilayers and cells: Hole formation and the relation to transport. *Bioconjugate Chemistry* **2004,** 15, (4), 774-782.

31. Majoros, I. J.; Myc, A.; Thomas, T.; Mehta, C. B.; Baker, J. R., PAMAM dendrimer-based multifunctional conjugate for cancer therapy: Synthesis, characterization, and functionality. *Biomacromolecules* **2006,** 7, (2), 572-579.

32. Nygren-Babol, L.; Sternesjo, A.; Jagerstad, M.; Bjorck, L., Affinity and rate constants for interactions of bovine folate-binding protein and folate derivatives determined by optical biosensor technology. Effect of stereoselectivity. *Journal of Agricultural and Food Chemistry* **2005,** 53, (13), 5473-5478.

33. Evans, E.; Ritchie, K., Dynamic strength of molecular adhesion bonds. *Biophysical Journal* **1997,** 72, (4), 1541-1555.

34. Taborda, C. P.; Rivera, J.; Zaragoza, O.; Casadevall, A., More is not necessarily better: Prozone-like effects in passive immunization with IgG. *Journal of Immunology* **2003,** 170, (7), 3621-3630.

35. Evans, E. B., Looking inside molecular bonds at biological interfaces with dynamic force spectroscopy. *Biophysical Chemistry* **1999,** 82, (2-3), 83-97.

36. Sulchek, T. A.; Friddle, R. W.; Langry, K.; Lau, E. Y.; Albrecht, H.; Ratto, T. V.; DeNardo, S. J.; Colvin, M. E.; Noy, A., Dynamic force spectroscopy of parallel individual Mucin1-antibody bonds. *Proceedings of the National Academy of Sciences of the United States of America* **2005,** 102, (46), 16638-16643.

37. Friddle, R. W.; Sulchek, T. A.; Albrecht, H.; De Nardo, S. J.; Noy, A., Counting and breaking individual biological bonds: Force spectroscopy of tethered ligand-receptor pairs. *Current Nanoscience* **2007,** 3, (1), 41-48.

CHAPTER 3

THE INTERACTION OF POLYCATIONIC POLYMERS WITH SUPPORTED LIPID BILAYERS AND CELLS: NANOSCALE HOLE FORMATION AND ENHANCED MEMBRANE PERMEABILITY BY NON-TARGETED NANOPARTICLES

3.1. BACKGROUND

The previous chapter examined a particular type of targeted nanoparticle whose scaffold consisted of an acetylated PAMAM dendrimer. Although our research group has had great success with this platform, it is by no means the sole candidate. Several polycationic polymers have been employed in gene and drug delivery applications, including poly-L-lysine (PLL), polyethylenimine (PEI), diethylaminoethyl-dextran (DEAE-DEX), and non-acetylated PAMAM dendrimers.[1-3] This chapter examines the interactions of these polycationic nanoparticles in their non-targeted form with cells and model membranes.

The generally accepted mechanism for internalization of polycationic polymers is through polycation-mediated endocytosis.[4-7] The mechanism consists of the polycationic nanoparticle first binding to the outer cell membrane and subsequently internalized into the cell via endocytosis. Once inside the cell, the nanoparticle is released from the endosome. The electrostatic interactions between the polycationic polymer and the cell membrane is thought to play a critical role in the process. Several research groups, including our own, have taken particular interest in the first step of the three-step process

of polycation-mediated endocytosis. To address this, groups have used both model and cell membranes. Studies involving model systems included incubation of polycationic nanoparticles such as PEI, PAMAM dendrimers and poly-(N-ethyl-4-vinylpyridinium bromide) with dye-containing vesicles. Following incubation, it was found that the dye was released from the interior of the vesicle, signifying that disruption of the model membrane had occurred.[8-10] *In vitro* studies have also demonstrated increased membrane permeability as determined by cytotoxicity (cytosolic enzyme leakage such as LDH) assays.[11, 12]

We previously reported that the positively charged PAMAM dendrimers cause membrane disruption, allowing the diffusion of molecules in and out of cells.[13] During the course of developing our targeted dendrimer-based platform, we noted that cells incubated with PAMAM dendrimers exhibited enzyme leakage while cells incubated with the acetylated form of the PAMAM dendrimer did not. This *in vitro* result was consistent with the proposed hole formation mechanism, as suggested by atomic force microscopy (AFM) on a supported 1,2-dimyristoyl-sn-glycero-3-phosphocholine (DMPC) model membrane.[14-17] There, it was shown that PAMAM dendrimers induce nanoscale defect formation in model membranes, while its acetylated forms aggregates, presumably within the model membrane. Although this body of work suggests that internalization of polycationic nanoparticles occurs via membrane hole formation, no clear connection had been made between the proposed model and *in vitro* studies.[16]

In this chapter, we correlate the formation of nanoscale holes using a series of common polycationic nanoparticles (PEI, PLL and DEAE-DEX) in model and real cell membranes. It is hypothesized that these polycationic nanoparticles will *(1)* induce

nanoscale hole formation in supported lipid bilayers (SLBs) *(2)* cause substantial permeability of the cell membrane allowing enhanced enzyme and dye diffusion. In addition, it is hypothesized that *(3)* neutral, linear polymers (PEG, PVA) will not induce hole formation in SLBs or induce membrane permeability in cell membranes. Within this chapter, AFM studies will demonstrate that nanoscale hole formation and/or expansion of pre-existing defects occurred in SLBs following incubation with the polycationic nanoparticles but not with the neutral linear polymers. *In vitro* studies will show that only those cells incubated with the polycationic nanoparticles were made permeable to molecules such as enzymes (LDH, Luc), propidium iodide (PI), and FITC. Interestingly, larger polycationic nanoparticles incubated with cells at low temperatures where the energy-dependent mechanism of endocytosis is thought to be inhibited have been shown to be still internalized, albeit to a less degree.[13] These results directly support the three hypothesis described above and suggest that polycationic nanoparticles can enter the cell through a hole formation process and not simply through the traditionally accepted polycation-mediated endocytosis. These studies have implications on the design and implementation of targeted delivery platforms.

3.2. EXPERIMENTAL

Materials and measurement of molar masses

PLL, PLL-FITC conjugate (PLL-FITC), PEI, and DEAE-DEX were purchased from Sigma-Aldrich. G5 PAMAM dendrimers were synthesized and then conjugated with FITC at the Michigan Nanotechnology Institute for Medicine and Biological Sciences, University of Michigan.[13] DMPC lipids were provided by Avanti Lipids,

Alabaster, AL. Chemical structures of the polycationic polymers used in this paper are illustrated in **Figure 3.1.**

The molar mass moments and molar mass distribution of each polymer sample was measured using gel permeation chromatography (GPC). The number average molar mass (M_n) and polydispersity index (PDI), a commonly used measure of the breadth of the molar mass distribution defined as the ratio of the weight and number average molar masses (M_w/M_n), of individual samples are listed in **Table 3.1**. GPC experiments were performed using an Alliance Waters 2690 separation module (Waters Corp., Milford, MA) equipped with a Waters 2487 UV absorbance detector (Waters Corp.), a Wyatt Dawn DSP laser photometer (Wyatt Technology Corp., Santa Barbara, CA), an Optilab DSP interferometric refractometer (Wyatt Technology Corp.), and TosoHaas TSK-Gel Guard PHW 06762 (75×7.5 mm, 12 μm), G 2000 PW 05761 (300 × 7.5 mm, 10 μm), G 3000 PW 05762 (300 × 7.5 mm, 10 μm), and G 4000 PW (300 × 7.5 mm, 17 μm) columns. Column temperatures were maintained at 25 ± 0.2 °C with a Waters temperature control module. Citric acid buffer (0.1 M) with 0.025 % sodium azide in water was used as a mobile phase. The pH of the mobile phase was adjusted to 2.74 using NaOH and the flow rate was maintained at 1 mL/min. Sample concentration was approximately 2 mg/mL and an injection volume of 100 μL was used for all samples. Molar mass moments of the polymers were determined using Astra software (version 4.7) (Wyatt Technology Corp.). Characterization of all polymers used here was completed by Mohammad T. Islam or Seungpyo Hong.

Preparation and AFM observation of supported DMPC lipid bilayers

A 0.67 mg/mL suspension of small, unilamellar vesicles (SUVs) was prepared as previously reported [13, 14, 18]. Supported lipid bilayers were formed by depositing 80 μL of liposome suspension on a 1×1 cm^2 piece of freshly cleaved mica. Following a 20 minute incubation period, the sample was gently rinsed with water to remove excess lipids and placed in the AFM for imaging as described in previous studies. All AFM measurements were performed in tapping mode on a Nanoscope IIIa Multimode scanning probe microscope from Digital Instruments (DI, Veeco Metrology Group, Santa Barbara, CA). The AFM was equipped with a liquid cell (DI) and a silicone nitride cantilever (DI model NPS, spring constant 0.32 N/m, length 100 μm) operating at a drive frequency of 6-9 kHz. After taking an initial image of the bilayer, approximately 20 μL of polymer solution was injected into the liquid cell. All solutions were prepared using high purity water (Nerl Diagnostics, East Providence, RI). The temperature inside the liquid cell was 28 °C and therefore above the gel to liquid transition temperature of supported DMPC bilayers.

Cell Lines

The KB and Rat2 cell lines were purchased from the American Type Tissue Collection (ATCC, Manassas, VA) and grown continuously as a monolayer at 37 °C, and 5% CO_2 in RPMI 1640 medium (Mediatech, Herndon, VA) and Dulbecco's modified Eagle's medium (DMEM, Gibco, Eggenstein, Germany), respectively. Rat2 cell line was transfected to permanently express the LUC gene using PAMAM dendrimer-mediated gene transfection as previously described.[13, 19, 20] The LUC expressing Rat2 cells is noted as Rat2pLUC. The RPMI 1640 and DMEM media were supplemented with penicillin

(100 units/mL), streptomycin (100 μg/mL), and 10% heat-inactivated fetal bovine calf serum (FBS) before use.

XTT, LUC, and LDH Assays and Flow Cytometry

Cytotoxicity of the polycationic polymers was assessed with a 2,3-bis(2-methoxy-4-nitro-5-sulfophenyl)-5[(phenylamino)carbonyl]-*2H*-tetrazolium hydroxide (XTT) assay kit (Cell Proliferation Kit II, Roche Molecular Biochemicals, Mannheim, Germany). KB and Rat2 cell lines (at a concentration of 5×10^4 cells/well) were prepared as monolayers in 96 well plates, followed by incubation with polymers in phosphate buffered saline (PBS) with Ca^{2+} and Mg^{2+} at 37 °C under 5% CO_2 for 4.5 hrs. Polymer solutions (supernatants) were removed and followed by washing with PBS twice. Mitochondrial activities in the cells were then measured using the assay kit.

The LDH and LUC activities in the cell supernatant after 3 hrs incubation were respectively analyzed using an LDH assay kit (Promega Co., Madison, WI) and a chemiluminescence assay(Promega Co., Madison, WI) as previously described.[13] The measured LDH and LUC activities were either recalculated by percentage to the activities of cell lysates of intact cells (% LDH released) or adjusted for the protein concentration of the sample (relative light unit (RLU)/mg protein). Flow cytometry was also performed according to our report.[13] Fluorescence signal intensities were measured by a Coulter EPICS/XL MCL Beckman-Coulter flow cytometer and data were analyzed using Expo32 software (Beckman-Coulter, Miami, FL). All in vitro assays were completed by Seungpyo Hong.

CLSM Observation

A concentration of 2×10^4 cells/mL of Rat2 cells was seeded on MatTek glass bottom petri dishes (35 mm) and incubated at 37 °C under 5% CO_2 for 24 hrs. The DMEM media was removed and 2 mL of each PLL-FITC and dendrimer-FITC conjugates in PBS (Ca^{2+}, Mg^{2+}) solution was added into the appropriate dish. The dishes were incubated with added solutions at 37 °C under 5% CO_2 for 1 hr. The conjugate-containing solutions were removed and the resulting cell monolayer was washed with PBS. Cells were fixed with 2% formaldehyde in the PBS (Ca^{2+}, Mg^{2+}) at room temperature for 10 min, followed by washing with PBS twice. Confocal and differential interference contrast (DIC) images were taken on an Olympus FV-500 confocal microscope using a 40×, 1.2 NA oil immersion objective. For the confocal images, the 488 nm line of an argon ion laser was used for excitation and the emission was filtered at 505 nm. Note that all confocal images were obtained by Seungpyo Hong.

3.3 RESULTS

Polycation-Induced Hole Formation on Aqueous Supported DMPC Lipid Bilayers

The polycationic nanoparticles used in this study (PLL, PEI and DEAE-DEX) were all shown to disrupt DMPC supported lipid bilayers. Several controls were performed for the AFM study. Before the introduction (through injection) of polymers into the solution containing the aqueous supported lipid bilayers, the bilayers were imaged alone for 8 to 10 minutes. These pre-imaging steps were done to ensure that the bilayers were stable and that pre-existing defects that appeared were not due to the act of imaging itself. A blank injection of water (the solvent in which the polymers were dissolved) was completed and resulted in no change to the bilayer over the course of a normal imaging

session (60 to 90 minutes). This shows that the injection itself is not responsible for the formation of defects. Finally, injections of 1 μg/mL of polyethylene glycol (PEG) and polyvinyl alcohol (PVA), two neutral polymers, were performed and resulted in no change to the supported bilayers over normal imaging time.

Images taken using AFM show that PEI, PLL and DEAE-DEX all disrupt DMPC supported lipid bilayers. **Figures 3.2, 3.3, and 3.4** are representative data sets of the polycationic polymers and DMPC lipid bilayer interactions. Although there is some variation, several repetitions were completed for each polymer confirming that the degrees of membrane/polymer interactions are qualitatively similar. Following the addition through injection of PLL into the AFM liquid cell at a final concentration of ~ 1 ug/mL **(Figure 3.2),** new defects in the bilayer are formed. The depth of these defects in the membrane is primarily in the range of 4.0-4.8 nm. Addition of PEI onto the bilayer, however, results in mostly the expansion of pre-existing defects **(Figure 3.3).** These expanded defects have measured 4.4 to 5.1 nm in depth which is consistent with the removal of a full bilayer. Interestingly, the introduction of DEAE-DEX to supported DMPC bilayers results in only 2 to 4 nm deep depressions.

Cytotoxicity of Polycation and Polycation-Induced Enzyme Leakage

The cytotoxicity of the polymers was determined using an XTT assay **(Figure 3.5).** The relative cell viability was calculated as:

$$[OD_{492nm}]_{sample}/[OD_{492nm}]_{control} \times 100.$$

The assay results show that the polymers are not cytotoxic up to a 12 μg/mL concentration (> 80% cell viability) for both KB and Rat2 cells. Based on these data, the assays performed to investigate the cytosolic enzyme release were carried out in polymer

concentrations of 6 and 12 μg/mL. Within this range, the polymers are non-cytotoxic so the observed enzyme release can be ascribed to an increase in cell membrane permeability as opposed to general lysis due to cell death.

The effect of positively charged polymers on the cell membranes was investigated in terms of cytosolic enzyme release from the cells using LDH and LUC assay techniques. As the polymer concentration increases, the amounts of both LDH and LUC released increased as illustrated in **Figure 3.6 and 3.7.** Induced membrane permeability as measured by LDH release shows a degree of cell type (KB and Rat2) dependence as shown in Figure 6. In both cell types (Figure 6), however, PEI induced more LDH leakage as compared to the other polycationic polymers. This is not surprising because PEI possesses a much greater charge/monomer ratio **(see Table 3.1)** as compared to the other polymers. G5-NH_2 and PLL cause similar amount of LDH release and the least LDH was released from the cells after exposure to DEAE-DEX among the polycationic polymers, particularly in the case of the Rat2 cells. PEG and PVA did not cause enzyme leakage. LUC release from Rat2pLUC exhibits a trend similar to the LDH release from cells seen as discussed above **(Figure 3.7).**

Binding and Internalization of PLL-FITC

PLL-FITC conjugate was used for direct observation by CLSM. This experiment was carried out to compare the internalization behavior of PEI, PLL, and DEAE-DEX polymers to that of dendrimeric G5-NH_2. **Figure 3.8** shows that PLL-FITC is internalized into the Rat2 cells resulting in strong fluorescence of FITC from inside the cells. In particular, the intracellular location of the internalized conjugates appears to exclude the nucleus. This internalization behavior is particularly interesting because

penetration of the polymers into the nucleus should be avoided for non-toxic gene delivery as it may alter the DNA sequence. G5-Ac-FITC, which remains neutral in water due to the conversion of all the surface primary amines groups to acetamide groups, is not internalized as shown in **Figure 3.8e** allowing the conjugate to be used as a negative control.[13] The DIC image is provided to show that an appropriate cell density was used **(Figure 3.8f).**

Diffusion of Small Molecules through the Permeabilized Membranes.

It is known that PI and FDA can be employed as indicators of diffusion-in and out, respectively.[13, 21] PI is readily internalized into cells with disrupted membranes but is excluded from cells with intact membranes. In contrast, FDA is able to traverse intact membranes and is then converted to fluorescein (FITC) by endogenous esterase in cells. The resulting FITC is unable to travel across intact membranes but is able to traverse permeabilized membrane. Therefore, it is assumed that PI fluorescence should increase and FITC fluorescence should decrease with increasing membrane permeability. Figure 9a shows the increase in PI signal intensity induced following the incubation of KB cells with the polycationic polymers. The greatest PI intensity increase is seen using PEI, followed by G5, DEAE-DEX, and PLL. Charge neutral PVA and PEG do not induce PI internalization. On the other hand, FITC fluorescence intensities are decreased after exposure to the polycationic polymers in a concentration-dependent manner **(Figure 3.9b).** The largest amount of intensity drop is observed in the PEI case, although DEAE-DEX, PLL, and G5 also show a decrease in FITC fluorescence intensity. As expected, PVA and PEG do not induce FITC escape.

3.4 DISCUSSION

Evidence for Hole Formation by Polycationic Polymers PEI, PLL, and DEAE-DEX

We previously reported nanoscale hole formation on both supported lipid bilayers and cellular membranes induced by positively charged PAMAM dendrimers [13-17]. In this study we test the possibility of extending the proposed mechanism of dendrimer/membrane interactions, i.e. hole formation by sphere-like PAMAM dendrimers, to the more common and inexpensive polycationic polymers PEI, PLL, and DEAE-DEX. Polycationic polymer-induced disruption of various supported phospholipid bilayers including dioleoyl phosphatidyl choline (DOPC), dioleoyl phosphatidyl serine (DOPS), 1-palmitoyl-2-oleoyl-sn-glycero-3-phosphatidic acid (POPA), and their mixtures has been reported using various methods. These techniques include quartz crystal microbalance with dissipation, leakage assay, ^{31}P NMR, and electrophoretic mobility.[9, 10, 22] Furthermore, polycationic polymer-induced permeabilization of living cell membranes has also been observed *in vitro* using enzyme assays and flow cytometry.[11, 13] In this paper, we correlate two separate types of studies (model membrane and *in vitro* studies) by performing simultaneous experiments at similar conditions to provide a better understanding of polymer/membrane interactions.

There are two basic types of disruption seen in AFM images: membrane hole formation and membrane thinning. 'Membrane hole formation' is the complete removal of the lipid bilayer from the mica surface, resulting in defects of 4 to 5 nm in depth. The apparent discrepancy between the expected depth for a removal of a full bilayer, 5 nm, and the depths experimentally measured in this study can be explained by the varying degrees of polymer adsorption to the surface of the mica. 'Membrane thinning,' which

could result from the re-orientation of lipids or the removal of a layer of lipid from the lipid bilayer, yields depressions ranging between approximately 2 and 3 nm.[23-26]

Although the effect of each of the polymers used in the study varies in degree, each of these commercial polycationic polymers induce disruption of the bilayers as shown in the AFM images **(Figures 3.2-3.4).** This study is consistent in terms of observing bilayer disruption but differs in both the type of disruption and concentration dependence as compared with the previous studies which examined the interaction of positively charged dendrimers with a DMPC supported lipid bilayers.[14] Our *in vitro* study shows enzyme (LDH with MW 135-140 kDa and ~4.3 nm in radius and LUC with MW 61 kDa and ~2.7 nm in radius) leakage out of the cells, polymer internalization into the cells, and diffusion in and out of small molecular probes (PI and FITC respectively) through the living cell membranes **(Figure 3.6-3.9)** which are also consistent with our previous report using cationic PAMAM dendrimers.[13] Therefore, it is clear that PEI, PLL, and DEAE-DEX also cause the formation of defects in both supported lipid bilayers and cell membranes.

Relationship between Polymer Properties and Membrane Permeabilization

As modern biotechnology tends towards the adaptation of biocompatible polymers for advanced biomedical applications, a fundamental understanding of these polymers, particularly in physiological conditions, should be obtained. In this paper, we try to provide a better understanding of the relationship between physical properties of polymers and biological membranes. GPC measurement enables us to rank hydrodynamic radii of the polycationic polymers in the following order: DEAE-DEX > PEI > PLL > G5 PAMAM. According to our AFM and *in vitro* studies, however, the

size of the polymers does not seem to markedly affect their ability to induce hole formation in the membranes. Instead, it was found that the degree of membrane permeability for the flexible polycationic polymers investigated here is strongly dependent on the number of formal charges on the polymer chain. As shown in **Table 3.1**, PEI has the greatest density of charged groups on its single polymeric chain among the polymers used in this study. Not surprisingly, a significantly high amount of LDH and LUC was released in both cell lines after incubation with PEI. Furthermore, changes in fluorescence in PI and FITC, as a result of interactions between PEI and cells, were greater than changes induced by the other polycationic polymers. This indicates that charge interactions play a key role in inducing changes of membrane permeability, i.e. nanoscale hole formation. Our data on PLL, DEAE-DEX, and G5-NH_2, however, suggests that electrostatic interactions are not the only factor contributing to the effectiveness of polymer-induced nanoporation. Although PLL has an order of magnitude higher charge/monomer ratio than DEAE-DEX and G5-NH_2, the difference among those polymers in terms of enzyme leakage, PI internalization, and FITC escape is not remarkable. One possible explanation is that efficacy of hole formation is dependent on the architecture of polymers. That is, sphere-like (PAMAM), branched (PEI), or ring-containing (DEAE-DEX) molecular structures are likely more effective than linear polymers (PLL) at increasing membrane permeability. Mecke *et al.* also suggested that the macromolecular architecture is an important factor in the polymer/membrane interactions.[14]

In summary, **Chapter 3** confirms our hypotheses that three commonly used polycationic nanoparticles (PEI, PLL and DEAE-DEX) *(1)* induce nanoscale hole

formation in supported lipid bilayers (SLBs) *(2)* cause substantial permeability of the cell membrane allowing enhanced enzyme and dye diffusion. In addition, we found that two neutral linear polymers, PEG and PVA, did not induce nanoscale hole formation in SLBs, or cause substantial permeability in cell membranes.

The conclusions we draw from these studies are two-fold. First, from a mechanistic standpoint, these linear polycationic polymers interact in a similar fashion to the spherical PAMAM dendrimer when exposed to model and real membranes. Although we had hypothesized this to be the case because of their similarity in their chemical make-up, it was not clear that the spherical shape of the dendrimer was not critical for hole formation within the membrane. **Chapter 4** will go into further detail regarding additional nanoparticle properties that mediate hole formation within membranes.

Second, from an application standpoint, these studies suggest that polycationic polymers are inappropriate as scaffolds for targeted delivery platforms. Indeed, the non-specific interactions these polycationic nanoparticles have with cell membranes would likely overwhelm any 'targeting' one could achieve using a targeting moiety. We have previously shown with our own targeted platform system that non-specific interactions dominate the nanoparticle-cell interactions when not fully acetylated following functionalization (*unpublished work by Thommey Thomas, MNiMBS*). In principle, one could similarly functionalize the other polycationic nanoparticles presented here and then acetylate their remaining amines to form a targeted platform. In practice, however, the ill-defined structures of PLL, PEI and DEAE-DEX as compared to that of the PAMAM dendrimer[27] make controlled functionalization of the linear polycationic polymers nearly

impossible. Given the clear importance of controlled functionalization, particularly in the case of targeted drug delivery platforms, these non-homogenous linear polycationic polymers are simply not appropriate.

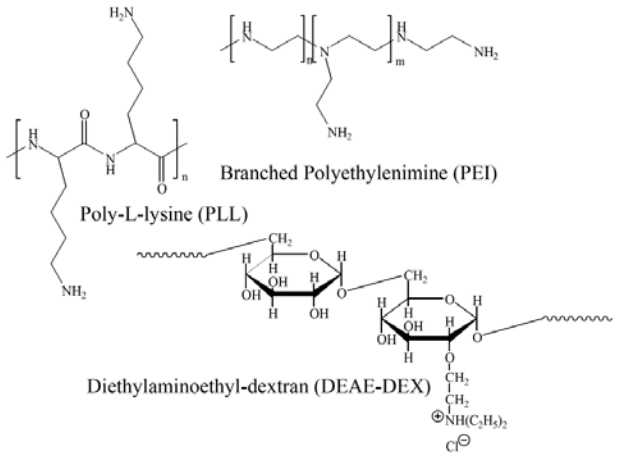

Figure 3.1. The structures of the linear polycationic nanoparticles used within these studies.

Table 1. Physicochemical properties of polycations used in this study

Polymer	M_n (PDI)[a]	Order of amines (°)	Charge/monomer ratio[b]	Zeta Potential (mV)[c]	Shape of chain
PLL	11210 (1.67)	1, 2	0.007519	17.59 ± 0.39	Linear, flexible
PLL-FITC	23620 (1.06)	1, 2	0.007519	-	Linear, flexible
PEI	78220 (3.44)	1, 2, 3	0.02290	45.18 ± 16.84	branched, flexible
DEAE-DEX	18490 (32.90)	3	0.00218	30.44 ± 2.71	Linear, intramolecular crosslinking
G5-NH_2	26530 (1.02)	1, 3	0.00885	19.24 ± 16.63	Sphere-like
PEG	16290 (1.22)	N/A	N/A	-1.07 ± 1.10	Linear, flexible
PVA	28490 (1.57)	N/A	N/A	-0.68 ± 1.36	Linear, inter-/intramolecular H bonding

[a] Measured by GPC.

[b] Theoretical number of charged groups per molecular weight of polymeric monomer.

[c] Measured by zeta potential/particle sizer NICOMP™ 380 ZLS (PSS·NICOMP, Santa Barbara, CA). The maximum count rate was 5 MHz and the measurements were carried out for 5 min. All the polymer samples were at a concentration of 1 mg/mL, pH 7.4 and measurement for each polymer were repeated 5 times.

Table 3.1 Physiochemical properties of polycationic polymers used in this study

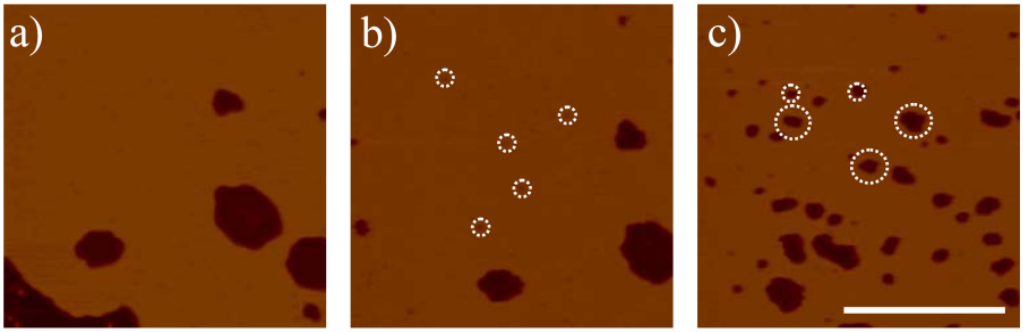

Figure 3.2 AFM images of supported DMPC lipid bilayers upon exposure to poly-L-lysine (PLL). 20 μL of 10 μg/ml PLL injected following image a), resulting in a final concentration of ~1.0 μg/ml in the AFM liquid cell. Total time between a) and c) is approximately 50 minutes. Several dotted white circles indicate formation of new holes in the lipid bilayers caused by PLL. Bar: 500 nm. Z-scale: 20 nm.

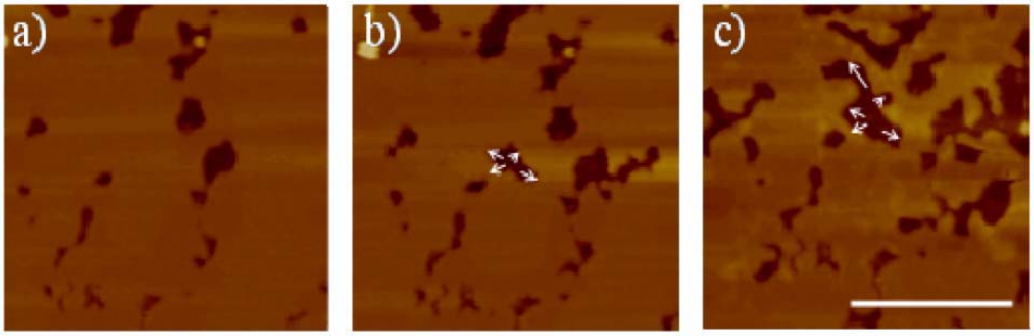

Figure 3.3 AFM images of supported DMPC lipid bilayers upon exposure to poly(ethylenimine) (PEI). 20 μL of 5μg/mL PEI injected following image a) resulting in a final concentration of ~0.5 μg/mL. An additional 20 μL of 10 μg/mL was injected after b), resulting in a final concentration of ~1.5 μg/mL. Total time between a) and c) is approximately 40 minutes. Note that there is no new hole formation but instead the pre-existing defects are expanded (see white arrows). Bar: 500 nm. Z-scale: 20 nm.

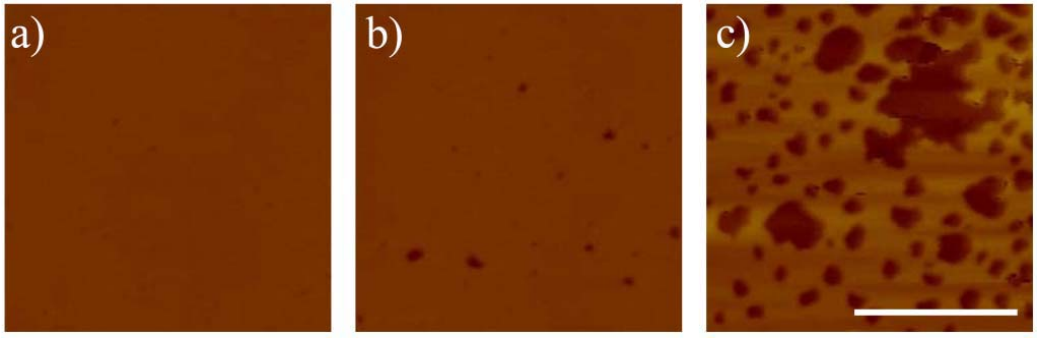

Figure 3.4 AFM images of supported DMPC lipid bilayers upon exposure to diethylaminoethyl-dextran (DEAE-DEX). 50 μL of 5 μg/mL DEAE-DEX injected following image a), resulting in a final concentration of ~1.3 µg/mL. Total time between a) and c) is approximately 90 minutes. Unlike that PLL and PEI create or expand defects in the lipid bilayers, DEAE-DEX induces membrane thinning. The newly formed defects are 2-4 nm deep instead of complete removal of the lipid bilayers (~4-5 nm deep). Bar: 500 nm. Z-scale: 20 nm. Elizabeth Janus is acknowledged for her help in obtaining these images.

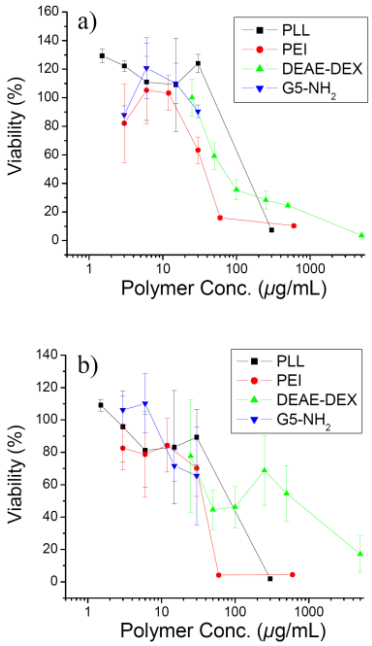

Figure 3.5 Cell viability determined by XTT assay of a) KB and b) Rat2 cells after incubation with PLL, PEI, DEAE-DEX, and G5-NH_2 PAMAM at 37 °C for 4.5 hrs. Note that all the polymers are not cytotoxic up to a concentration of 12 μg/mL Note that this data was obtained by S. Hong.

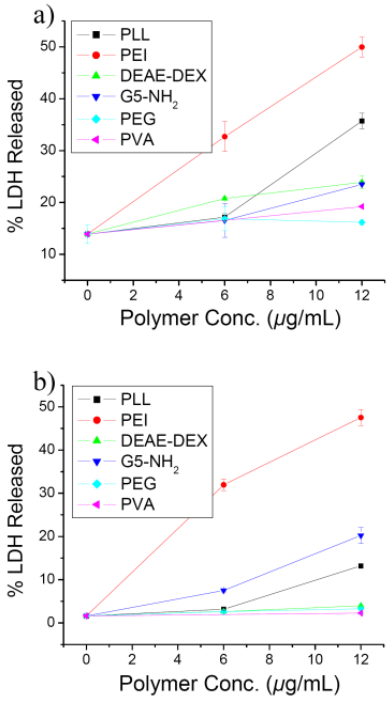

Figure 3.6 Dose-dependent LDH release from a) KB and b) Rat2 cell lines incubated with PLL, PEI, DEAE-DEX, G5-NH_2 PAMAM, PEG, and PVA at 37 °C for 3 hrs. All the polycationic polymers induce LDH leakage but the neutral polymers PEG and PVA do not cause any significant leakage. Note that these studies were completed by Seungpyo Hong.

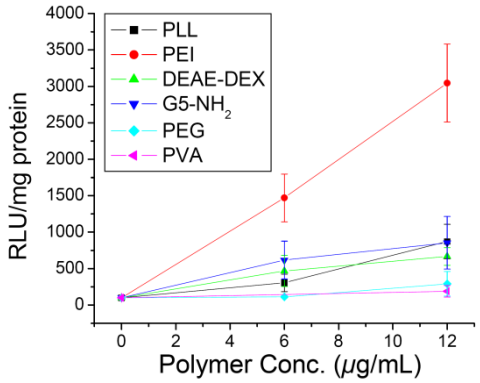

Figure 3.7 Dose-dependent luciferase (LUC) release from Rat2pLUC cell line incubated with PLL, PEI, DEAE-DEX, G5-NH_2 PAMAM, PEG, and PVA at 37 °C for 3 hrs. Before the incubation, Rat2 cells were transfected by PAMAM dedrimer-mediated cell transfection to express LUC in their cytosols. As seen in the LDH assay data in Figure 6, all the polycationic polymers used in this study also cause LUC leakage but the neutral polymers do not. Note that these studies were completed by Seungpyo Hong.

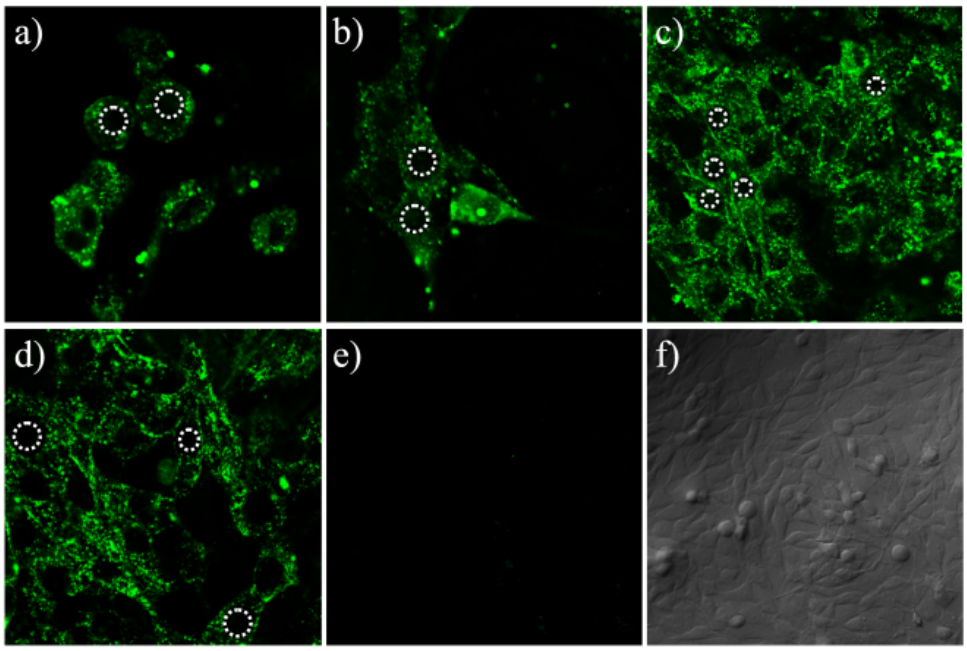

Figure 3.8. Confocal microscopy images of Rat2 cells incubated with a) 6 μg/ml PLL-FITC and b) 12 μg/ml PLL-FITC conjugates. c) A zoomed-out image of b). Rat2 cells incubated with d) 6 μg/ml G5-NH_2-FITC and e) 12 μg/ml G5-Ac-FITC conjugates. f) Differential interference contrast (DIC) image of e), shown to illustrate that there are a decent amount of the cells at the focal plane although nothing can be seen in the fluorescence image e). Note that the green fluorescence from either PLL-FITC or G5-NH_2-FITC does not occur from within cell nuclei which are indicated by several dotted white circles. The location of the nuclei and the exclusion of the polycationic polymers were confirmed in previously published work using DAPI staining of the nucleus (*15*). Note that these studies were completed by Seungpyo Hong.

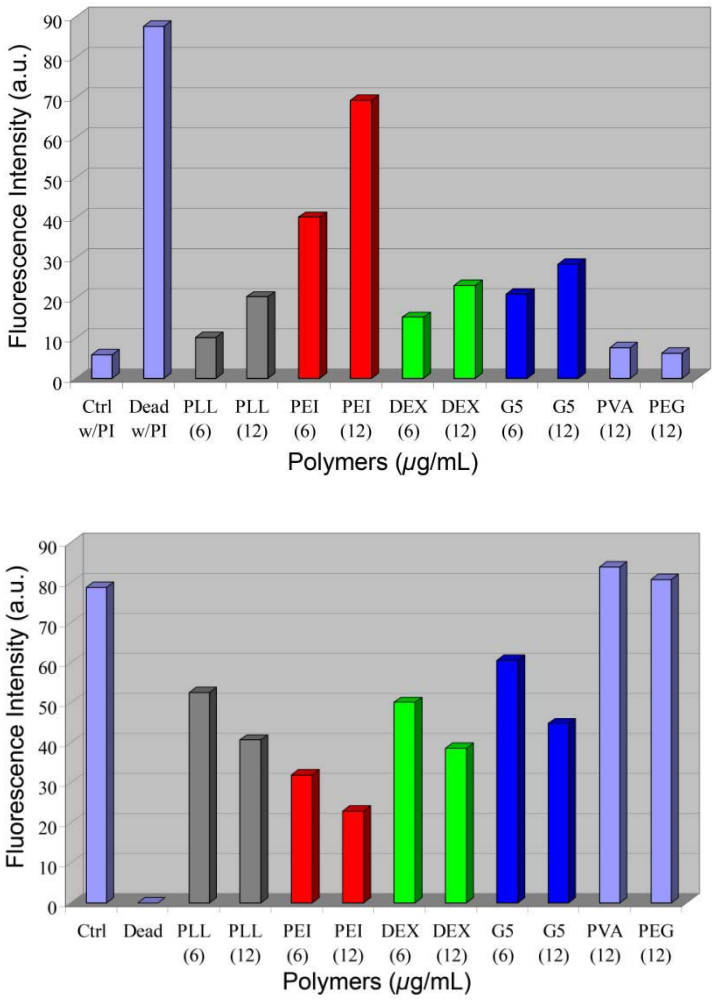

Figure 3.9. Fluorescence intensity of a) propidium iodide (PI) and b) fluorescein (FITC) from KB cells measured by flow cytometer. Note that fluorescence intensity of PI should increase while that of FITC should decrease with increase of membrane permeability. All the polycationic polymers cause an increase of PI fluorescence intensities and a decrease of FITC fluorescence. However the neutral polymers do not cause such changes. Note that these studies were completed by Seungpyo Hong.

3.6 REFERENCES

1. Cho, Y. W.; Kim, J. D.; Park, K., Pollycation gene delivery systems: escape from endosomes to cytosol. *Journal of Pharmacy and Pharmacology* **2003,** 55, (6), 721-734.

2. Davis, M. E., Non-viral gene delivery systems. *Current Opinion in Biotechnology* **2002,** 13, (2), 128-131.

3. Segura, T.; Shea, L. D., Materials for non-viral gene delivery. *Annual Review of Materials Research* **2001,** 31, 25-46.

4. Rolland, A. P., From genes to gene medicines: Recent advances in nonviral gene delivery. *Critical Reviews in Therapeutic Drug Carrier Systems* **1998,** 15, (2), 143-198.

5. Behr, J. P., Synthetic Gene-Transfer Vectors. *Accounts Of Chemical Research* **1993,** 26, (5), 274-278.

6. Boussif, O.; Lezoualch, F.; Zanta, M. A.; Mergny, M. D.; Scherman, D.; Demeneix, B.; Behr, J. P., A Versatile Vector For Gene And Oligonucleotide Transfer Into Cells In Culture And In-Vivo - Polyethylenimine. *Proceedings Of The National Academy Of Sciences Of The United States Of America* **1995,** 92, (16), 7297-7301.

7. Kopatz, I.; Remy, J. S.; Behr, J. P., A model for non-viral gene delivery: through syndecan adhesion molecules and powered by actin. *Journal Of Gene Medicine* **2004,** 6, (7), 769-776.

8. Purohit, G.; Sakthivel, T.; Florence, A. T., Interaction of cationic partial dendrimers with charged and neutral liposomes. *International Journal of Pharmaceutics* **2001,** 214, (1-2), 71-76.

9. Yaroslavov, A. A.; Kuchenkova, O. Y.; Okuneva, I. B.; Melik-Nubarov, N. S.; Kozlova, N. O.; Lobyshev, V. I.; Menger, F. M.; Kabanov, V. A., Effect of polylysine on transformations and permeability of negative vesicular membranes. *Biochimica Et Biophysica Acta-Biomembranes* **2003,** 1611, (1-2), 44-54.

10. Zhang, Z. Y.; Smith, B. D., High-generation polycationic dendrimers are unusually effective at disrupting anionic vesicles: Membrane bending model. *Bioconjugate Chemistry* **2000,** 11, (6), 805-814.

11. Fischer, D.; Li, Y. X.; Ahlemeyer, B.; Krieglstein, J.; Kissel, T., In vitro cytotoxicity testing of polycations: influence of polymer structure on cell viability and hemolysis. *Biomaterials* **2003,** 24, (7), 1121-1131.

12. Benns, J. M.; Mahato, R. I.; Kim, S. W., Optimization of factors influencing the transfection efficiency of folate-PEG-folate-graft-polyethylenimine. *Journal of Controlled Release* **2002,** 79, (1-3), 255-269.

13. Hong, S. P.; Bielinska, A. U.; Mecke, A.; Keszler, B.; Beals, J. L.; Shi, X. Y.; Balogh, L.; Orr, B. G.; Baker, J. R.; Holl, M. M. B., Interaction of poly(amidoamine) dendrimers with supported lipid bilayers and cells: Hole formation and the relation to transport. *Bioconjugate Chemistry* **2004,** 15, (4), 774-782.

14. Mecke, A.; Uppuluri, S.; Sassanella, T. M.; Lee, D.-K.; Ramamoorthy, A.; Baker, J. R.; Orr, B. G.; Banaszak Holl, M. M., Direct Observation of Lipid Bilayer Disruption by Polyamidoamine Dendrimers. *Chemistry and Physics of Lipids* **2004,** 132, 3-14.

15. Mecke, A.; Lee, D. K.; Ramamoorthy, A.; Orr, B. G.; Holl, M. M. B., Membrane thinning due to antimicrobial peptide binding: An atomic force microscopy study of MSI-78 in lipid bilayers. *Biophysical Journal* **2005,** 89, (6), 4043-4050.

16. Mecke, A.; Lee, D. K.; Ramamoorthy, A.; Orr, B. G.; Holl, M. M. B., Synthetic and natural polycationic polymer nanoparticles interact selectively with fluid-phase domains of DMPC lipid bilayers. *Langmuir* **2005,** 21, (19), 8588-8590.

17. Mecke, A.; Majoros, I. J.; Patri, A. K.; Baker, J. R.; Holl, M. M. B.; Orr, B. G., Lipid bilayer disruption by polycationic polymers: The roles of size and chemical functional group. *Langmuir* **2005,** 21, (23), 10348-10354.

18. Mecke, A.; Uppuluri, S.; Sassanella, T. M.; Lee, D. K.; Ramamoorthy, A.; Baker, J. R.; Orr, B. G.; Holl, M. M. B., Direct observation of lipid bilayer disruption by poly(amidoamine) dendrimers. *Chemistry and Physics of Lipids* **2004,** 132, (1), 3-14.

19. Bielinska, A.; KukowskaLatallo, J. F.; Johnson, J.; Tomalia, D. A.; Baker, J. R., Regulation of in vitro gene expression using antisense oligonucleotides or antisense expression plasmids transfected using starburst PAMAM dendrimers. *Nucleic Acids Research* **1996,** 24, (11), 2176-2182.

20. Bielinska, A. U.; KukowskaLatallo, J. F.; Baker, J. R., The interaction of plasmid DNA with polyamidoamine dendrimers: mechanism of complex formation and analysis of alterations induced in nuclease sensitivity and transcriptional activity of the complexed DNA. *Biochimica Et Biophysica Acta-Gene Structure and Expression* **1997,** 1353, (2), 180-190.

21. Umebayashi, Y.; Miyamoto, Y.; Wakita, M.; Kobayashi, A.; Nishisaka, T., Elevation of plasma membrane permeability on laser irradiation of extracellular latex particles. *Journal of Biochemistry* **2003,** 134, (2), 219-224.

22. Rossetti, F. F.; Reviakine, I.; Csucs, G.; Assi, F.; Voros, J.; Textor, M., Interactions between poly(L-Lysine)-g-poly(ethylene glycol) and Supported Phospholipid Bilayers. *Biophysical Journal* **2004,** 86, (1), 174A-174A.

23. Harroun, T. A.; Heller, W. T.; Weiss, T. M.; Yang, L.; Huang, H. W., Experimental evidence for hydrophobic matching and membrane-mediated interactions in lipid bilayers containing gramicidin. *Biophysical Journal* **1999,** 76, (2), 937-945.

24. Heller, W. T.; Waring, A. J.; Lehrer, R. I.; Harroun, T. A.; Weiss, T. M.; Yang, L.; Huang, H. W., Membrane thinning effect of the beta-sheet antimicrobial protegrin. *Biochemistry* **2000,** 39, (1), 139-145.

25. Ludtke, S.; He, K.; Huang, H., Membrane thinning caused by magainin 2. *Biochemistry* **1995,** 34, (51), 16764-16769.

26. Mazzuca, C.; Stella, L.; Venanzi, M.; Formaggio, F.; Toniolo, C.; Pispisa, B., Mechanism of membrane activity of the antibiotic trichogin GA IV: A two-state transition controlled by peptide concentration. *Biophysical Journal* **2005,** 88, (5), 3411-3421.

27. Hong, S. P.; Leroueil, P. R.; Janus, E. K.; Peters, J. L.; Kober, M. M.; Islam, M. T.; Orr, B. G.; Baker, J. R.; Holl, M. M. B., Interaction of polycationic polymers with supported lipid bilayers and cells: Nanoscale hole formation and enhanced membrane permeability. *Bioconjugate Chemistry* **2006,** 17, (3), 728-734.

CHAPTER 4

EXAMINING THE INTERACTION OF A VARIETY OF COVALENTLY-LINKED CATIONIC NANOPARTICLES WITH SUPPORTED LIPID BILAYERS USING AFM

4.1. BACKGROUND

Nanoparticles are currently employed or proposed for a variety of products including drug and gene delivery materials,[1, 2] industrial applications such as catalysts,[3] and consumer products including paints[4] and lotions.[5] Although the technical benefits of using nanoparticles for each particular implementation are clear; the broader impacts of the release of such materials into the environment have yet to be understood.[6-8] One concern is the cytotoxicity of these materials. An interaction of particular interest is that between the cell plasma membrane and nanoparticles, as this is the basic structure of the cell that may be breached with concomitant cytotoxicity.

A great deal of empirical evidence suggests that nanoparticles are effective disruptors of cell plasma membranes. Ready access to this work is provided by a number of recently published papers demonstrating both *in vitro,*[9-13] as well as *in vivo*[13-18] nanoparticle activity with membranes. Specifically, cell level data have demonstrated evidence for membrane permeability via enzyme leakage assays[7, 10, 12, 19] and dye diffusion studies.[12] Direct evidence that the nanoparticles disrupt lipid bilayers was provided by electron paramagnetic resonance (EPR).[20, 21] Studies on supported lipid bilayers (SLBs) have identified two general types of disruption: (1) nanoscale hole formation and (2) membrane thinning. These mechanisms have been explored using oriented circular dichroism (OCD),[22, 23] X-ray diffraction,[22] solid state NMR,[24] molecular

modeling,[10, 25, 26] and atomic force microscopy (AFM).[10, 12, 23-25, 27, 28] The AFM/SLB assay has proven to be a particularly powerful tool for studying this problem because it provides images of the disruption events on the nanometer scale. This assay is completed by first depositing a drop of 1 mg/mL lipid vesicle solution on a cleaved mica surface. Following an incubation time of approximately 20 minutes, excess lipid is removed by gently rinsing the newly formed SLB with water. After a stable image of the SLB using tapping/AC mode AFM is obtained, nanoparticles are introduced and imaging continues until the SLB is once again stable. An interesting example of the AFM/SLB assay used MSI-78 as the nanoparticle and demonstrated that localized ~1 nm diameter membrane thinning events occurred, as opposed to a continuous even thinning over the entire membrane.[23] In contrast, previous experiments implementing dye diffusion enzyme leakage assays or membrane curvature experiments were also not able to provide nanoscale mechanistic information. Recent AFM experiments performed in parallel with dye diffusion and enzyme leakage assays have provided direct evidence of the formation of nanoscale holes in SLBs and provided a common mechanism that is consistent with all three of the previous experimental observations.[10, 12]

We have previously shown that the degree of SLB disruption caused by polymer nanoparticles (e.g., hole formation, membrane thinning), correlates with the level of enzyme leakage, dye diffusion, cytotoxicity, and nanoparticle uptake measured in vitro (this AFM data is shown in Figures 4.3b-d and 4).[10, 12, 27] In addition, the degree of membrane disruption parallels the degree of non-selective tissue uptake observed *in vivo*.[29] This correlation between the AFM/SLB assays and the *in vitro* and *in vivo* studies inspired us to examine the disruption between other nanoparticles that are well-precedented to disrupt and/or translocate across cell membranes. We therefore chose the

AFM/SLB assay to explore the behavior of a number of other important materials including a pentanol-core G3 dendron, the cell penetrating peptide MSI-78,[30] the TAT sequence[31] employed by HIV virus, amine-coated gold nanoparticles,[19, 32] and amine-terminated silica.[33, 34] This set of particles, when combined with our previous studies on G3, G5, and G7 PAMAM dendrimers,[10] polyethyleneimine (PEI) and diethylaminoethyl-dextran (DEAE-DEX)[12], presents a wide range of physical properties (organic vs. inorganic; small vs. large; flexible vs. rigid; spherical vs. irregular) that may affect the degree of membrane disruption.

4.2 EXPERIMENTAL

Liposome preparation

1,2-dimyristoyl-sn-glycero-3-phosphocholine was purchased from Avanti Lipids, Alabaster, AL. A 2 mg/ml suspension of small, unilamellar vesicles (SUVs) was prepared as follows. Fourteen (14) mg of the powdered DMPC was dissolved in approximately 1 mL of chloroform inside a 10 ml round bottom flask. The solvent was then evaporated using a rotary evaporator to form a thin lipid film. This film was hydrated by adding 0.1 M NaCl solution followed by shaking and sonication until the lipids were completely dissolved. The resulting large, multilamellar vesicles (LMVs) were broken down to SUVs by using a probe sonicator. The resulting suspension was placed in a bench-top centrifuge and spun at full speed for 20 minutes. The supernatant was removed and placed in another 2.5 mL glass vial. The resulting clear suspension was diluted further with 0.1 M NaCl solution to obtain a final lipid concentration of 2 mg/mL. Lipids solutions were further diluted with 0.1 NaCl as needed. All water used in the

experiments was ultrapure (type I) water. SUVs were used within one week of fabrication.

Sample Preparation

A drop of 1 mg/mL DMPC liposome suspension was placed on a 1 cm× 1 cm piece of freshly cleaved mica attached to a metal sample puck by double sided tape. After an incubation time of about 20 min, excess lipids were removed by gently rinsing with water. It is critical that the bilayer remain hydrated at all times. The sample was placed in the AFM and imaged under a water drop to confirm that a bilayer had formed and remained unchanged between subsequent images. Note that images were obtained in either tapping or AC mode. Nanoparticles were then introduced via a syringe onto the surface of the substrate. The volume introduced per injection was 20 μL. Subsequent images were captured showing the progression of the nanoparticles' effect on the model membrane.

Images were obtained using Veeco MultiMode IIIA and PicoPlus Molecular Imaging AFMs and were done so using their respective liquid cells and a syringe. Images were obtained in tapping and AC mode, respectively. Concentrations of nanoparticles are estimated based on volume of nanoparticles introduced to the liquid cell divided by the total volume of the appropriate liquid cell. Note that both mass and molar concentrations are given where appropriate for ease of comparison between particles.

Nanoparticles for Experiment

Nanoparticle	Number of e^+ at pH 7.2	Molecular weight (g/mol particle)	Physical Radius of Particle (nm)	Approximate Surface Area (nm^2)	Charge Density (e^+/surface area (nm^2))	Type of Interaction
MSI-78	9	2,640	1.1	15	0.6	Defect Eroder
TAT	50	33,000	2.5	79	0.6	Defect Inducer
PAMAM G3-NH_2	32	69	1.6	32	1	Surface Aggregator
PAMAM G5-NH_2	128	28,000	2.3	64	2.	Defect Eroder
PAMAM G7-NH_2	512	117,000	3.6	162	3.	Defect Inducer
G3-NH_2 Dendron	16	3,642	1	13	1.2	Defect Aggregator
PEI	14	78,220	3	110	0.1	Defect Inducer
DEAE-DEX	0.1	18,000	2	50	2×10^{-3}	Defect Inducer
Au-NH_2	80	87,800	2	50	1.5	Defect Eroder
Silica-NH_2	13,000	104,000,000	25	7,854	2	Defect Inducer

Table 4.1. Physical properties of nanoparticles used in this study.

MSI-78 (natural, net-positively charged protein)

MSI-78 (1a), a 22 amino acid protein with 9 of those residues positively charged at pH 7.2 was obtained from A. Ramamoorthy's Research Group (Department of Chemistry, University of Michigan) and dissolved in Millipore water. Approximately 20 uL of 30 mg/mL MSI-78 was injected onto a DMPC supported lipid bilayer (1b) yielding a final concentration of 1.2 mg/mL (450 nM) MSI-78. Subsequent images were (1c-1d) were taken over a period of 40 minutes.

TAT (natural, net positively charged protein)

TAT (2a), a 275 amino acid protein with 50 of those residues positively charged at pH 7.2, was obtained from C. Fierke's Research Group (Department of Chemistry, University of Michigan) and dissolved in Millipore water. Approximately 150 uL of 500 n*M* TAT protein was injected onto a DMPC supported lipid bilayer (2b) yielding a final concentration of ~300 n*M* TAT (10 ug/mL) TAT. Subsequent images (2c-2d) were taken over a period of 25 minutes.

PAMAM Dendrimers (flexible spherical synthetic polycationic polymer)

PAMAM dendrimers were purchased from Dendritech then purified and characterized by the Michigan Nanotechnology Institute for Medicine and Biological Sciences at the University of Michigan (Ann Arbor, MI) and dissolved in Millipore water. Approximated 25 n*M* of G3-NH_2(32) (3a), G5-NH_2(128) (3b), and G7-NH_2(256) (3c), were introduced to supported DMPC bilayers. This corresponds to 0.1 ug/mL (G3-NH_2), 0.7 ug/mL (G5-NH_2) and 3.0 ug/mL (G7-NH_2). Approximately 500 nM of pentanol core-based G3-NH_2(16) (3d) were introduced to supported DMPC bilayer. This corresponds to 0.04 ug/mL G3-NH_2 dendron. Subsequent images were taken over a period of 30-60 minutes. Note that the number of amines per PAMAM dendrimer is based on theoretical values.

PEI (irregular synthetic polycationic polymer)

PEI was purchased from Sigma Aldrich and dissolved in millipore water without any further purification. Approximately 20 uL of 1 ug/mL PEI (Mn: 78,220, PDI: 3.44) was injected onto a DMPC supported lipid bilayer (3a) yielding a final concentration of ~ 1 μg/mL PEI. Subsequent images (1c-1d) were taken over a period of 40 minutes.

DEAE-DEX (irregular synthetic polycationic polymer)

DEAE-DEX (2a) was purchased from Sigma Aldrich and dissolved in Millipore water without any further purification. Approximately 20 μL of 1 ug/mL DEAE-DEX (Mn: 18,490; PDI: 32.90) was injected onto a DMPC supported lipid (2b) bilayer yielding a final concentration of ~1 μg/mL DEAE-DEX. Subsequent images (2c-2d) were taken over a period of 90 minutes.

Au-NH_2 (small rigid inorganic sphere, surface modified with positive charges)

Au-NH_2 nanoparticles (5a) consisting of ~2 nm gold cores surface-modified with ~80 alkyl amines per particle (determined using potentiometric titration) yielding a final diameter of ~ 5 nm, were fabricated via standard procedure[19] by V. Rotello's research group and dissolved in Millipore water. Approximately 40 μL of 2.5 μM Au-NH_2 were injected onto a DMPC supported bilayer (5b) yielding a final concentration of 500 nM (44 μg/mL) Au-NH_2 nanoparticles. Subsequent images (5c-5d) were taken over a period of 30 minutes.

Si-NH_2 (large rigid inorganic sphere, surface modified with positive charges)

Si-NH_2 nanoparticles (6b) consisting of ~50 nm silica modified with ~13,000 amino groups (determined using potentiometric titration) with were obtained from G. Kisker GbR (Frankfurt, Germany) and dissolved in Millipore water. Approximately 60 uL of 10 mg/mL were injected onto a DMPC supported bilayer (6b) yielding a final concentration of 3 mg/mL (30 nM) Si-NH_2 nanoparticles. Subsequent images (6c-6d) were taken over a period of 45 minutes.

4.3 RESULTS AND DISCUSSION

Many small biological nanomaterials found in nature are capable of traversing cell membranes. Examples include MSI-78[35] and TAT.[36] The ability to penetrate cell membranes is not only advantageous for the host and virus, respectively, but potentially also a useful tool for scientists seeking to utilize these natural transportation systems for cellular delivery. The interaction between MSI-78 and the SLB was found to be concentration-dependent. At lower concentrations (~2 μg/mL), non-uniform membrane thinning of SLBs is observed.[24] At higher MSI-78 concentrations (1.2 mg/mL), the erosion of pre-existing holes in the lipid bilayer is found. (Figure 4.1) TAT, a larger protein in comparison to MSI-78, induces the formation of holes in the bilayer (Figure 4.2) at significantly lower concentrations than was required for MSI-78. These SLB studies are consistent with cell level studies that have shown both of these biological proteins are internalized,[36] and more indirectly, are capable of disrupting cell membranes.[9-12]

A variety of polymers have been used to mimic the ability of natural particles to breech cellular membranes. PAMAM dendrimers are highly charged spherical polymers that have been employed as transfection agents in drug delivery.[2, 12, 37, 38] Earlier studies by our group showed that the positively charged polymers interact with the supported lipid bilayer in a generation-defined dependent fashion.[25, 27] That is, G3-NH_2 dendrimers ($32e^+$) accumulate around the edges of pre-existing defects, while the more highly charged G5-NH_2 ($128e^+$) and G7-NH_2 ($512e^+$) expand pre-existing defects and form new defects, respectively (Figure 4.3b-d). In order to consider a change in topology while keeping a constant chemical composition, we now present the results for pentanol-core

G3-NH_2 dendrons ($16e^+$) (Figure 4.3a). The number of positive charges listed represent the theoretical number of amine terminal groups on each dendrimers, with all amine groups expected to be protonated.under the conditions employed[39, 40] Following addition to the SLB, G3-NH_2 dendrons were shown to both accumulate around the edges of pre-existing defects, as well as expand those defects. Two commonly utilized linear polycationic polymers, PEI and DEAE-DEX, have also previously been shown to induce the formation of nanoscale defects within the model membrane (Figure 4.4).[12] In these cases, however, no polymer accumulation around SLB defects was witnessed.

Given the wide range of rigid nanoparticles currently in use, two inorganic nanoparticles, Au-NH_2 and silica-NH_2, were selected for testing. Gold nanoparticles are perhaps the most well studied class of nanoparticles, and like dendrimers, have been utilized as transfection agents.[32] The versatility of gold nanoparticles both in their tunable size and functionality make them a convenient choice in examining the effect rigidity has on nanoparticle-membrane interaction. Experiments using 2 nm gold nanoparticles coated with an alkylamine substituent (total diameter: ~5-6 nm) show that supported lipid bilayers were disrupted primarily by expanding pre-existing defects. This is reminiscent of what was seen in the case of G5-NH_2.. Initially upon lipid erosion, the underlying mica surface is clean. However, after 6 min the Au-NH_2 nanoparticles, possibly aggregated with lipid, are observed to aggregate on the negatively charged mica. PEI and PAMAM dendrimers have also been observed to bind to the mica surface.[10, 12] These Au-NH_2-SLB interactions suggest that rigid-inorganic cores do not alter the gross nanoparticle-membrane interaction seen with the other classes of nanoparticles.

Although biology and thus nano-medicine primarily focuses on the 1-15 nm scale, the 50 nm size of the silica-NH_2 particles remain pertinent given industrial uses of

particles in this size range. Given the rigid inorganic core and amine-terminated surface, silica-NH_2 particles provide an example which is both significantly larger and does not contain a flexible, organic core. Despite these differences, the silica-NH_2 nanoparticles induced the formation of holes following addition to the supported lipid bilayer (Figure 4.6). This is similar to what was seen in the G7-NH_2 case.

Taking a broad view of these interactions, we note that the nanoparticles we studied can be divided into three subcategories: 1) particles that aggregate around defects and on the lipid bilayer surface (pentanol-core G3-NH_2 dendron, PAMAM G3-NH_2,) but are not effective at inducing defects 2) particles that encounter the surface, do not directly induce defects, but instead diffuse to existing and expand them (Au-NH_2, MSI-78, PAMAM G5-NH_2,) and 3) and particles that are capable of directly inducing defects in lipid bilayers (TAT, PAMAM G7-NH_2, PEI, DEAE-DEX and silica-NH_2). Based on these studies, cationic nanoparticles with quite different sizes, shapes and flexibility are all capable of disrupting SLBs in the nanomolar range.

When making qualitative comparisons between these particles, one must recall that the concentrations used for the imaging experiments differ so as to focus on the concentration range where the particles disrupt the bilayer. Keeping this in mind, we note that cationic charge density does not serve as a good predictor of the interaction across nanoparticle classes. However, the *surface area* of the cationic nanoparticle does roughly correlate with the degree of nanoparticle-lipid interaction. Those particles that have greater surface areas (> ~60 nm^2) are generally more effective at inducing SLB disruption than those with smaller surface area (< ~60 nm^2), while these latter particles were more likely to aggregate on the surface around pre-existing defects.

The results presented within this paper are consistent with several studies previously performed by other groups. A thermodynamic model describing the mechanism of interaction between PAMAM dendrimers, and more generally nanoparticles, and lipid bilayers has recently been completed by Ginzburg and Balijepalli.[41] Within the model it shown that charged nanoparticles with diameters comparable to that of a lipid bilayer show an increased tendencies to induce defect formation within lipid bilayers. Our results, as well as those of Ginzburg and Balijepalli, are also consistent with the observations of Oberdorster *et al.* who demonstrated that ultrafine particles (diameter ~20 nm) induce an increased inflammatory response over 'fine particles' (diameter ~250 nm) per unit mass.[42, 43] Here, Oberdorster *et al* attributed the origin of this difference to the larger ratio of surface to mass inherently present in ultrafine particles over fine particles.[42] Note that in the work of Oberdorster *et al.* surface area was defined per mass of sample, whereas for the work presented in this paper surface area is defined per particle. This difference in the definition of particle characteristics results in Oberdorster *et al.* concluding that for a given mass of sample that the smaller particles will be more disruptive. In this paper, surface area is defined per particle, resulting in the conclusion that for a given number of nanoparticles, the larger particles **(**r = 1.5-25 nm**)** which have greater surface area) are more disruptive. Note that with the exception of silica amine nanoparticles, also nanoparticles investigated within this study as well as the one presented by Ginzburg and Balijepalli fall within the ultrafine particle regime (r = 0-20 nm)**.** Although surface area is a general parameter for predicting how cationic nanoparticles interact with SLBs, the trends presented here indicate that it is not the only important parameter. The nanoparticle-SLB interactions

are likely also dependent on a *number* of other parameters including charge density, shape, and flexibility.

4.4 CONCLUSION

This results presented in this paper demonstrate that disruption of lipid bilayers is a common property of cationic nanoparticles. Each cationic nanoparticle presented here, regardless of shape (spherical vs. irregular), chemical composition (organic vs. inorganic), deformability (flexible vs. rigid), charge density, or size, disrupts supported lipid bilayers. Our previously published studies demonstrated that effectiveness of a particle in causing nanoscale disruption of supported lipid bilayers correlated well the particle's ability to both induce cell membrane permeability and to internalize into the cell.[10, 12, 13] The data presented here indicates that the hypothesis that nanoscale hole formation may be a biologically relevant process should be extended to a variety of additional materials including MSI-78, TAT, and cationic gold and silica particles. The generality of the bilayer disruption is extremely important because many examples of natural and synthetic nanoparticles utilize amine terminations to achieve water solubility and other functions. Given the growing use of nanoparticles in consumer products, industrial applications and in medicine, it is imperative that we understand observed and potential effects of nanoparticles on biological membranes and the basic science underpinning these interactions.

4.5 FIGURES

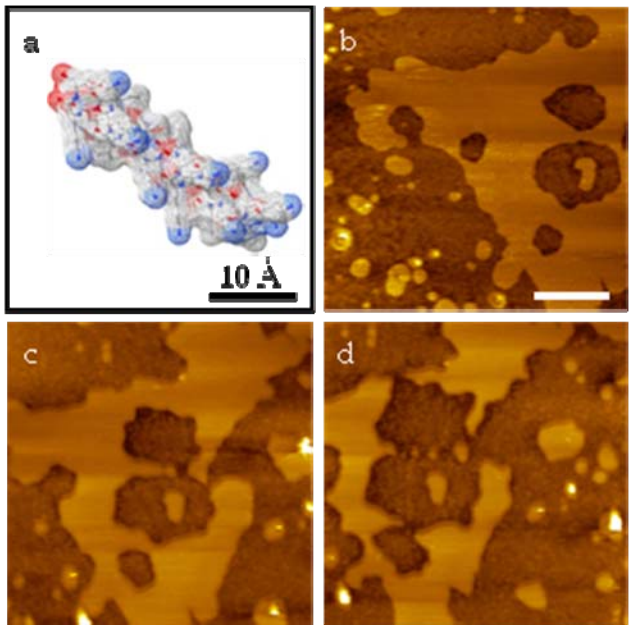

Figure 4.1a-d. (1a). Space filling model of MSI-78, a 22 amino acid protein with 9 of those residues positively charged at pH 7.2. MSI-78 were injected onto a DMPC lipid bilayer (1b) resulting in a final concentration of ~450 nM (1.2 mg/mL) MSI-78. Subsequent images over ~40 minutes were obtained (1c-d) which showed the removal of lipid, primarily through the expansion of pre-existing defects as seen with G5-NH2 dendrimers. Note that the perimeter surrounding the defects is ~1 nm thinner then the full lipid bilayer (~5 nm). This 'thinning effect' is consistent with what had been previously shown at lower concentration of MSI-78 (2 µg/mL) and suggests that the thinning of the bilayer precedes full removal of lipid. Scale bar is 500 nm.

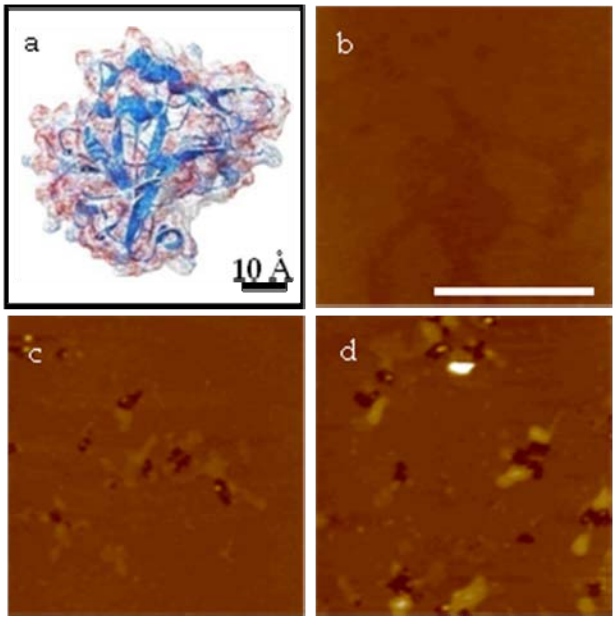

Figure 4.2a-d. (4.2a) Space-filling model of TAT, a 275 amino acid protein with 50 of those residues positively charged at pH 7.2. TAT protein was injected onto a DMPC lipid bilayer (4.2b) yielding a final concentration of 300 nN (10 μg/mL) TAT. Subsequent images (4.2c-d) taken over a period of 20 minutes showed the formation and expansion of defects in the bilayer. Scale bar is 500 nm.

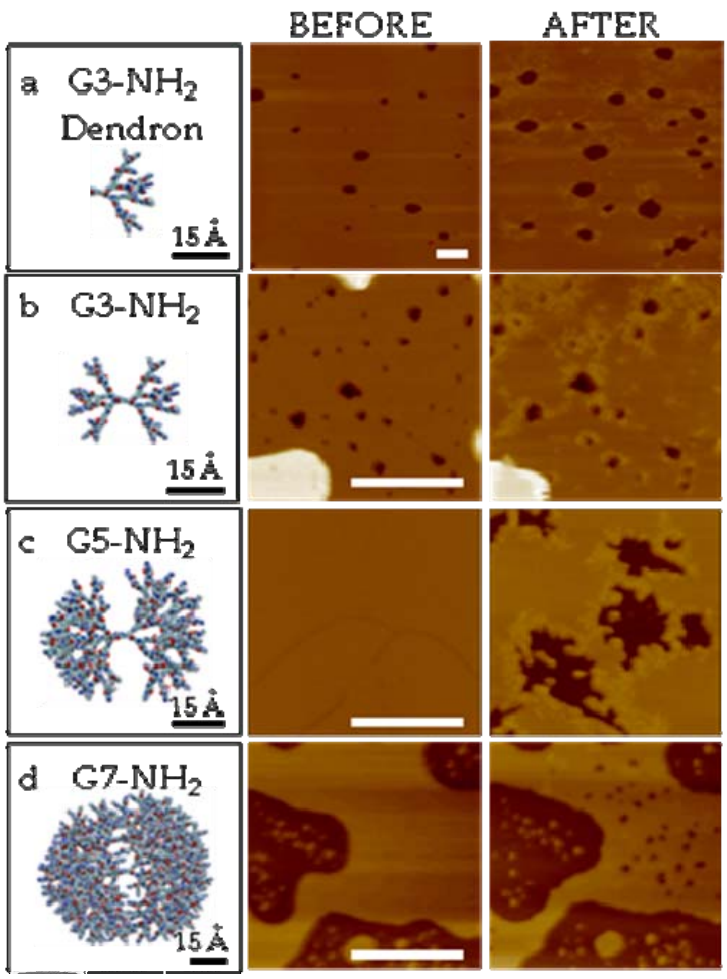

Figure 4.3a-d (4.3a) G3-NH_2 dendron ($16e^+$) primarily expanding pre-existing defects, eventually accumulating around the edges (4.3b) G3-NH_2 ($32e^+$) accumulated around the edges of pre-existing defects (4.3c) G5-NH_2 ($128e^+$) primarily expanded pre-existing defects, eventually accumulating around the edges and (4.3d) G7-NH_2 (512 e^+) primarily induced the formation of defects on lipid terraces. (4.3a) G3-NH_2 dendron concentration was ~100 nM (G3-NH_2 dendron = 0.04 µg/mL). Dendrimer concentrations used were ~25 nM (4.3b-d) (G3-NH_2 = 0.01 µg/mL; G5-NH_2 = 0.07 µg/mL; G7-NH_2 = 3 µg/mL. Scale bars are 500 nm. (Dendrimer work was completed by Almut Mecke).

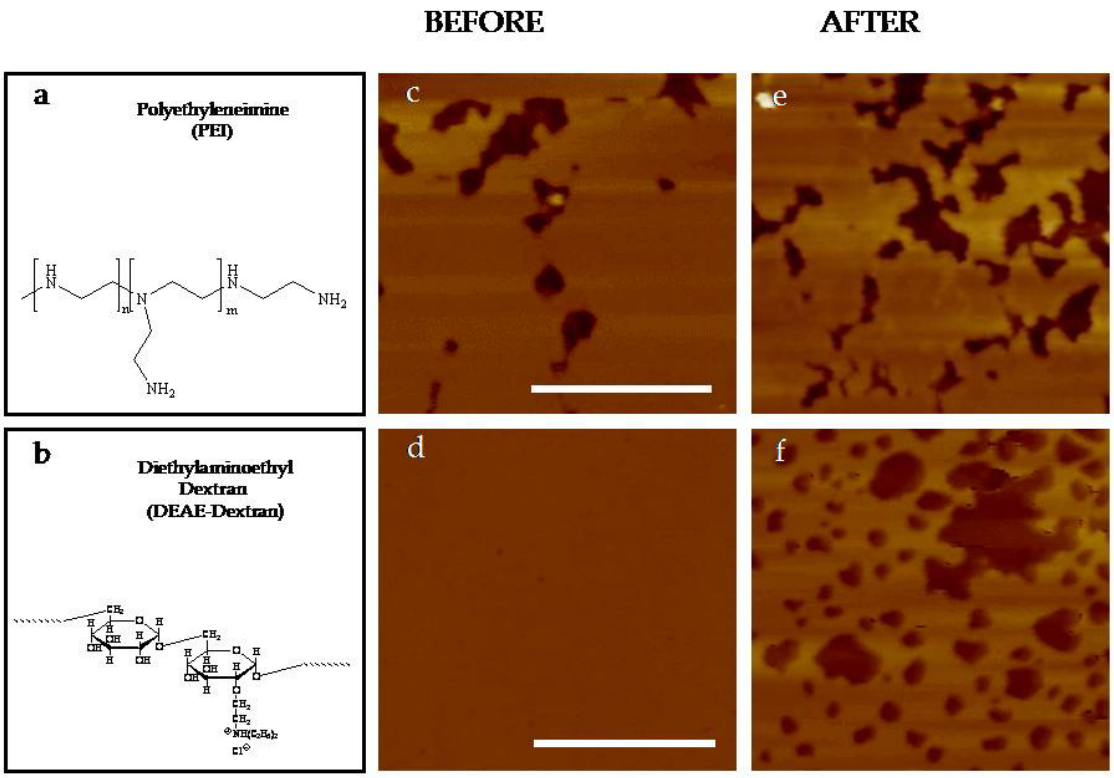

Figure 4.4a-d. PEI (M_w: 78,220, PDI: 3.44, d = 6.6 nm) and DEAE-DEX (M_w: 18,490; PDI: 3.290, d = 4.2 nm) were injected onto DMPC supported lipid bilayers (4.4c and 4.4d, respectively) yielding a final concentration of 1 µg/mL polymer in both cases. Images following injection showed that PEI expanded pre-existing defects (4.4e) similar to what was seen with the G5-NH2 while DEAE-DEX induced thinning of the bilayer similar to what was seen with MSI-78 at low concentration (4.4d). Note that diameters were based on the M_w values and assuming a spherical shape with a density of 1.0 g/cm^3. Scale bars are 500 nm.

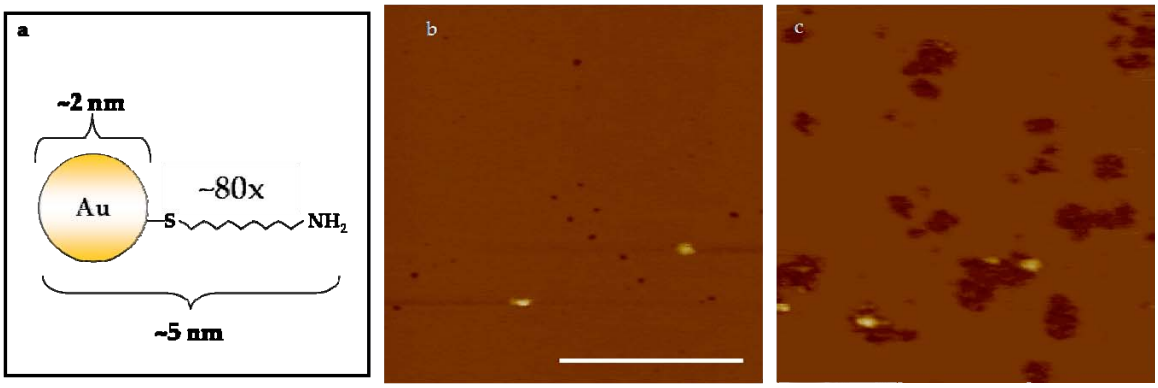

Figure 4.5a-c. Au-NH_2 nanoparticles (4.5a) were injected onto a DMPC supported lipid bilayer (4.5b) yielding a final concentration of ~500 nM (44 µg/mL) Au-NH_2. The Au-NH_2 nanoparticles expanded pre-existing defects within the supported lipid bilayer and appeared to aggregate on the mica surface (4.5c) Scale bar is 500 nm.

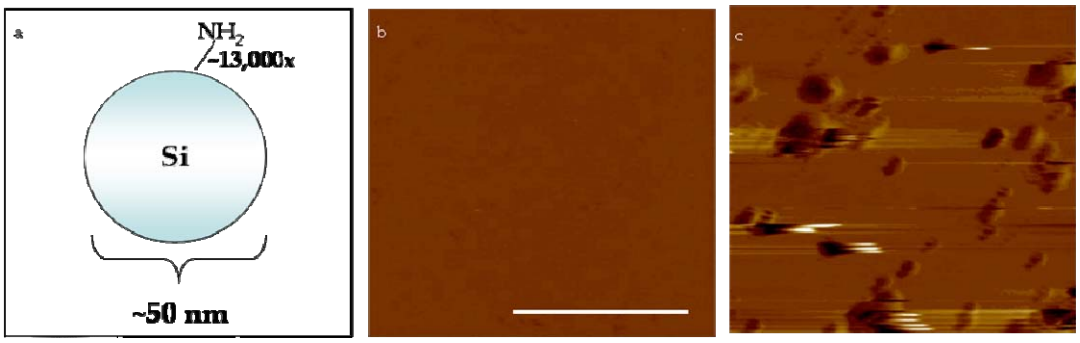

Figure 4.6a-c. 50 nm amine coated silica spheres (~13,000 NH_2/sphere) (4.6a) were introduced onto a DMPC lipid bilayer (4.6b) yielding a final concentration of ~3 mg/mL (30 nM) of the silica spheres. The addition of the positively charged spheres resulted in the formation of circular defects on the bilayer ranging from 20-150 nm in diameter (4.6c). The formation of the new defects within the bilayer is similar to what was seen with G7-NH_2 PAMAM dendrimers. Scale bar is 500 nm.

REFERENCES 4.6

1. Popielarski, S. R.; Pun, S. H.; Davis, M. E., A nanoparticle-based model delivery system to guide the rational design of gene delivery to the liver. 1. Synthesis and characterization. *Bioconjugate Chemistry* **2005,** 16, (5), 1063-1070.

2. Bielinska, A. U.; Yen, A.; Wu, H. L.; Zahos, K. M.; Sun, R.; Weiner, N. D.; Baker, J. R.; Roessler, B. J., Application of membrane-based dendrimer/DNA complexes for solid phase transfection in vitro and in vivo. *Biomaterials* **2000,** 21, (9), 877-887.

3. Bell, A. T., The impact of nanoscience on heterogeneous catalysis. *Science* **2003,** 299, (5613), 1688-1691.

4. Allen, N. S.; Edge, M.; Ortega, A.; Liauw, C. M.; Stratton, J.; McIntyre, R. B., Behaviour of nanoparticle (ultrafine) titanium dioxide pigments and stabilisers on the photooxidative stability of water based acrylic and isocyanate based acrylic coatings. *Polymer Degradation and Stability* **2002,** 78, (3), 467-478.

5. Luppi, B.; Cerchiara, T.; Bigucci, F.; Basile, R.; Zecchi, V., Polymeric nanoparticles composed of fatty acids and polyvinylalcohol for topical application of sunscreens. *Journal of Pharmacy and Pharmacology* **2004,** 56, (3), 407-411.

6. Maynard, A. D.; Kuempel, E. D., Airborne nanostructured particles and occupational health. *Journal Of Nanoparticle Research* **2005,** 7, (6), 587-614.

7. Magrez, A.; Kasas, S.; Salicio, V.; Pasquier, N.; Seo, J. W.; Celio, M.; Catsicas, S.; Schwaller, B.; Forro, L., Cellular toxicity of carbon-based nanomaterials. *Nano Letters* **2006,** 6, (6), 1121-1125.

8. Xia, T.; Kovochich, M.; Brant, J.; Hotze, M.; Sempf, J.; Oberley, T.; Sioutas, C.; Yeh, J. I.; Wiesner, M. R.; Nel, A. E., Comparison of the abilities of ambient and manufactured nanoparticles to induce cellular toxicity according to an oxidative stress paradigm. *Nano Letters* **2006,** 6, (8), 1794-1807.

9. Fischer, D.; Li, Y. X.; Ahlemeyer, B.; Krieglstein, J.; Kissel, T., In vitro cytotoxicity testing of polycations: influence of polymer structure on cell viability and hemolysis. *Biomaterials* **2003,** 24, (7), 1121-1131.

10. Hong, S. P.; Bielinska, A. U.; Mecke, A.; Keszler, B.; Beals, J. L.; Shi, X. Y.; Balogh, L.; Orr, B. G.; Baker, J. R.; Holl, M. M. B., Interaction of poly(amidoamine) dendrimers with supported lipid bilayers and cells: Hole formation and the relation to transport. *Bioconjugate Chemistry* **2004,** 15, (4), 774-782.

11. Hussain, S. M.; Hess, K. L.; Gearhart, J. M.; Geiss, K. T.; Schlager, J. J., In vitro toxicity of nanoparticles in BRL 3A rat liver cells. *Toxicology in Vitro* **2005,** 19, (7), 975-983.

12. Hong, S. P.; Leroueil, P. R.; Janus, E. K.; Peters, J. L.; Kober, M. M.; Islam, M. T.; Orr, B. G.; Baker, J. R.; Holl, M. M. B., Interaction of polycationic polymers with supported lipid bilayers and cells: Nanoscale hole formation and enhanced membrane permeability. *Bioconjugate Chemistry* **2006,** 17, (3), 728-734.

13. Leroueil, P. R.; Hong, S. Y.; Mecke, A.; Baker, J. R.; Orr, B. G.; Holl, M. M. B., Nanoparticle interaction with biological membranes: Does nanotechnology present a janus face? *Accounts of Chemical Research* **2007,** 40, (5), 335-342.

14. Monteiro-Riviere, N. A.; Nemanich, R. J.; Inman, A. O.; Wang, Y. Y. Y.; Riviere, J. E., Multi-walled carbon nanotube interactions with human epidermal keratinocytes. *Toxicology Letters* **2005,** 155, (3), 377-384.

15. Oberdorster, E., Manufactured nanomaterials (Fullerenes, C-60) induce oxidative stress in the brain of juvenile largemouth bass. *Environmental Health Perspectives* **2004,** 112, (10), 1058-1062.

16. Oberdorster, E.; Cheek, A. O., Gender benders at the beach: Endocrine disruption in marine and estuarine organisms. *Environmental Toxicology and Chemistry* **2001,** 20, (1), 23-36.

17. Oberdorster, G.; Gelein, R. M.; Ferin, J.; Weiss, B., Association of Particulate Air-Pollution and Acute Mortality - Involvement of Ultrafine Particles. *Inhalation Toxicology* **1995,** 7, (1), 111-124.

18. Tinkle, S. S.; Antonini, J. M.; Rich, B. A.; Roberts, J. R.; Salmen, R.; DePree, K.; Adkins, E. J., Skin as a route of exposure and sensitization in chronic beryllium disease. *Environmental Health Perspectives* **2003,** 111, (9), 1202-1208.

19. Goodman, C. M.; McCusker, C. D.; Yilmaz, T.; Rotello, V. M., Toxicity of gold nanoparticles functionalized with cationic and anionic side chains. *Bioconjugate Chemistry* **2004,** 15, (4), 897-900.

20. Ottaviani, M. F.; Sacchi, B.; Turro, N. J.; Chen, W.; Jockusch, S.; Tomalia, D. A., An EPR study of the interactions between starburst dendrimers and polynucleotides. *Macromolecules* **1999,** 32, (7), 2275-2282.

21. Kapoor, S.; Kartha, S.; Meisel, D., EPR and pulse radiolysis studies on electron transfer in transition metal dithiolenes at the surface of colloidal TiO2. *Research on Chemical Intermediates* **2001,** 27, (4-5), 317-332.

22. Heller, W. T.; Waring, A. J.; Lehrer, R. I.; Harroun, T. A.; Weiss, T. M.; Yang, L.; Huang, H. W., Membrane thinning effect of the beta-sheet antimicrobial protegrin. *Biochemistry* **2000,** 39, (1), 139-145.

23. Mecke, A.; Lee, D. K.; Ramamoorthy, A.; Orr, B. G.; Holl, M. M. B., Synthetic and natural polycationic polymer nanoparticles interact selectively with fluid-phase domains of DMPC lipid bilayers. *Langmuir* **2005,** 21, (19), 8588-8590.

24. Mecke, A.; Lee, D. K.; Ramamoorthy, A.; Orr, B. G.; Holl, M. M. B., Membrane thinning due to antimicrobial peptide binding: An atomic force microscopy study of MSI-78 in lipid bilayers. *Biophysical Journal* **2005,** 89, (6), 4043-4050.

25. Mecke, A.; Uppuluri, S.; Sassanella, T. M.; Lee, D. K.; Ramamoorthy, A.; Baker, J. R.; Orr, B. G.; Holl, M. M. B., Direct observation of lipid bilayer disruption by poly(amidoamine) dendrimers. *Chemistry and Physics of Lipids* **2004,** 132, (1), 3-14.

26. Livadaru, L.; Kovaenko, A., Fundamental mechanism of translocation across liquidlike membranes: Toward control over nanoparticle behavior. *Nano Letters* **2006,** 6, (1), 78-83.

27. Mecke, A.; Majoros, I. J.; Patri, A. K.; Baker, J. R.; Holl, M. M. B.; Orr, B. G., Lipid bilayer disruption by polycationic polymers: The roles of size and chemical functional group. *Langmuir* **2005,** 21, (23), 10348-10354.

28. Spurlin, T. A.; Gewirth, A. A., Poly-L-lysine-induced morphology changes in mixed anionic/zwitterionic and neat zwitterionic-supported phospholipid bilayers. *Biophysical Journal* **2006,** 91, (8), 2919-2927.

29. Nigavekar, S. S.; Sung, L. Y.; Llanes, M.; El-Jawahri, A.; Lawrence, T. S.; Becker, C. W.; Balogh, L.; Khan, M. K., H-3 dendrimer nanoparticle organ/tumor distribution. *Pharmaceutical Research* **2004,** 21, (3), 476-483.

30. Drin, G.; Cottin, S.; Blanc, E.; Rees, A. R.; Temsamani, J., Studies on the internalization mechanism of cationic cell-penetrating peptides. *Journal of Biological Chemistry* **2003,** 278, (33), 31192-31201.

31. Richard, J. P.; Melikov, K.; Vives, E.; Ramos, C.; Verbeure, B.; Gait, M. J.; Chernomordik, L. V.; Lebleu, B., Cell-penetrating peptides - A reevaluation of the mechanism of cellular uptake. *Journal of Biological Chemistry* **2003,** 278, (1), 585-590.

32. Sandhu, K. K.; McIntosh, C. M.; Simard, J. M.; Smith, S. W.; Rotello, V. M., Gold nanoparticle-mediated Transfection of mammalian cells. *Bioconjugate Chemistry* **2002,** 13, (1), 3-6.

33. Mori, H.; Lanzendorfer, M. G.; Muller, A. H. E.; Klee, J. E., Organic-inorganic nanoassembly based on complexation of cationic silica nanoparticles and weak anionic polyelectrolytes in aqueous and alcohol media. *Langmuir* **2004,** 20, (5), 1934-1944.

34. Bagwe, R. P.; Hilliard, L. R.; Tan, W. H., Surface modification of silica nanoparticles to reduce aggregation and nonspecific binding. *Langmuir* **2006,** 22, (9), 4357-4362.
35. Fuchs, P. C.; Barry, A. L.; Brown, S. D., In vitro antimicrobial activity of MSI-78, a magainin analog. *Antimicrobial Agents and Chemotherapy* **1998,** 42, (5), 1213-1216.

36. Fawell, S.; Seery, J.; Daikh, Y.; Moore, C.; Chen, L. L.; Pepinsky, B.; Barsoum, J., TAT-mediated delivery of heterologous proteins into cells. *Proceedings of the National Academy of Sciences of the United States of America* **1994,** 91, (2), 664-668.

37. Shukla, R.; Thomas, T. P.; Peters, J. L.; Desai, A. M.; Kukowska-Latallo, J.; Patri, A. K.; Kotlyar, A.; Baker, J. R., HER2 specific tumor targeting with dendrimer conjugated anti-HER2 mAb. *Bioconjugate Chemistry* **2006,** 17, (5), 1109-1115.

38. Thomas, T. P.; Patri, A. K.; Myc, A.; Myaing, M. T.; Ye, J. Y.; Norris, T. B.; Baker, J. R., In vitro targeting of synthesized anti body-conjugated dendrimer nanoparticles. *Biomacromolecules* **2004,** 5, (6), 2269-2274.

39. Majoros, I. J.; Myc, A.; Thomas, T.; Mehta, C. B.; Baker, J. R., PAMAM dendrimer-based multifunctional conjugate for cancer therapy: Synthesis, characterization, and functionality. *Biomacromolecules* **2006,** 7, (2), 572-579.

40. Majoros, I. J.; Thomas, T. P.; Mehta, C. B.; Baker, J. R., Poly(amidoamine) dendrimer-based multifunctional engineered nanodevice for cancer therapy. *Journal of Medicinal Chemistry* **2005,** 48, (19), 5892-5899.

41. Ginzburg, V. V.; Balijepalli, S., Modeling the Thermodynamics of the Interaction of Nanoparticles with Cell Membranes. *Nano Letters* **2007,** 7, (12), 3716-3722.

42. Oberdorster, G., Pulmonary effects of inhaled ultrafine particles. *International Archives of Occupational and Environmental Health* **2001,** 74, (1), 1-8.

43. Oberdorster, G.; Oberdorster, E.; Oberdorster, J., Nanotoxicology: An emerging discipline evolving from studies of ultrafine particles. *Environmental Health Perspectives* **2005,** 113, (7), 823-839.

CHAPTER 5

THE IMPORTANCE OF SUPRAMOLECULAR STRUCTURE FOR NANOPARTICLE FUNCTION

5.1 BACKGROUND

The nanoparticles investigated in the previous chapters are formed through covalent linkages of their respective sub-parts. In this **Chapter 5**, we examine the interaction of a type of charged, non-covalently linked 'nanoparticles' called micelles. Above critical micelle concentration (CMC), detergent molecules self-assemble to form micelles which are regular structure similar in size to those nanoparticles investigated in **Chapters 3-4**. Within this chapter we use atomic force microscopy (AFM) to address, on a nanoscale level, the behavior of two common ionic detergents as individual molecules (below CMC), as well as in their supramolecular micelle forms (above CMC). The two species discussed, the negatively charged sodium dodecylsulfate (SDS, $C_{12}H_{25}SO_4Na$, CMC = 7-10 mM) and the positively charged cetyltrimethylammonium bromide (CTAB, $C_{16}H_{33}N(CH_3)_3Br$, CMC = 1mM), were chosen because they are well documented to disrupt biological membranes above CMC.[1] Like the covalently linked nanoparticles investigated in the previous chapters, we find that the above CMC charged detergents SDS and CTAB remove lipid from SLBs. Interestingly, pre-existing defects within the SLBs are occluded when these same detergents are introduced at concentrations below their respective CMCs. This chapter shows that non-covalently linked nanoparticles

induce defects within model cell membranes similar to covalently-linked charged nanoparticles.

The ashen-fat used by the ancient Babylonians to remove mud from their clothes is not far removed from the present-day detergents we purchase at the local drug store. Indeed, the mechanism by which hydrophobic materials are removed can be explained in a simple fashion: the hydrocarbon chain of the detergent molecule interacts with the hydrophobic material and the resulting composite is made soluble in water by the presence of the detergent's hydrophilic head. However, this explanation masks the fact that these molecules function via a supramolecular organization that generates an active form, called a micelle, which is on the order of tens of nanometers in size. The ratio of the hydrophobic tail length to hydrophilic head area is the primary parameter that determines the size of the micelle and the critical micelle concentration (CMC).[1] Below CMC, the surfactant molecules are present as individual molecules in solution. At the CMC, it becomes energetically favorable for the amphiphilic molecules to arrange themselves into structures such as spherical micelles and, at higher concentrations, rod-like structures. These ordered, nanoscale micelles and rods are the active form of the detergent that dissolves oils and other biological entities including membrane components such as proteins and lipids.[2]

Previous studies have examined the activity of various detergents both below and above CMC in the presence of lipid vesicles[3-6] and supported lipid bilayers.[4, 5, 7] Below CMC, single detergent molecules incorporate into the lipid domain, decreasing surface tension and enlarging the previously lipid-only domain.[2, 4, 5, 7, 8] Above CMC, the detergent removes the lipid either by an exchange of detergent molecules between the

detergent micelle and lipid domain, or by encapsulation of the lipid by the detergent micelle. This set of experimental observations has been further supported by a theoretical analysis that described the interaction as primarily a function of CMC and the equilibrium partition coefficient.[9] The majority of studies to date employed methods which sample macroscopic volumes such as light scattering,[10-12] nuclear magnetic resonance (NMR),[13, 14] radio tracers[15] and isothermal titration calorimetry,[10, 16, 17] and were thus unable to make measurements with nanoscale resolution regarding the detergent insertion or erosion process. Recently, Morandant and Kirat published an AFM study of the interaction of Triton X-100 with mixed dioleoylphosphatidylcholine/dipalmitoylphosphatidylcholine (DOPC/DPPC) supported lipid bilayers on mica.[7] Triton X-100 (polyoxoethylene(10) isooctylphenyl ether, 4-$(C_8H_{17})C_6H_4(OCH_2CH_2)_nOH$ [n = ~10]) is a non-ionic detergent that is highly effective at disrupting biological membranes. In their study, they noted that below CMC Triton X-100 inserted into the lipid bilayer but did not dissolve it, while above CMC, the detergent preferentially dissolved the liquid-phase DOPC regions as compared to the gel-phase DPPC regions. Not only does this demonstrate that form affects function (i.e., single molecule vs. micelle), and that lipid phase further mediates this function, it raises additional questions regarding the effect of detergent charge. In particular, how does head group charge affect the interaction between lipid and detergent, both in the single-molecule and micelle form?

5.2 EXPERIMENTAL

5.2.1 Materials

Sodium dodecyl sulfate (SDS) and cetyltrimethyl ammonium bromide (CTAB) were purchased from Sigma-Aldrich. Solutions of SDS and CTAB above and below their respective CMCs were made using deionized water. The CMCs for SDS and CTAB are 7-10 mM and 1 mM, respectively.[1]

Images were obtained using either a Nanoscope IIIa MultiMode Scanning Probe Microscope (Veeco, Santa Barbara, CA) or a PicoPlus instrument (Molecular Imaging, Tempe, AZ). Imaging was completed using the appropriate liquid cell for each instrument. Silicon nitride cantilevers (NPS (Veeco), spring constant 0.32 N/m) were used at a drive frequency of 6-12 kHz.

5.2.2 Imaging

A 1 mg/mL suspension of small, unilamellar vesicles (SUVs) were prepared as previously reported.[18] 60-80 μL of the DMPC liposome suspension was placed on a 1 cm × 1 cm piece of freshly cleaved mica attached to a metal sample puck by double sided tape. After an incubation period of about 20 min, excess lipids were removed by gently rinsing with deionized water. The sample was placed in the AFM and imaged to confirm that a bilayer had formed. After it was determined the bilayer was stable (i.e., remained unchanged over a period of ~10 minutes), detergent was introduced via a syringe onto the surface of the lipid bilayer. Final concentration of detergent within the liquid was estimated based on the molarity of the detergent introduced to the liquid cell divided by the total volume of the appropriate liquid cell. Imaging was performed at 24-25°C. Under our imaging conditions, the lipids imaged were in the liquid crystalline phase as evidenced by the presence, and subsequent disappearance, of the gel crystalline phase during the ~10 minute stabilization period.

5.2.3 Image Analysis

Height analysis was completed using each instrument's respective software and exported as JPEGs. All images (with the exception of Figures 3a and 3b) are displayed on a 20 nm scale. The contrast of Figures 1c and 1d was enhanced using Photoshop to yield Figures 3a and 3b. This was done to enable the reader to more easily distinguish the lipid-detergent boundaries. Root-mean squared (RMS) roughness values were calculated using the imaging software, Gywddion.

5.3 RESULTS AND DISCUSSION

Concentrations of detergent were selected below CMC so that the effects of detergent molecules could be studied in the absence of micelles. When SDS below CMC was introduced to a DMPC supported lipid bilayer (SLB), (Figure 1a), pre-existing defects were filled (Figure 1b-d). The occluded regions possess an identical height and an equivalent root-mean square (RMS) roughness to that measured on the bilayer regions before and after SDS introduction. When CTAB below CMC was introduced to a supported DMPC lipid bilayer, (Figure 2a), the pre-existing defects were once again filled (Figure 2b-d). In contrast to SDS, the CTAB occluded region is ~ 1 nm thinner than the lipid bilayer and differed in RMS roughness. Both SDS and CTAB occlude the pre-existing defects in the DMPC SLB and maintain a distinguishable perimeter identical in shape to the original bilayer defect.

To highlight the existence of the persistent boundary between the occluded region and the lipid bilayer, a magnified view of the filling of a single defect is provided for both SDS and CTAB (Figures 3a and 3b, respectively). In both cases, it is clear that the defect

occluded while maintaining the distinct boundary of the original defect perimeter. The defects appear to occlude by initial interaction of the detergent with the defect edge followed by filling to the center. For both SDS and CTAB, the height and the RMS roughness of the occluded region remains constant during the entire filling process. If mixing between lipid and detergent were occurring, we would have expected the original defect perimeter to disappear. Furthermore, if mixing was occurring during the filling process, we would have expected the measured height and/or RMS roughness to vary, particularly for CTAB occlusion where a ~ 1 nm difference in height is observed. However, neither the disappearance of the perimeter nor varying occlusion height was observed over the time scale of these experiments.

Based upon the measured height of the occluded regions, it appears that detergent molecules fill the pre-existing membrane defects with a bilayer of detergent. This is consistent with the models of occlusion structure proposed in Fig. 7a for SDS and Fig. 7b for CTAB. Interestingly, this observation differs from the *uniform* intercalation of detergent into lipid vesicles and lipid bilayers that has been proposed previously.[5, 8, 9, 13] These earlier conclusions were reached based on a variety of bulk techniques including light scattering,[10] and nuclear magnetic resonance.[13] The previous AFM studies, which concluded that detergent partitioned directly into the lipid bilayer, differed in that the published images do not have pre-existing defects present and the detergent employed was not charged.[7] Unlike the previous AFM studies employing non-ionic detergent, we did not observe swelling of the lipid bilayer. This is additional evidence that charged detergent molecules do not partition into the bilayer over the time scale of these experiments. The results highlighted in Figures 1 and 2 indicate that non-uniform

distribution of detergent is possible and that the lipid bilayer can even template the detergent into a bilayer structure. The C12 methylene chain of SDS should be sufficient to provide a bilayer of equivalent thickness to DMPC. It is perhaps surprising that the C16 chain of CTAB results in a 1 nm thinner bilayer. This suggests that the CTAB bilayer is partially interdigitated or has a substantial tilt angle. Another possible interpretation for the occluded regions would involve an admixture of detergent and lipid. The AFM data does not directly address the composition of the occlusions and based upon the data presented this alternative cannot be ruled out. However, we believe the persistence of the perimeter, consistency of the occlusion height and uniform RMS roughness provide substantial evidence against the mixed lipid/detergent hypothesis.

Experiments were also carried out with concentrations of detergent above the CMC such that SDS and CTAB would be in the form of nanoscale micelles. When SDS above CMC was introduced to a DMPC bilayer with pre-existing defects, lipid was removed thus increasing the number of 5 nm deep defects present (Figure 4a). When CTAB above CMC was introduced to a similar DMPC bilayer, the perimeter of the pre-existing bilayer defects grew large (Figure 4b). However, the depth of the defects changes to 2.5 nm. In order to probe the origin of this change in defect depth, SDS above CMC was added to the CTAB-lipid sample, resulting in the formation of the 5 nm depth expected for defects in a DMPC bilayer (Figure 5). This served as confirmation that the initial measured 2.5 nm defects were not the result of an overall decrease in the bilayer height, but instead the result of a 2.5 nm coating atop the mica inside the defect. In previous studies, we have noted that polycationic polymers will coat mica inside a lipid bilayer defect.[19] By analogy, we considered two possible models to explain the presence

of a 2.5 nm mica coating leading to an observed 2.5 nm defect in the lipid bilayer: (1) a monolayer of CTAB with positively charged head-group bound to the negatively charged mica and alkyl chains pointing into the water and (2) an interdigitated CTAB bilayer with charge head-groups bound to mica and directed toward the water (as shown in Figure 7d). In order to better understand the structure of the 2.5 nm layer coating the mica, we performed two experiments. First, we deposited a water solution of CTAB above CMC onto mica and observed 2.5 nm high regions (Figure 6). These have been previously characterized as interdigitated, tilted bilayers of CTAB.[20] This firmly established that a 2.5 nm coating of CTAB on mica, and by extension a 2.5 nm defect in DMPC filled with CTAB, is consistent with the data illustrated in **Figure 5.4b**, and was a reasonable hypothesis. Second, we performed a contact angle experiment with a 2.5 nm coating of CTAB on mica and found complete wetting by water. The results of these experiments are consistent with model (2) as depicted in **Figure 5.7d**. The wetting experiments are inconsistent with the presence of a monolayer of CTAB with the alkyl chains oriented away from the surface as required by the AFM height measurement. It is possible that the negative charge of the mica substrate chosen may have influenced the behavior of the charged detergents. Indeed, it is likely that the electrostatic interaction between the positively charged moiety of the CTAB molecule and the negatively charged mica substrate is responsible for CTAB's tendency to remain on the mica substrate. Despite having opposing charges, both detergents nonetheless interacted with the SLB in very similar fashions. This indicates that both the occlusion and erosion interactions observed are common properties of charged detergents.

Despite the similarity in behavior between these self-aggregated micelles and the covalently linked nanoparticles, it is not clear that their respective mechanisms of lipid removal are the same. As discussed in the beginning of this chapter, detergent micelles remove lipid either by an exchange of detergent molecules between the detergent micelle and lipid domain, or by encapsulation of the lipid by the detergent micelle. Clearly, no such exchange occurs during lipid removal by the covalently-linked nanoparticles. However, lipid may bind to the surface of the charged nanoparticle, integrating itself within the nanoparticle structure as shown below **(Figure 5.8).** Using a PAMAM dendrimer as example, we see that this structure vaguely resembles a mixed lipid-detergent micelle **(Figure 5.8).** One can imagine that larger nanoparticles would be more effective at removing lipid than smaller nanoparticles at equimolar concentrations because of the additional space available for the lipid molecules to bind. A trend showing increased hole formation activity with increased nanoparticle size has been shown by Hong *et al* using PAMAM dendrimers, and is consistent with this argument.[21] However, there is also evidence for an optimal nanoparticle size for lipid removal which runs contrary to this argument.[22] More detailed mechanistic studies examining the removal lipid by nanoparticles must be completed before mechanistic analogies such as these are given serious credence. These studies, in the form of atomistic simulations using PAMAM dendrimers and DMPC SLBs, are currently being undertaken by CV Kelly.

5.4 CONCLUSIONS

In this chapter, two major observations are presented. First, solutions of charged detergents below CMC, as exemplified by SDS and CTAB, did not erode, insert into, and/or induce holes in DMPC supported lipid bilayers over the ~10 minute time scale of the experiments. However, the defects present were occluded by the detergent. Second, solutions of charged detergents above CMC did erode lipid bilayers over a ~ 10 minute time scale. The defects formed in the SLBs by these non-covalently linked nanoparticles were very similar to those defects formed by the more traditional nanoparticles investigated in **Chapters 3-4.** This shows that non-covalent aggregations of charged material are capable of inducing defects within cell membranes.

5.5 FIGURES

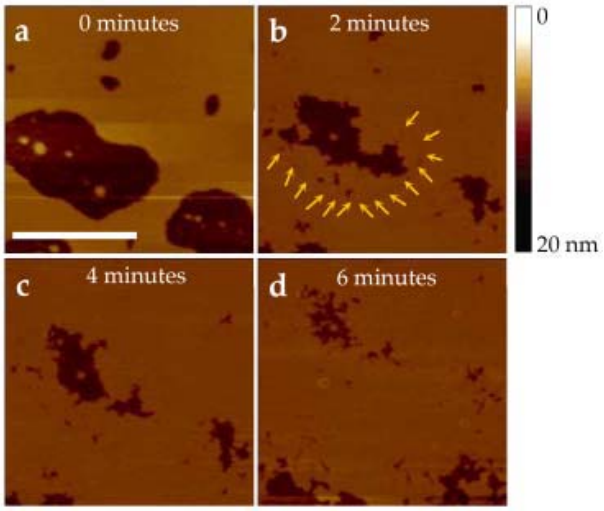

Figure 5.1. SDS below CMC (0.04 mM) introduced to DMPC mica-SLB with pre-existing defects. **(a)** Image before SDS addition. **(b-d)** Images post SDS addition. Arrows highlight lipid-detergent boundary. Scale bar 500 nm.

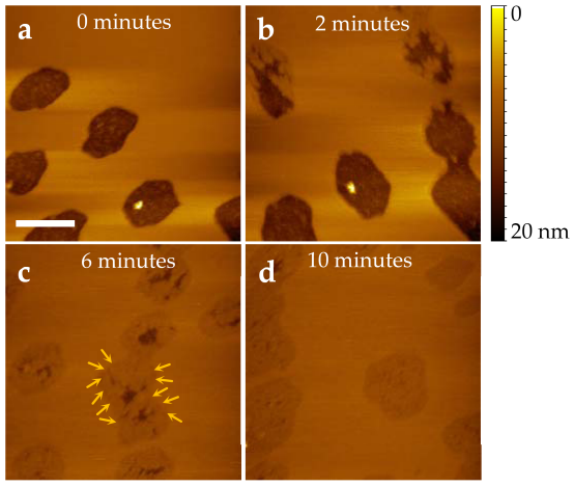

Figure 5.2. CTAB below CMC (0.1 mM) introduced to DMPC mica-SLB with pre-existing defects. (a) Image before SDS addition. (b-d) Images post CTAB addition. Arrows highlight lipid-detergent boundary. Scale bar 500 nm

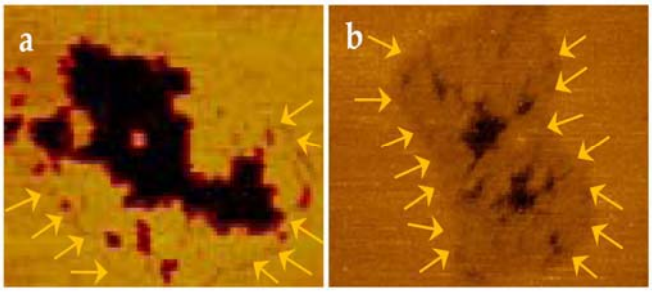

Figure 5.3. Zoomed in image of **(a)** ***1c*** and **(b)** ***2c*** highlighting persistent lipid-detergent boundaries for SDS and CTAB, respectively.

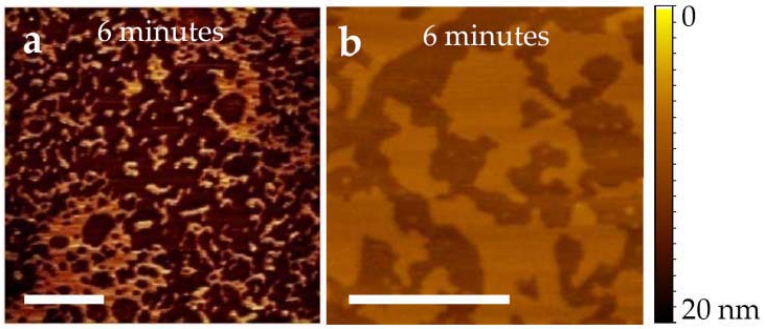

Figure 5.4. **(a)** DMPC mica-SLB after addition of SDS above CMC (20 mM). **(b)** DMPC mica-SLB after addition of CTAB above CMC (5 mM). Scale bar 500 nm.

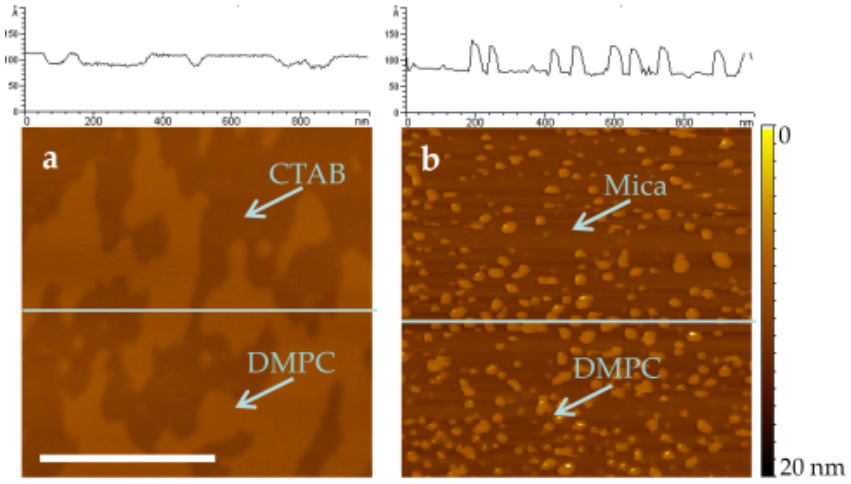

Figure 5.5. **(a)** DMPC mica-SLB after addition of CTAB above CMC (5 mM). **(b)** After addtion of SDS above CMC (20 mM) to *(a)*. Scale bar 500 nm.

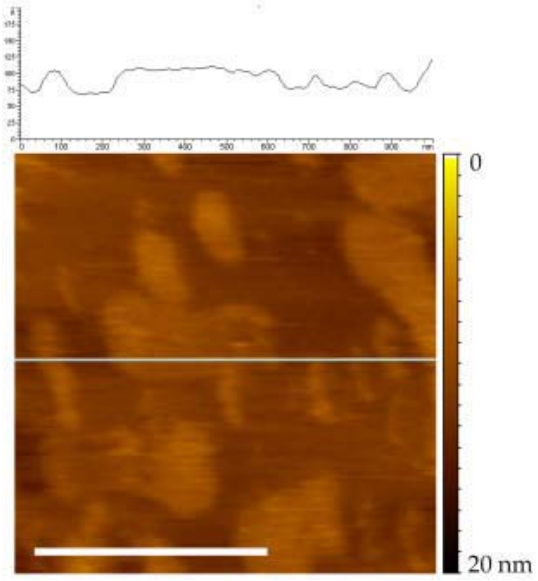

Figure 5.6. CTAB above CMC deposited on mica. Line scan shows ~2.5 nm height for CTAB. Scale bar 500 nm

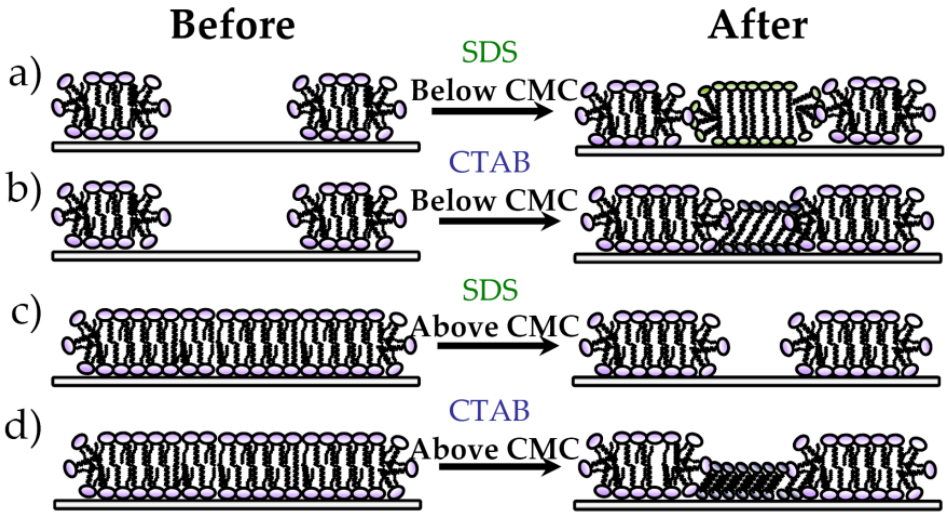

Figure 5.7. **(a)** Below CMC, SDS occludes defects. **(b)** Below CMC, CTAB occludes defects. **(c)** Above CMC, SDS removes lipid from bilayer. **(d)** Above CMC, CTAB removes lipid leaving a CTAB bilayer. Note in all cases the tilt angle of the detergent bilayer (*a, b, d*) is not ascertained from these studies. CTAB bilayer is drawn *(b, d)* based previously published studies.

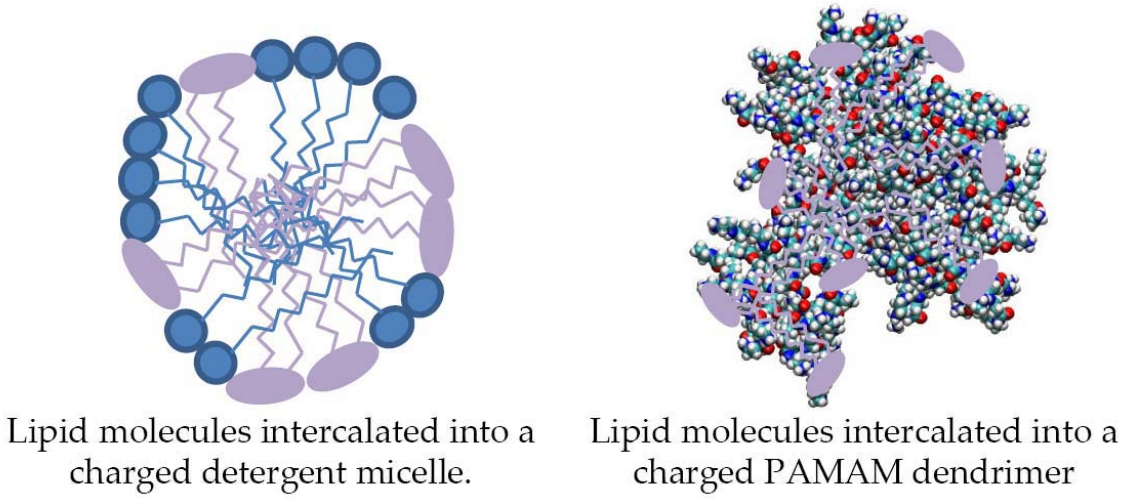

Figure 5.8 (a) Lipid (purple) intercalated into a charged detergent micelle (blue) and (b) lipid intercalated into a charged PAMAM dendrimer

5.6 REFERENCES

1. Neugebauer, J. M., Detergents - an Overview. *Methods in Enzymology* **1990,** 182, 239-253.

2. le Maire, M.; Champeil, P.; Moller, J. V., Interaction of membrane proteins and lipids with solubilizing detergents. *Biochimica Et Biophysica Acta-Biomembranes* **2000,** 1508, (1-2), 86-111.

3. Dennis, E. A., Kinetic Dependence of Phospholipase A2 Activity on Detergent Triton X-100. *Journal of Lipid Research* **1973,** 14, (2), 152-159.

4. Deo, N.; Somasundaran, P., Effects of sodium dodecyl sulfate on mixed liposome solubilization. *Langmuir* **2003,** 19, (18), 7271-7275.

5. Kragh-Hansen, U.; le Maire, M.; Moller, J. V., The mechanism of detergent solubilization of liposomes and protein-containing membranes. *Biophysical Journal* **1998,** 75, (6), 2932-2946.

6. de la Maza, A.; Parra, J. L., Vesicle-Micelle Structural Transitions of Phospholipid-Bilayers and Sodium Dodecyl-Sulfate. *Langmuir* **1995,** 11, (7), 2435-2441.

7. Morandat, S.; El Kirat, K., Membrane resistance to Triton X-100 explored by real-time atomic force microscopy. *Langmuir* **2006,** 22, (13), 5786-5791.

8. Kumaran, V., Effect of surface charges on the curvature moduli of a membrane. *Physical Review E* **2001,** 6405, (5), 051922.

9. Lichtenberg, D., Characterization of the Solubilization of Lipid Bilayers by Surfactants. *Biochimica Et Biophysica Acta* **1985,** 821, (3), 470-478.

10. Keller, S.; Heerklotz, H.; Jahnke, N.; Blume, A., Thermodynamics of lipid membrane solubilization by sodium dodecyl sulfate. *Biophysical Journal* **2006,** 90, (12), 4509-4521.

11. Pata, V.; Ahmed, F.; Discher, D. E.; Dan, N., Membrane solubilization by detergent: Resistance conferred by thickness. *Langmuir* **2004,** 20, (10), 3888-3893.

12. Deforesta, B.; Lemaire, M.; Orlowski, S.; Champeil, P.; Lund, S.; Moller, J. V.; Michelangeli, F.; Lee, A. G., Membrane Solubilization by Detergent - Use of Brominated Phospholipids to Evaluate the Detergent-Induced Changes in Ca-2+-Atpase Lipid Interaction. *Biochemistry* **1989,** 28, (6), 2558-2567.

13. Klose, G.; Madler, B.; Schafer, H.; Schneider, K. P., Structural characterization of POPC, and C12E4 in their mixed membranes at reduced hydration by solid state H-2 NMR. *Journal of Physical Chemistry B* **1999,** 103, (15), 3022-3029.

14. Thomas, M. J.; Pang, K.; Chen, Q.; Lyles, D.; Hantgan, R.; Waite, M., Lipid exchange between mixed micelles of phospholipid and triton X-100. *Biochimica Et Biophysica Acta-Biomembranes* **1999,** 1417, (1), 144-156.

15. Ueno, M., Partition Behavior of a Nonionic Detergent, Octyl Glucoside, between Membrane and Water Phases, and Its Effect on Membrane-Permeability. *Biochemistry* **1989,** 28, (13), 5631-5634.

16. Tan, A. M.; Ziegler, A.; Steinbauer, B.; Seelig, J., Thermodynamics of sodium dodecyl sulfate partitioning into lipid membranes. *Biophysical Journal* **2002,** 83, (3), 1547-1556.

17. Heerklotz, H.; Lantzsch, G.; Binder, H.; Klose, G.; Blume, A., Application of Isothermal Titration Calorimetry for Detecting Lipid-Membrane Solubilization. *Chemical Physics Letters* **1995,** 235, (5-6), 517-520.

18. Tokumasu, F.; Jin, A. J.; Dvorak, J. A., Lipid membrane phase behaviour elucidated in real time by controlled environment atomic force microscopy. *Journal of Electron Microscopy* **2002,** 51, (1), 1-9.

19. Hong, S. P.; Leroueil, P. R.; Janus, E. K.; Peters, J. L.; Kober, M. M.; Islam, M. T.; Orr, B. G.; Baker, J. R.; Holl, M. M. B., Interaction of polycationic polymers with supported lipid bilayers and cells: Nanoscale hole formation and enhanced membrane permeability. *Bioconjugate Chemistry* **2006,** 17, (3), 728-734.

20. Perkin, S.; Kampf, N.; Klein, J., Stability of self-assembled hydrophobic surfactant layers in water. *Journal of Physical Chemistry B* **2005,** 109, (9), 3832-3837.

21. Hong, S. P.; Bielinska, A. U.; Mecke, A.; Keszler, B.; Beals, J. L.; Shi, X. Y.; Balogh, L.; Orr, B. G.; Baker, J. R.; Holl, M. M. B., Interaction of poly(amidoamine) dendrimers with supported lipid bilayers and cells: Hole formation and the relation to transport. *Bioconjugate Chemistry* **2004,** 15, (4), 774-782.

22. Mecke, A.; Uppuluri, S.; Sassanella, T. M.; Lee, D. K.; Ramamoorthy, A.; Baker, J. R.; Orr, B. G.; Holl, M. M. B., Direct observation of lipid bilayer disruption by poly(amidoamine) dendrimers. *Chemistry and Physics of Lipids* **2004,** 132, (1), 3-14.

CHAPTER 6

CONCLUSIONS AND OUTLOOK

This dissertation has examined the interactions of targeted and non-targeted nanoparticles with cells and model membranes. The force pulling studies presented within Chapter 2 showed that in the presence of free FA, the number of binding events between the multivalent targeted nanodevice G5-Ac_{70}-$FA_{7.2}$ significantly decreased. Interestingly, however, the average rupture force under these free FA blocking conditions was significantly higher than under non-blocking conditions. Due to the expected distributions of FAs present on the surface of the G5-Ac_{70}-FA_n, we are not at this point able to make conclusions regarding the difference in binding seen between G5-Ac_{70}-$FA_{2.7,}$ and G5-Ac_{70}-$FA_{4.7}$ and G5-Ac_{70}-$FA_{7.2.}$

Chapters 3-5 examine the interaction of a variety of charged nanoparticles with a model membrane using atomic force microscopy (AFM). Each of the covalently-linked cationic nanoparticle investigated, regardless of shape (spherical vs. irregular), chemical composition (organic vs. inorganic), deformability (flexible vs. rigid), charge density, or size, disrupted supported lipid bilayers. It was shown that the degree of membrane disruption tracked grossly with nanoparticle surface area. In addition, Chapter 5 shows the non-covalently linked charged nanoparticles in the form of detergent micelles behave similarly to the covalently-linked nanoparticles investigated in Chapters 3-4. The formation of defects on the model membranes by charged nanoparticles is consistent with

cell-level studies and suggests that hole formation within the membrane is one of the mechanisms through which nanoparticles are internalized and/or induce toxicity.

There are several ways in which to improve our understanding of targeted multivalent platforms, G5-FA_n. First, it is necessary to repeat these studies with a number of tips for each G5-FA_n. The studies presented here relied on the measurements obtained from a single tip for each G5-FA_n. Given the expected distributions of FA on the surface of the dendrimer scaffold, it is simply necessary if we are to draw any conclusion regarding the distribution of binding configurations. Second, we could perform the force pulling studies on a G5-FA_1 or equivalent model to determine if the dislocations presented in Chapter 2 represent, as hypothesized, a single FA unbinding from the FBP substrate. The synthetic difficulties associated with making a G5-FA_1 would likely require a substitution of some sort. For example, one could imagine forgoing the dendrimer altogether and attaching a FA to the focal point of a dendron, or to the end of the PEG linker. Although this does introduce a new variable (the effect of the G5 itself), theoretically it should not alter the force required to rupture the FA-FBP bond. Third, we could obtain absolute forces of unbinding using dynamic force microscopy. The study completed in Chapter 2 yielded relative forces which is acceptable when comparing rupture forces within a single system. However, if we had interest in comparing our G5-FA_n system to other multivalent systems, we would need to obtain absolute forces. As a final suggestion for improving the force pulling studies, we could orient the FBP on the substrate. By orienting the FBP on the substrate, we could be sure that we were measuring the variation in the number of FAs binding, and not simply

the difference in binding strength due to the variation in the orientation of the receptor itself.

The intention of Chapters 3-5 was to determine which physical parameters dictate whether a nanoparticle will breach a cellular membrane. Suffice it to say, the simplicity of this goal masked the complexity of the problem. It was hypothesized that charge density played a significant role in the nanoparticle-membrane interaction, so much so that the other parameters could be considered secondary. This hypothesis was driven by our observation that PAMAM dendrimers of higher generations (e.g., G7) were more effective at inducing defects than small generations (e.g., G3 and G5). Interestingly, however, it did not appear that charge density dominated nanoparticle-membrane interactions. Instead, it was nanoparticle surface area that tracked best with the degree of membrane disruption. That said, this trend was far from exact and it is very likely that other physical parameters such as charge density help mediate nanoparticle-membrane interactions.

One tactic for teasing out the effect of each of the physical parameters would be to systematically vary one parameter more carefully. Unfortunately, systematically varying any parameter is not trivial for most synthetic nanoparticles. However, PAMAM dendrimers do lend themselves nicely to this line of experimentation. For example, the G7 PAMAM dendrimer has nominally 512 primary amines and largely induces the formation of defects whereas G3 PAMAM dendrimer has nominally 16 primary amines and does little more than aggregate around pre-existing defects. By acetylating 496 of the G7's primary amines, we can directly compare the effect of size. Similarly, one can

imagine varying the percentage of amine groups acetylated for a particular dendrimer generation and examining how this effects the dendrimer interaction both with membranes It is possible that this type of one-parameter variation could be applied to other systems such as modified gold nanoparticles. For example, one could systematically vary the size of the gold core while maintain the number of alkyl amine groups on the surface. These studies should be completed using both the AFM/SLB assay, as well as the more traditional cell-level assays in order to obtain a more complete picture of the interactions. Although this line of study would be tedious, it would yield a much clearer understanding of the how the physical parameters of nanoparticles affect their interaction with membranes.

As manufacturers increasingly push the limits of how small conventional materials can be made, materials of nanoscale size are becoming more and more important. Although the fabrication of new goods is generally good, our understanding of the interaction between nanoparticles and their environment has not yet caught up with our technology. The short time frame over which manufactured nanomaterials have been developed has not allowed us to fully understand their associated toxicity, the importance of which is just beginning to be appreciated. As such, there remains a great deal of study to be done not only on those particles already utilized, but also on those currently being developed. While it is only natural to search for new ways to improve products, we must nonetheless remain cognizant of the potential dangers associated with technological advancements.

BIBLIOGRAPHY

BIBLIOGRAPHY

Allen, N. S.; Edge, M.; Ortega, A.; Liauw, C. M.; Stratton, J.; McIntyre, R. B., Behaviour of nanoparticle (ultrafine) titanium dioxide pigments and stabilisers on the photooxidative stability of water based acrylic and isocyanate based acrylic coatings. *Polymer Degradation and Stability* **2002,** 78, (3), 467-478.

Allen, T. M.; Cullis, P. R., Drug delivery systems: Entering the mainstream. *Science* **2004,** 303, (5665), 1818-1822.

Andresen, T. L.; Jensen, S. S.; Jorgensen, K., Advanced strategies in liposomal cancer therapy: Problems and prospects of active and tumor specific drug release. *Progress in Lipid Research* **2005,** 44, (1), 68-97.

Artemov, D.; Mori, N.; Ravi, R.; Bhujwalla, Z. M., Magnetic resonance molecular imaging of the HER-2/neu receptor. *Cancer Research* **2003,** 63, (11), 2723-2727.

Bagwe, R. P.; Hilliard, L. R.; Tan, W. H., Surface modification of silica nanoparticles to reduce aggregation and nonspecific binding. *Langmuir* **2006,** 22, (9), 4357-4362.

Bell, A. T., The impact of nanoscience on heterogeneous catalysis. *Science* **2003,** 299, (5613), 1688-1691.

Bielinska, A. U.; Yen, A.; Wu, H. L.; Zahos, K. M.; Sun, R.; Weiner, N. D.; Baker, J. R.; Roessler, B. J., Application of membrane-based dendrimer/DNA complexes for solid phase transfection in vitro and in vivo. *Biomaterials* **2000,** 21, (9), 877-887.

Borm, P. Y. A.; Costa, D.; Castranova, V.; Donaldson, K.; Driscoll, K.; Dungworth, D.; Green, F.; Greim, H.; Harkema, J.; Jarabek, A.; Kane, A. B.; Kuempel, E. D.; Mauderly, J. L.; McCunney, R. J.; Miller, F.; Morgan, D.; Mossman, B.; Muhle, H.; Nauss, K.; Nikula, K.; Oberdorster, G.; Olin, S. S.; Pepelko, W.; Pinkerton, K. E.; Schultz, M.; Utell, M. J.; Vallyathan, V.; Vu, V.; Warheit, D. B.; Witschi, H., The relevance of the rat lung response to particle overload for human risk assessment: A workshop consensus report. *Inhalation Toxicology* **2000,** 12, (1-2), 1-17.

Brannon-Peppas, L.; Blanchette, J. O., Nanoparticle and targeted systems for cancer therapy. *Advanced Drug Delivery Reviews* **2004,** 56, (11), 1649-1659.

Braun, K.; Pipkorn, R.; Waldeck, W., Development and characterization of drug delivery systems for targeting mammalian cells and tissues: A review. *Current Medicinal Chemistry* **2005,** 12, (16), 1841-1858.

Campbell, I. G.; Jones, T. A.; Foulkes, W. D.; Trowsdale, J., Folate-Binding Protein Is a Marker for Ovarian-Cancer. *Cancer Research* **1991,** 51, (19), 5329-5338.

Carrithers, M. D.; Lerner, M. R., Synthesis and characterization of bivalent peptide ligands targeted to G-protein-coupled receptors. *Chemistry & Biology* **1996,** 3, (7), 537-542.

Chen, X. Y.; Plasencia, C.; Hou, Y. P.; Neamati, N., Synthesis and biological evaluation of dimeric RGD peptide-paclitaxel conjugate as a model for integrin-targeted drug delivery. *Journal of Medicinal Chemistry* **2005,** 48, (4), 1098-1106.

de la Maza, A.; Parra, J. L., Vesicle-Micelle Structural Transitions of Phospholipid-Bilayers and Sodium Dodecyl-Sulfate. *Langmuir* **1995,** 11, (7), 2435-2441.

Deforesta, B.; Lemaire, M.; Orlowski, S.; Champeil, P.; Lund, S.; Moller, J. V.; Michelangeli, F.; Lee, A. G., Membrane Solubilization by Detergent - Use of Brominated Phospholipids to Evaluate the Detergent-Induced Changes in Ca-2+-Atpase Lipid Interaction. *Biochemistry* **1989,** 28, (6), 2558-2567.

Dennis, E. A., Kinetic Dependence of Phospholipase A2 Activity on Detergent Triton X-100. *Journal of Lipid Research* **1973,** 14, (2), 152-159.

Deo, N.; Somasundaran, P., Effects of sodium dodecyl sulfate on mixed liposome solubilization. *Langmuir* **2003,** 19, (18), 7271-7275.

Drin, G.; Cottin, S.; Blanc, E.; Rees, A. R.; Temsamani, J., Studies on the internalization mechanism of cationic cell-penetrating peptides. *Journal of Biological Chemistry* **2003,** 278, (33), 31192-31201.

Dubey, P. K.; Mishra, V.; Jain, S.; Mahor, S.; Vyas, S. P., Liposomes modified with cyclic RGD peptide for tumor targeting. *Journal of Drug Targeting* **2004,** 12, (5), 257-264.

Duncan, R., The dawning era of polymer therapeutics. *Nature Reviews Drug Discovery* **2003,** 2, (5), 347-360.

Duncan, R.; Izzo, L., Dendrimer biocompatibility and toxicity. *Advanced Drug Delivery Reviews* **2005,** 57, (15), 2215-2237.

Evans, E.; Ritchie, K., Dynamic strength of molecular adhesion bonds. *Biophysical Journal* **1997,** 72, (4), 1541-1555.

Evans, E. B., Looking inside molecular bonds at biological interfaces with dynamic force spectroscopy. *Biophysical Chemistry* **1999,** 82, (2-3), 83-97.

Farokhzad, O. C.; Jon, S. Y.; Khadelmhosseini, A.; Tran, T. N. T.; LaVan, D. A.; Langer, R., Nanopartide-aptamer bioconjugates: A new approach for targeting prostate cancer cells. *Cancer Research* **2004,** 64, (21), 7668-7672.

Fawell, S.; Seery, J.; Daikh, Y.; Moore, C.; Chen, L. L.; Pepinsky, B.; Barsoum, J., TAT-mediated delivery of heterologous proteins into cells. *Proceedings of the National Academy of Sciences of the United States of America* **1994,** 91, (2), 664-668.

Fischer, D.; Li, Y. X.; Ahlemeyer, B.; Krieglstein, J.; Kissel, T., In vitro cytotoxicity testing of polycations: influence of polymer structure on cell viability and hemolysis. *Biomaterials* **2003,** 24, (7), 1121-1131.

Friddle, R. W.; Sulchek, T. A.; Albrecht, H.; De Nardo, S. J.; Noy, A., Counting and breaking individual biological bonds: Force spectroscopy of tethered ligand-receptor pairs. *Current Nanoscience* **2007,** 3, (1), 41-48.

Fuchs, P. C.; Barry, A. L.; Brown, S. D., In vitro antimicrobial activity of MSI-78, a magainin analog. *Antimicrobial Agents and Chemotherapy* **1998,** 42, (5), 1213-1216.

Ginzburg, V. V.; Balijepalli, S., Modeling the Thermodynamics of the Interaction of Nanoparticles with Cell Membranes. *Nano Letters* **2007,** 7, (12), 3716-3722.

Goodman, C. M.; McCusker, C. D.; Yilmaz, T.; Rotello, V. M., Toxicity of gold nanoparticles functionalized with cationic and anionic side chains. *Bioconjugate Chemistry* **2004,** 15, (4), 897-900.

Gopalakr.Pv; Karush, F., Antibody Affinity .7. Multivalent Interaction of Anti-Lactoside Antibody. *Journal of Immunology* **1974,** 113, (3), 769-778.

Gu, F. X.; Karnik, R.; Wang, A. Z.; Alexis, F.; Levy-Nissenbaum, E.; Hong, S.; Langer, R. S.; Farokhzad, O. C., Targeted nanoparticles for cancer therapy. *Nano Today* **2007,** 2, (3), 14-21.

Gwinn, M. R.; Vallyathan, V., Nanoparticles: Health effects - Pros and cons. *Environmental Health Perspectives* **2006,** 114, (12), 1818-1825.

Heerklotz, H.; Lantzsch, G.; Binder, H.; Klose, G.; Blume, A., Application of Isothermal Titration Calorimetry for Detecting Lipid-Membrane Solubilization. *Chemical Physics Letters* **1995,** 235, (5-6), 517-520.

Heller, W. T.; Waring, A. J.; Lehrer, R. I.; Harroun, T. A.; Weiss, T. M.; Yang, L.; Huang, H. W., Membrane thinning effect of the beta-sheet antimicrobial protegrin. *Biochemistry* **2000,** 39, (1), 139-145.

Hong, S.; Leroueil, P. R.; Majoros, I. J.; Orr, B. G.; Baker, J. R.; Holl, M. M. B., The binding avidity of a nanoparticle-based multivalent targeted drug delivery platform. *Chemistry & Biology* **2007,** 14, (1), 105-113.

Hong, S. P.; Bielinska, A. U.; Mecke, A.; Keszler, B.; Beals, J. L.; Shi, X. Y.; Balogh, L.; Orr, B. G.; Baker, J. R.; Holl, M. M. B., Interaction of poly(amidoamine) dendrimers with supported lipid bilayers and cells: Hole formation and the relation to transport. *Bioconjugate Chemistry* **2004,** 15, (4), 774-782.

Hong, S. P.; Leroueil, P. R.; Janus, E. K.; Peters, J. L.; Kober, M. M.; Islam, M. T.; Orr, B. G.; Baker, J. R.; Holl, M. M. B., Interaction of polycationic polymers with supported lipid bilayers and cells: Nanoscale hole formation and enhanced membrane permeability. *Bioconjugate Chemistry* **2006,** 17, (3), 728-734.

Hood, J. D.; Bednarski, M.; Frausto, R.; Guccione, S.; Reisfeld, R. A.; Xiang, R.; Cheresh, D. A., Tumor regression by targeted gene delivery to the neovasculature. *Science* **2002,** 296, (5577), 2404-2407.

Hussain, S. M.; Hess, K. L.; Gearhart, J. M.; Geiss, K. T.; Schlager, J. J., In vitro toxicity of nanoparticles in BRL 3A rat liver cells. *Toxicology in Vitro* **2005,** 19, (7), 975-983.

Jackson, J. B.; Halas, N. J., Silver nanoshells: Variations in morphologies and optical properties. *Journal of Physical Chemistry B* **2001,** 105, (14), 2743-2746.

Jain, R. K., Barriers to Drug-Delivery in Solid Tumors. *Scientific American* **1994,** 271, (1), 58-65.

Jin, Z. H.; Josserand, V.; Foillard, S.; Boturyn, D.; Dumy, P.; Favrot, M. C.; Coll, J. L., In vivo optical imaging of integrin alpha(v)-beta(3) in mice using multivalent or monovalent cRGD targeting vectors. *Molecular Cancer* **2007,** 6.

Kamat, P. V., Photophysical, photochemical and photocatalytic aspects of metal nanoparticles. *Journal of Physical Chemistry B* **2002,** 106, (32), 7729-7744.

Kapoor, S.; Kartha, S.; Meisel, D., EPR and pulse radiolysis studies on electron transfer in transition metal dithiolenes at the surface of colloidal TiO2. *Research on Chemical Intermediates* **2001,** 27, (4-5), 317-332.

Keller, S.; Heerklotz, H.; Jahnke, N.; Blume, A., Thermodynamics of lipid membrane solubilization by sodium dodecyl sulfate. *Biophysical Journal* **2006,** 90, (12), 4509-4521.

Klose, G.; Madler, B.; Schafer, H.; Schneider, K. P., Structural characterization of POPC, and C12E4 in their mixed membranes at reduced hydration by solid state H-2 NMR. *Journal of Physical Chemistry B* **1999,** 103, (15), 3022-3029.

Kragh-Hansen, U.; le Maire, M.; Moller, J. V., The mechanism of detergent solubilization of liposomes and protein-containing membranes. *Biophysical Journal* **1998,** 75, (6), 2932-2946.

Kreuter, J., Nanoparticulate systems for brain delivery of drugs. *Advanced Drug Delivery Reviews* **2001,** 47, (1), 65-81.

Kukowska-Latallo, J. F.; Candido, K. A.; Cao, Z. Y.; Nigavekar, S. S.; Majoros, I. J.; Thomas, T. P.; Balogh, L. P.; Khan, M. K.; Baker, J. R., Nanoparticle targeting of anticancer drug improves therapeutic response in animal model of human epithelial cancer. *Cancer Research* **2005,** 65, (12), 5317-5324.

Kumaran, V., Effect of surface charges on the curvature moduli of a membrane. *Physical Review E* **2001,** 6405, (5), 051922.

Langer, R., Drug delivery and targeting. *Nature* **1998,** 392, (6679), 5-10.

le Maire, M.; Champeil, P.; Moller, J. V., Interaction of membrane proteins and lipids with solubilizing detergents. *Biochimica Et Biophysica Acta-Biomembranes* **2000,** 1508, (1-2), 86-111.

Leroueil, P. R.; Hong, S. Y.; Mecke, A.; Baker, J. R.; Orr, B. G.; Holl, M. M. B., Nanoparticle interaction with biological membranes: Does nanotechnology present a janus face? *Accounts of Chemical Research* **2007,** 40, (5), 335-342.

Li, M.; Schnablegger, H.; Mann, S., Coupled synthesis and self-assembly of nanoparticles to give structures with controlled organization. *Nature* **1999,** 402, (6760), 393-395.

Lichtenberg, D., Characterization of the Solubilization of Lipid Bilayers by Surfactants. *Biochimica Et Biophysica Acta* **1985,** 821, (3), 470-478.

Link, S.; El-Sayed, M. A., Shape and size dependence of radiative, non-radiative and photothermal properties of gold nanocrystals. *International Reviews in Physical Chemistry* **2000,** 19, (3), 409-453.

Liu, Y.; Steiniger, S. C. J.; Kim, Y.; Kaufmann, G. F.; Felding-Habermann, B.; Janda, K. D., Mechanistic studies of a peptidic GRP78 ligand for cancer cell-specific drug delivery. *Molecular Pharmaceutics* **2007,** 4, (3), 435-447.

Livadaru, L.; Kovaenko, A., Fundamental mechanism of translocation across liquidlike membranes: Toward control over nanoparticle behavior. *Nano Letters* **2006,** 6, (1), 78-83.

Luo, Y.; Bernshaw, N. J.; Lu, Z. R.; Kopecek, J.; Prestwich, G. D., Targeted delivery of doxorubicin by HPMA copolymer-hyaluronan bioconjugates. *Pharmaceutical Research* **2002,** 19, (4), 396-402.

Luppi, B.; Cerchiara, T.; Bigucci, F.; Basile, R.; Zecchi, V., Polymeric nanoparticles composed of fatty acids and polyvinylalcohol for topical application of sunscreens. *Journal of Pharmacy and Pharmacology* **2004,** 56, (3), 407-411.

Maaheimo, H.; Renkonen, R.; Turunen, J. P.; Penttila, L.; Renkonen, O., Synthesis of a Divalent Sialyl-Lewis-X O-Glycan, a Potent Inhibitor of Lymphocyte-Endothelium Adhesion - Evidence That Multivalency Enhances the Saccharide Binding to L-Selectin. *European Journal of Biochemistry* **1995,** 234, (2), 616-625.

Maeda, H., The enhanced permeability and retention (EPR) effect in tumor vasculature: The key role of tumor-selective macromolecular drug targeting. In *Advances in Enzyme Regulation, Vol 41*, 2001; Vol. 41, pp 189-207.

Magrez, A.; Kasas, S.; Salicio, V.; Pasquier, N.; Seo, J. W.; Celio, M.; Catsicas, S.; Schwaller, B.; Forro, L., Cellular toxicity of carbon-based nanomaterials. *Nano Letters* **2006,** 6, (6), 1121-1125.

Majoros, I. J.; Myc, A.; Thomas, T.; Mehta, C. B.; Baker, J. R., PAMAM dendrimer-based multifunctional conjugate for cancer therapy: Synthesis, characterization, and functionality. *Biomacromolecules* **2006,** 7, (2), 572-579.

Majoros, I. J.; Thomas, T. P.; Mehta, C. B.; Baker, J. R., Poly(amidoamine) dendrimer-based multifunctional engineered nanodevice for cancer therapy. *Journal of Medicinal Chemistry* **2005,** 48, (19), 5892-5899.

Maynard, A. D.; Kuempel, E. D., Airborne nanostructured particles and occupational health. *Journal Of Nanoparticle Research* **2005,** 7, (6), 587-614.

Meadows, D. C.; Gervay-Hague, J., Targeting HIV. *Chemmedchem* **2006,** 1, (1), 16-29.

Mecke, A.; Lee, D. K.; Ramamoorthy, A.; Orr, B. G.; Holl, M. M. B., Synthetic and natural polycationic polymer nanoparticles interact selectively with fluid-phase domains of DMPC lipid bilayers. *Langmuir* **2005,** 21, (19), 8588-8590.

Mecke, A.; Lee, D. K.; Ramamoorthy, A.; Orr, B. G.; Holl, M. M. B., Membrane thinning due to antimicrobial peptide binding: An atomic force microscopy study of MSI-78 in lipid bilayers. *Biophysical Journal* **2005,** 89, (6), 4043-4050.

Mecke, A.; Majoros, I. J.; Patri, A. K.; Baker, J. R.; Holl, M. M. B.; Orr, B. G., Lipid bilayer disruption by polycationic polymers: The roles of size and chemical functional group. *Langmuir* **2005,** 21, (23), 10348-10354.

73. Mecke, A.; Uppuluri, S.; Sassanella, T. M.; Lee, D. K.; Ramamoorthy, A.; Baker, J. R.; Orr, B. G.; Holl, M. M. B., Direct observation of lipid bilayer disruption by poly(amidoamine) dendrimers. *Chemistry and Physics of Lipids* **2004,** 132, (1), 3-14.

Monteiro-Riviere, N. A.; Nemanich, R. J.; Inman, A. O.; Wang, Y. Y. Y.; Riviere, J. E., Multi-walled carbon nanotube interactions with human epidermal keratinocytes. *Toxicology Letters* **2005,** 155, (3), 377-384.

Montet, X.; Funovics, M.; Montet-Abou, K.; Weissleder, R.; Josephson, L., Multivalent effects of RGD peptides obtained by nanoparticle display. *Journal of Medicinal Chemistry* **2006,** 49, (20), 6087-6093.

Morandat, S.; El Kirat, K., Membrane resistance to Triton X-100 explored by real-time atomic force microscopy. *Langmuir* **2006,** 22, (13), 5786-5791.

Mori, H.; Lanzendorfer, M. G.; Muller, A. H. E.; Klee, J. E., Organic-inorganic nanoassembly based on complexation of cationic silica nanoparticles and weak anionic polyelectrolytes in aqueous and alcohol media. *Langmuir* **2004,** 20, (5), 1934-1944.

Murray, C. B.; Kagan, C. R.; Bawendi, M. G., Synthesis and characterization of monodisperse nanocrystals and close-packed nanocrystal assemblies. *Annual Review of Materials Science* **2000,** 30, 545-610.

Napier, M. E.; Desimone, J. M., Nanoparticle drug delivery platform. *Polymer Reviews* **2007,** 47, (3), 321-327.

Nel, A.; Xia, T.; Madler, L.; Li, N., Toxic potential of materials at the nanolevel. *Science* **2006,** 311, (5761), 622-627.

Neugebauer, J. M., Detergents - an Overview. *Methods in Enzymology* **1990,** 182, 239-253.

Nigavekar, S. S.; Sung, L. Y.; Llanes, M.; El-Jawahri, A.; Lawrence, T. S.; Becker, C. W.; Balogh, L.; Khan, M. K., H-3 dendrimer nanoparticle organ/tumor distribution. *Pharmaceutical Research* **2004,** 21, (3), 476-483.

Nygren-Babol, L.; Sternesjo, A.; Jagerstad, M.; Bjorck, L., Affinity and rate constants for interactions of bovine folate-binding protein and folate derivatives determined by optical biosensor technology. Effect of stereoselectivity. *Journal of Agricultural and Food Chemistry* **2005,** 53, (13), 5473-5478.

Oberdorster, E., Manufactured nanomaterials (Fullerenes, C-60) induce oxidative stress in the brain of juvenile largemouth bass. *Environmental Health Perspectives* **2004,** 112, (10), 1058-1062.

Oberdorster, E.; Cheek, A. O., Gender benders at the beach: Endocrine disruption in marine and estuarine organisms. *Environmental Toxicology and Chemistry* **2001,** 20, (1), 23-36.

Oberdorster, G., Pulmonary effects of inhaled ultrafine particles. *International Archives of Occupational and Environmental Health* **2001,** 74, (1), 1-8.

Oberdorster, G.; Gelein, R. M.; Ferin, J.; Weiss, B., Association of Particulate Air-Pollution and Acute Mortality - Involvement of Ultrafine Particles. *Inhalation Toxicology* **1995,** 7, (1), 111-124.

Oberdorster, G.; Oberdorster, E.; Oberdorster, J., Nanotoxicology: An emerging discipline evolving from studies of ultrafine particles. *Environmental Health Perspectives* **2005,** 113, (7), 823-839.

Ottaviani, M. F.; Sacchi, B.; Turro, N. J.; Chen, W.; Jockusch, S.; Tomalia, D. A., An EPR study of the interactions between starburst dendrimers and polynucleotides. *Macromolecules* **1999,** 32, (7), 2275-2282.

Paciotti, G. F.; Myer, L.; Weinreich, D.; Goia, D.; Pavel, N.; McLaughlin, R. E.; Tamarkin, L., Colloidal gold: A novel nanoparticle vector for tumor directed drug delivery. *Drug Delivery* **2004,** 11, (3), 169-183.

Pata, V.; Ahmed, F.; Discher, D. E.; Dan, N., Membrane solubilization by detergent: Resistance conferred by thickness. *Langmuir* **2004,** 20, (10), 3888-3893.

Perkin, S.; Kampf, N.; Klein, J., Stability of self-assembled hydrophobic surfactant layers in water. *Journal of Physical Chemistry B* **2005,** 109, (9), 3832-3837.

Pillai, O.; Dhanikula, A. B.; Panchagnula, R., Drug delivery: an odyssey of 100 years. *Current Opinion in Chemical Biology* **2001,** 5, (4), 439-446.

Popielarski, S. R.; Pun, S. H.; Davis, M. E., A nanoparticle-based model delivery system to guide the rational design of gene delivery to the liver. 1. Synthesis and characterization. *Bioconjugate Chemistry* **2005,** 16, (5), 1063-1070.

Quintana, A.; Raczka, E.; Piehler, L.; Lee, I.; Myc, A.; Majoros, I.; Patri, A. K.; Thomas, T.; Mule, J.; Baker, J. R., Design and function of a dendrimer-based therapeutic nanodevice targeted to tumor cells through the folate receptor. *Pharmaceutical Research* **2002,** 19, (9), 1310-1316.

Richard, J. P.; Melikov, K.; Vives, E.; Ramos, C.; Verbeure, B.; Gait, M. J.; Chernomordik, L. V.; Lebleu, B., Cell-penetrating peptides - A reevaluation of the mechanism of cellular uptake. *Journal of Biological Chemistry* **2003,** 278, (1), 585-590.

Ross, J. F.; Chaudhuri, P. K.; Ratnam, M., Differential Regulation of Folate Receptor Isoforms in Normal and Malignant-Tissues in-Vivo and in Established Cell-Lines - Physiological and Clinical Implications. *Cancer* **1994,** 73, (9), 2432-2443.

Salmaso, S.; Semenzato, A.; Caliceti, P.; Hoebeke, J.; Sonvico, F.; Dubernet, C.; Couvreur, P., Specific antitumor targetable beta-cyclodextrin-poly(ethylene glycol)-folic acid drug delivery bioconjugate. *Bioconjugate Chemistry* **2004,** 15, (5), 997-1004.

Sandhu, K. K.; McIntosh, C. M.; Simard, J. M.; Smith, S. W.; Rotello, V. M., Gold nanoparticle-mediated Transfection of mammalian cells. *Bioconjugate Chemistry* **2002,** 13, (1), 3-6.

Satchi-Fainaro, R.; Duncan, R.; Barnes, C. M., Polymer therapeutics for cancer: Current status and future challenges. In *Polymer Therapeutics Ii: Polymers as Drugs, Conjugates and Gene Delivery Systems*, 2006; Vol. 193, pp 1-65.

Schiffelers, R. M.; Ansari, A.; Xu, J.; Zhou, Q.; Tang, Q. Q.; Storm, G.; Molema, G.; Lu, P. Y.; Scaria, P. V.; Woodle, M. C., Cancer siRNA therapy by tumor selective delivery with ligand-targeted sterically stabilized nanoparticle. *Nucleic Acids Research* **2004,** 32, (19).

Shipway, A. N.; Katz, E.; Willner, I., Nanoparticle arrays on surfaces for electronic, optical, and sensor applications. *Chemphyschem* **2000,** 1, (1), 18-52.

Shukla, R.; Thomas, T. P.; Peters, J. L.; Desai, A. M.; Kukowska-Latallo, J.; Patri, A. K.; Kotlyar, A.; Baker, J. R., HER2 specific tumor targeting with dendrimer conjugated anti-HER2 mAb. *Bioconjugate Chemistry* **2006,** 17, (5), 1109-1115.

Shukla, S. K.; Petrucci, F.; Caimi, S.; Alimonti, A.; Cusumano, R., Cancer 'Chemotherapia specifica' ninety years after Paul Ehrlich. *Chemotherapy* **2007,** 53, (5), 309-312.

Spurlin, T. A.; Gewirth, A. A., Poly-L-lysine-induced morphology changes in mixed anionic/zwitterionic and neat zwitterionic-supported phospholipid bilayers. *Biophysical Journal* **2006,** 91, (8), 2919-2927.

Stella, B.; Arpicco, S.; Peracchia, M. T.; Desmaele, D.; Hoebeke, J.; Renoir, M.; D'Angelo, J.; Cattel, L.; Couvreur, P., Design of folic acid-conjugated nanoparticles for drug targeting. *Journal of Pharmaceutical Sciences* **2000,** 89, (11), 1452-1464.

Sudimack, J.; Lee, R. J., Targeted drug delivery via the folate receptor. *Advanced Drug Delivery Reviews* **2000,** 41, (2), 147-162.

Sulchek, T. A.; Friddle, R. W.; Langry, K.; Lau, E. Y.; Albrecht, H.; Ratto, T. V.; DeNardo, S. J.; Colvin, M. E.; Noy, A., Dynamic force spectroscopy of parallel individual Mucin1-antibody bonds. *Proceedings of the National Academy of Sciences of the United States of America* **2005,** 102, (46), 16638-16643.

Taborda, C. P.; Rivera, J.; Zaragoza, O.; Casadevall, A., More is not necessarily better: Prozone-like effects in passive immunization with IgG. *Journal of Immunology* **2003,** 170, (7), 3621-3630.

Tan, A. M.; Ziegler, A.; Steinbauer, B.; Seelig, J., Thermodynamics of sodium dodecyl sulfate partitioning into lipid membranes. *Biophysical Journal* **2002,** 83, (3), 1547-1556.

Thomas, M. J.; Pang, K.; Chen, Q.; Lyles, D.; Hantgan, R.; Waite, M., Lipid exchange between mixed micelles of phospholipid and triton X-100. *Biochimica Et Biophysica Acta-Biomembranes* **1999,** 1417, (1), 144-156.

Thomas, T. P.; Majoros, I. J.; Kotlyar, A.; Kukowska-Latallo, J. F.; Bielinska, A.; Myc, A.; Baker, J. R., Targeting and inhibition of cell growth by an engineered dendritic nanodevice. *Journal of Medicinal Chemistry* **2005,** 48, (11), 3729-3735.

Thomas, T. P.; Patri, A. K.; Myc, A.; Myaing, M. T.; Ye, J. Y.; Norris, T. B.; Baker, J. R., In vitro targeting of synthesized anti body-conjugated dendrimer nanoparticles. *Biomacromolecules* **2004,** 5, (6), 2269-2274.

Tinkle, S. S.; Antonini, J. M.; Rich, B. A.; Roberts, J. R.; Salmen, R.; DePree, K.; Adkins, E. J., Skin as a route of exposure and sensitization in chronic beryllium disease. *Environmental Health Perspectives* **2003,** 111, (9), 1202-1208.

Tokumasu, F.; Jin, A. J.; Dvorak, J. A., Lipid membrane phase behaviour elucidated in real time by controlled environment atomic force microscopy. *Journal of Electron Microscopy* **2002,** 51, (1), 1-9.

Uckun, F. M.; Narla, R. K.; Zeren, T.; Yanishevski, Y.; Myers, D. E.; Waurzyniak, B.; Ek, O.; Schneider, E.; Messinger, Y.; Chelstrom, L. M.; Gunther, R.; Evans, W., In vivo toxicity, pharmacokinetics, and anticancer activity of genistein linked to recombinant human epidermal growth factor. *Clinical Cancer Research* **1998,** 4, (5), 1125-1134.

Ueno, M., Partition Behavior of a Nonionic Detergent, Octyl Glucoside, between Membrane and Water Phases, and Its Effect on Membrane-Permeability. *Biochemistry* **1989,** 28, (13), 5631-5634.

Warheit, D. B.; Webb, T. R.; Colvin, V. L.; Reed, K. L.; Sayes, C. R., Pulmonary bioassay studies with nanoscale and fine-quartz particles in rats: Toxicity is not dependent upon particle size but on surface characteristics. *Toxicological Sciences* **2007,** 95, (1), 270-280.

Weitman, S. D.; Lark, R. H.; Coney, L. R.; Fort, D. W.; Frasca, V.; Zurawski, V. R.; Kamen, B. A., Distribution of the Folate Receptor Gp38 in Normal and Malignant-Cell Lines and Tissues. *Cancer Research* **1992,** 52, (12), 3396-3401.

Weitman, S. D.; Weinberg, A. G.; Coney, L. R.; Zurawski, V. R.; Jennings, D. S.; Kamen, B. A., Cellular-Localization of the Folate Receptor - Potential Role in Drug Toxicity and Folate Homeostasis. *Cancer Research* **1992,** 52, (23), 6708-6711.

West, J. L.; Halas, N. J., Engineered nanomaterials for biophotonics applications: Improving sensing, imaging, and therapeutics. *Annual Review of Biomedical Engineering* **2003,** 5, 285-292.

Winter, P. M.; Caruthers, S. D.; Kassner, A.; Harris, T. D.; Chinen, L. K.; Allen, J. S.; Lacy, E. K.; Zhang, H. Y.; Robertson, J. D.; Wickline, S. A.; Lanza, G. M., Molecular Imaging of angiogenesis in nascent vx-2 rabbit tumors using a novel alpha(v)beta(3)-targeted nanoparticle and 1.5 tesla magnetic resonance imaging. *Cancer Research* **2003,** 63, (18), 5838-5843.

Wittmaack, K., Search of the most relevant parameter for quantifying lung inflammatory response to nanoparticle exposure: Particle number, surface area, or what? *Environmental Health Perspectives* **2007,** 115, (2), 187-194.

Woodrow Wilson International Center for Scholars: Project on Emerging Technologies. http://www.nanotechproject.org/ (October 2, 2007)

Xia, T.; Kovochich, M.; Brant, J.; Hotze, M.; Sempf, J.; Oberley, T.; Sioutas, C.; Yeh, J. I.; Wiesner, M. R.; Nel, A. E., Comparison of the abilities of ambient and manufactured nanoparticles to induce cellular toxicity according to an oxidative stress paradigm. *Nano Letters* **2006,** 6, (8), 1794-1807.

Zhi, P. X.; Qing, H. Z.; Gao, Q. L.; Ai, B. Y., Inorganic nanoparticles as carriers for efficient cellular delivery. *Chemical Engineering Science* **2006,** 61, (3), 1027-1040.